1-1-2011

Force Analysis of Human Lumbar Spine Using a Forward Kinematics Model

Krunal Patel
Ryerson University

FORCE ANALYSIS OF HUMAN LUMBAR SPINE USING A FORWARD KINEMATICS MODEL

by

Krunal Patel
Bachelor of Engineering
Ryerson University, 2009

A Thesis
presented to Ryerson University

in partial fulfillment of the
requirements for the degree of
Master of Applied Science
in the Program of
Mechanical Engineering

Toronto, Ontario, Canada, 2011

AUTHOR'S DECLARATION

I hereby declare that I am the sole author of this thesis.

I authorize Ryerson University to lend this thesis to other institutions or individuals for the purpose of scholarly research.

Krunal Patel

Ryerson University

I further authorize Ryerson University to reproduce this thesis by photocopying or by other means, in total or in part, at the request of other institution or individuals for the purpose of scholarly research.

Krunal Patel

Ryerson University

ABSTRACT

FORCE ANALYSIS OF HUMAN LUMBAR SPINE USING FORWARD KINEMATICS MODEL

Krunal Patel, Master of Applied Science, 2011

Department of Mechanical and Industrial Engineering, Ryerson University

The purpose of this study is to present a forward kinematics model of the human lumbar spine and to compare the internal loads and trunk flexion extension with existing literature. The forward kinematics model of lumbar spine with 30 DOF was designed using Solidworks and used Matlab to simulate the results for different postures. The forward kinematics model predicted similar trend for trunk flexion extension, compression force, shear forces and moment as described in literature for in vivo studies. The comparison between the proposed model and in vivo measurement showed a pressure difference of less than 15% on the disc L4-L5 for all activities whereas the compression force and moment differed by ~17% on the disc L5-S1. The modeling methodology presented in this thesis provides a more accurate representation of compression forces and moments of the human lumbar spine since the model makes no assumptions regarding muscle force and does not rely on any other software for kinematics data.

ACKNOWLEDGEMENTS

First and foremost, I would like to show my sincere appreciation for my advisor, Dr. Ahmad Ghasempoor, for his enthusiasm, firm encouragement and faith in my abilities. I am forever indebted to Dr. Ahmad Ghasempoor for this opportunity to work in biomechanics field under his supervision at Ryerson. There were many challenges and frustrating stages while modeling lumbar spine that would have been far more difficult to handle without him.

I would also like to express my deepest thanks to Dr. Mohammad Abdoli for sharing his vast knowledge in biomedical field during the modeling of lumbar spine and for the many great conversations we have had about human anatomy that gave me an in depth knowledge that otherwise could not have been obtained from literature.

I would like to give a very special thanks to my parents and sisters who have always supported me throughout my life and I am also eternally obliged to my best friend for her infinite patience and unconditional support. I would not have accomplished this without her resolute dedication.

I would also like to extend my gratitude to all my friends with whom I shared light moments and for all those mind refreshing conversations we had over "Chai time" that rescued me from losing my sanity more times than I can remember.

DEDICATION

I dedicate this work to my family, especially my mom and dad, who have always supported me throughout life no matter what I chose and have never judged my actions and always pray for my success day and night.

I also dedicate this work to my best friend and some very close friends, who tirelessly care and support me in my times of need, despair, depression, and even tolerate my temper tantrums.

TABLE OF CONTENTS

LIST OF FIGURES

LIST OF TABLES

LIST OF APPENDICES

NOMENCLATURE

N	Newton
Nm	Newton meter
MPa	Mega Pascal (10^6 Pascal)
kg	Kilograms
mm	Millimeter (10^{-3} m)
kN/m	kilo newton per meter
N/mm	Newton per milimeter
cm	Centimeter (10^{-2} m)
DOF	Degrees of freedom
2D	2 Dimensional
3D	3 Dimensional
t	Time
S	Seconds
F	Force
a	acceleration
m	mass
M	moment

Chapter 1: Introduction

1.1 Introduction

In human body, muscular and skeletal systems are essential for everyday movements. The muscular system is composed of the muscle fibres with the main function of contractility. Tendons are attached to the bones and produce greater amount of force under compression and sustain the body posture in various conditions as well as stabilize the body temperature. [1, 2]

In this thesis, the main focus is on the human lumbar spine specifically lumbar vertebrae, lumbar muscles, intervertebral discs, joints, and ligaments. The connections, functions and other parameters of these elements are briefly described in Chapter 3. The goal of studying human lumbar spine is to prevent the low back injuries due to the instability of the spine and to provide a data base for researchers for further studies. Musculoskeletal disorders in lower back are of concern in everyday and extreme activities alike. These include sports, work around the house and garden, lifting, sitting, driving, office work, and dealing with heavy industrial equipments [3]. According to National Institute of Neurological Disorders and stroke (NINDS), Americans spend approximately $50 billion each year for the low back pain while National health services indicated that one in three people in United Kingdom are suffering from the lower back pain problems [4]. As stated in Ahmadi et al., nearly 80% of people experience back pain in their life after the age of 30 [5]. Low back pain is a universally shared problem and its direct and indirect cost effect on industries is enormous. Many industries are now adopting safer lifting or manual material handling techniques due to the increasing risk of injuries and long term absence of workers. While lifting or handling material, squat lift and kyphotic lift is recommended as compared to stoop lift and lordotic lift. According to studies, many workers prefer stoop lift because it requires less energy and is easy to operate but also because in many cases squat lift is not possible due to the size of the load and lift set up [6].

Low back pain is also common problem in some athletes. Lundin et al. [7] have found that the severe low back pain rate is higher in wrestlers (54%) compare to soccer (37%) and tennis (32%) players. Back pain is the common reason for these players to miss the tournaments or loss of

playing time in sports. Hainline, [8] has reported that about 38% of professional tennis players have missed at least one tournament due to the low back pain.

Most of the times, low back pain problems are caused by the prolonged sitting, awkward posture of spine, heavy lifting, repetitive bending and twisting as well as sports injuries. In office work, workers are required to sustain a single posture for long periods of time. According to Sondergaard et al. [9] sitting is a dynamic task which causes the pressure on the lower back which results in increased stress and pain in lower back. Bazrgari et al. [6] states that the sudden unexpected loading conditions as well as larger applied forces can increase the risk factors of nervous system damage by increasing the muscle forces, trunk movements and spinal loads. Wang et al. [10] have shown that dynamic loading is a risk factor for low back pain and the associate risk is three times higher compared to awkward posture. All of these studies indicate that the instability in spine causes the low back pain but it is still not clear that which segment of the structure causes the low back pain [7].

Human spinal column is divided into five sections: cervical curvature, thoracic, curvature, lumbar curvature, sacrum and coccyx these consist of 33 bones in total. These bones are connected with ligaments and tendons to provide stable posture of the body with help of discs, joints and ligaments where muscles provide forces; discs provide cushion to the spinal column, vertebrae are responsible for stabilizing the skulls, joints provide locking system to vertebrae and ligaments provide resistance against excessive movements. [1]

1.2 Research Objective

The objective of this study was to examine the reaction forces, moments, muscles forces and pressure on lumbar discs, and resulting movements of lumbar spine during the various activities. To examine these variables a forward kinematics model of lumbar spine was created. The model uses anatomically accurate CAD models of spine to create a dynamic representation of the lumbar spine in response to various loading scenarios.

1.3 Thesis Organization

This thesis is organized in five chapters. Chapter one contains introduction. Chapter two includes literature review about the existing technologies for the measurement of lumbar spine forces, and moments as well as motions. Chapter three provides details on methodology; it explains in detail the lumbar components and also emphasises the main aspects of forward kinematics modeling using Simulink. Chapter four presents the results of the case studies; results for lumbar motion, compression and shear forces and moments of the lumbar spine. Chapter five discusses the results and compares them with literature and Chapter six concludes the thesis by highlighting the major findings of the forward kinematics modeling of the lumbar spine.

Chapter 2: Literature review

2.1 Introduction

Lumbar spine is a complex yet sensitive structure of the body. Due to this sensitivity the lower back, is prone to injuries under bad posture or heavy loadings. About 40% of people suffer from the back pain between the age of 25 to 74 [11].

The number of low back pain patients are increasing day by day which causes problems not only in work places but also affects the economy due to the long term leave of absence of injured workers. Low back injuries may be caused by the loss of stability of the spine. Prediction of the dynamic response of the spine in biomechanical analysis is important in different loading conditions [12], because musculoskeletal disorders in lower back are of major concern in both active and inactive occupations [13]. Both active and inactive works can increase the instability of spine in certain ways to some degrees leading to injuries and pain disorders of lower-back [14]. Instability in spine could be due to sudden perturbation [15], prolonged sitting [9, 16-17], whole body vibration [18, 19], awkward posture of spine [20, 21], heavy lifting [22, 23], unsupported sitting or standing [24, 25], repetitive bending [26], sports injuries as well as larger applied forces [27, 28].

Modeling of the spine using the computerized model is necessary because it can be used for assessing reaction forces and motions in lumbar spine. The data collected using physical test from human subjects varies from person to person due to the fact that not all persons have the same upper body weight. Another reason for using models is that sensors cannot easily be introduced into the spine of a human subject due to the risk of degeneration of the discs [29]. Modeling can help researchers understand the internal mechanisms of lumbar spine at extreme levels of load and motion where physical test is limited for ethical reasons.

This chapter will discuss the current modeling methodologies that are being used to evaluate the lumbar spine motion, forces and moments including in vivo – in vitro measurements, finite element modeling and rigid body modeling.

2.2 In vivo and In vitro experiments of the lumbar spine

The main purpose of 'in vivo' and 'in vitro' experiments is to provide a database of anthropometric measurements of alive human or subject. Previously published data can be validated and appropriate adjustments can be made using these measurements. Also, results produced by computerized model might be confirmed by comparing the measurements. Establishing an understanding of loading of the spine is greatly important but it is almost impossible to quantify the load in the spine because the force or pressure transducer cannot be transferred into a living human being for ethical reasons. Results produced by computerized model can only be validated through in vivo or in vitro measurements. Wilke cited human body as chain of rigid segments and gives great importance to anthropometric data [29]. In 1960s and 1970s the most important data were provided by Nachemson's using the direct in vivo measurements [30]. The dynamic measurements for different postures were presented as absolute values and unfortunately the anthropometric data were missing from the results. "Since then, very few data have corroborated those findings"[29]. Recently, intradiscal pressures were measured on the subject for various postures by Wilke et al. [29] which are describe below.

H. –J. Wilke et al. [29] have measured the intradiscal pressure on non- degenerated disc of a subject. After getting the approval from the state ethical review board of Germany the experimental study was performed on a 45 year old male with weight of 70 kg with no previous back pain history. Initially lumbar spine discs were evaluated for the non-degeneration or dehydration sign using the MRI-scan and based on the evaluation L4-L5 disc was chosen for the pressure measurement. The intradiscal pressure was measured for several activities such as standing, lifting, sitting, bending in a various posture after implanting the pressure transducer in to the subject. Results indicate that balancing of the spine and proper technique while lifting and trunk support while sitting can reduce the intradiscal pressure on the discs. The intradiscal pressure values: squat lift 1.7 MPa; stoop lift with round back 2.3 MPa; exercise fingertip- floor distance 1.6 MPa; crate of beer held close at chest level 1.0 MPa; crate of beer held away about 60 cm 1.8 MPa; walking with one crate 1.0 MPa; lifting two crates 2.1 MPa; walking with two crates 0.9 MPa; relaxed erect sitting 0.45 MPa; erect sitting bent forward 0.63 MPa; flexed forward with elbows on thigh 0.43 MPa; flexed actively forward 0.9 MPa. These results were in

good agreement in comparison with Nachemson's data except for standing, and sitting. The authors have claimed that this difference were due to the use of different transducer. [29]

Another in vivo measurement was carried out combined with finite element method by Bazrgari et al. [6] to estimate trunk muscle forces and internal spine loads for squat lift and stoop lift. The measurements were performed on healthy fifteen subjects with average height of 177 ± 7 cm and with weight of 74 ± 11 kg by attaching the light emitting diode (LED). These subjects were asked to perform sagittal symmetric squat and stoop lift with load of 180N and without load (0N) and with no instruction on lumbar posture. Average thorax and pelvis rotations were prescribed based on the in vivo measurement for four different cases which are shown in the Figure (2-1).

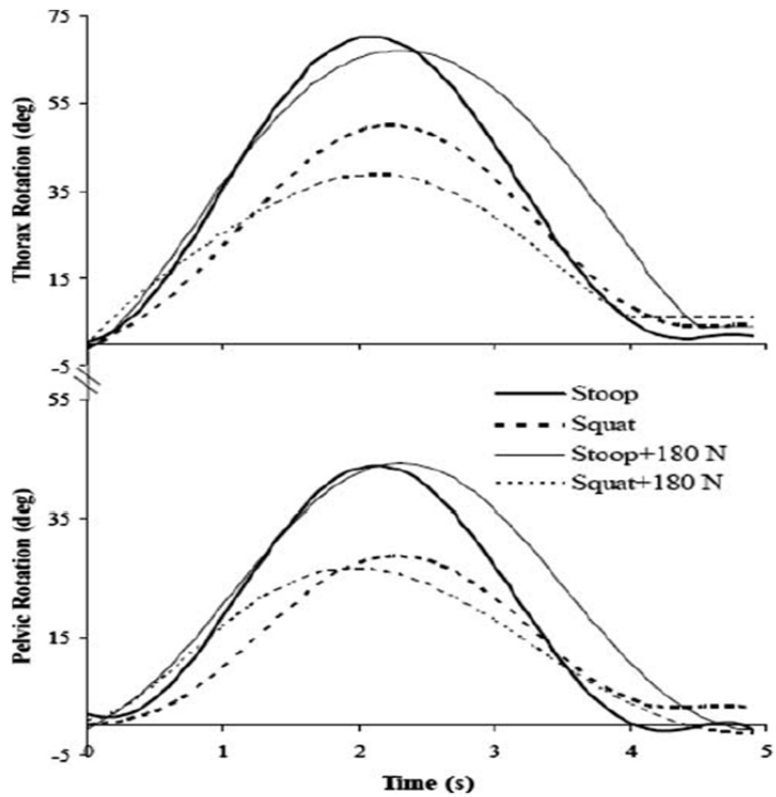

Figure 2-1: Thorax (top) and pelvis (bottom) rotations based on in vivo measurement [6]

Measured thorax and pelvis rotations were transferred in to the finite element model to predict the maximum net internal moments, compression forces, shear forces and lumbar muscle forces. The thorax and pelvis rotations have indicated that magnitude of load has no significant effect on these rotations whereas moment, shear, compression and muscle forces show significant difference. Also, the compression and shear forces were higher in stoop lift compared to squat

lift while lifting the load of 0N and 180N with difference reaching maximum of ~800N for compression and ~200N for shear forces. The maximum shear and compression forces and moments are shown in the Figure (2-2) for forces and moment curve on disc L5-S1.

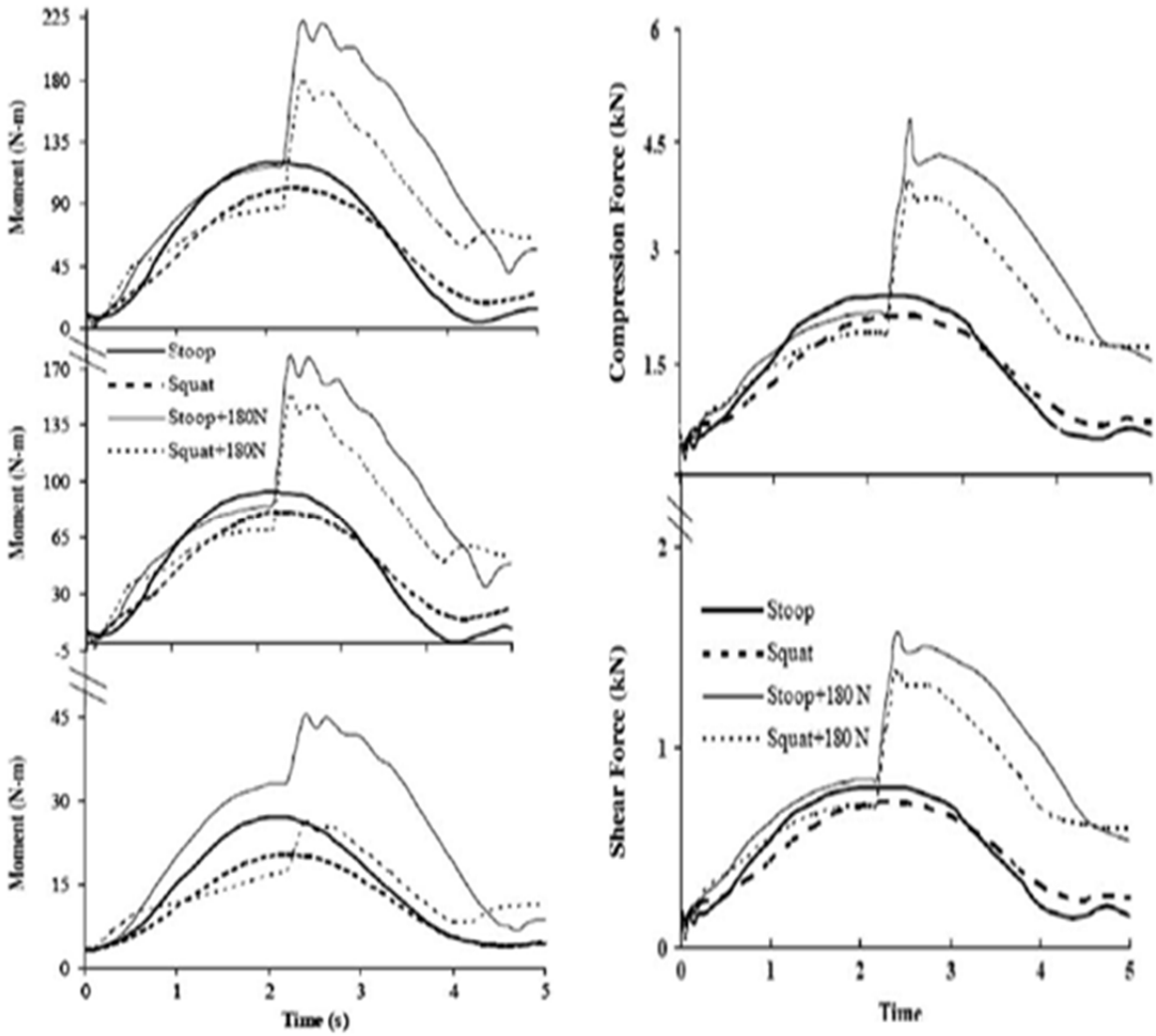

Figure 2-2: Predicted sagittal moment (N.m) at the L5-S1 level; net external moment (top left), moment resisted by muscle forces (left middle), passive ligamentous spine moment (bottom left); maximum shear and compression forces for L5-S1 level (bottom right and top right respectively [6]

A number of studies have indicated that maintaining same posture during sitting or driving can be a major risk factor for the development of the low-back pain [9, 31, 32]. Relationship between the musculoskeletal discomfort and low-back pains are reported in many articles and are used to serve the purpose of research study in current Simulink model; some of the articles are

summarized below to help understand the relationship between prolonged sitting and driving and low-back pain.

Authors, Sondergaard et al. [9] have investigated the relation between the centre of pressure displacement and variations in lumbar curvature in prolonged sitting postural moment by means of nonlinear and linear analysis. Corlett, 2006 and Pope et al. [31, 32] have suggested that "the prolonged sitting could be the risk factor for development of the low back-pain." This study revealed the important aspects between discomfort and back pain as discomfort is related to the sitting postural change and sustaining same posture for long period of time. Considering the fact that sitting is a dynamic task, data were collected for the discomfort ratings (between 0 to 5 where 0 represented no discomfort and 5 represented worst), kinetics and kinematics for prolonged sitting postures. Using the collected data, discomfort index for the body parts, anterior-posterior displacement, medial-lateral directions, and lumbar curvature were calculated. From the displacements of the center pressure and lumbar curvature the mean, standard deviation as well as entropy values were extracted which were later used to assess the variability and complexity of the sitting posture. These results were evaluated in terms of discomfort to understand the correlation between discomfort and sitting position. The standard deviation of displacement was positively correlated and entropies were negatively correlated with direction and lumbar curvature while mean had no correlation. The study concluded that increasing the degree of variability and reduction in complexity is interrelated with the discomfort in the sitting posture.

Geffen et al. [13] have analyzed that the limited settings in static sitting have been associated with lower back pain in inactive occupations. Inactive occupations such as office work and vehicle driving are the worldwide concerns for the lower back pain due to the awkward posture of body (spine). To prevent lumbar discomfort for the long term static sitting authors have developed passive motion technique to adjust the pelvis orientation independent from the trunk. To study the effect of the lower back loads, computer-aided simulator chair with the adjustable pelvis posture were used in the experiments on eighteen healthy males. In these experiments the body segments orientation, seat reaction forces and interface back pressure distribution were measured. Seat reaction forces were taken for the sagittal and frontal plane during the quasi-static actuated pelvis rotation. The pelvis rotations in sagittal and frontal directions were 19±3

degrees and 9±3 degrees, respectively. The strong relations for the sagittal in upward direction and frontal in lateral direction were found with the centre of back pressure. These results have shown that decoupled pelvis adjustment could be useful intervention to control the loads in lumbar region for prolonged static sitting. Applying this technique can control the periodic lumbar motion by improving the tolerance for the prolonged static sitting. [13]

Indeed, in vivo – in vitro measurements are more preferable for lumbar spine analysis because most of the dynamic models cannot comprise complex geometry of the spine and required validation for specific cases. However, dynamic models are used by many researches to understand the mechanical behaviour of the spine because it is almost impossible to quantify the load in the spine due to the fact that the force or pressure transducer cannot be transferred into a living human being for ethical reasons.

2.3 Lumbar Spine Models

Most of the lumbar spine modeling efforts reported in the literature is done using finite element method (FEM) or rigid body dynamics with aid of electromyography, MRI scan or CT scan. The early models are designed based on mathematical equations. The models reviewed so far, whether FE based or rigid body based, use inverse kinematics approach to investigate static and dynamic motion responses as well as internal forces. Inverse kinematics is a technique in which the desired position and orientation is assumed to be known or is planned. Using the kinematics relationship, internal forces required for achieving certain sets of positions and orientations are calculated. Because of redundancy problem while acquiring the desired position and orientation using inverse kinematics, one could have multiple results or no results. The redundancy is caused by the fact that there are not enough equilibrium equations available to determine all the muscle forces [33]. In the case of multiple plausible results, optimization is typically used to pick a best set of answers.

While using the inverse kinematics technique in lumbar spine to find the motion responses and internal pressures or loads of the body, many researchers have encountered problems with final outputs of such models since optimality criteria are somewhat arbitrary. Another drawback of this technique is that it is not suitable for very high or very low loadings [34]. Studies have

shown that inverse kinematics technique is also not reliable for intervertebral translation because the input geometric data were dependent of other softwares and intervertebral translations were very sensitive to small changes in input data [35].

These methods are either interdependent or have their own limitations because of the mechanical complexity of the spine which makes it rather difficult to compare and analyse the results of the techniques [36] as well as these techniques do not provide good agreement in higher motion or higher loadings.

2.4 Finite Element analysis of the lumbar spine model

Finite element method has been used in modeling of lumbar spine by a number of researchers. It is a commonly used technique to scrutinize the biomechanical behaviour of lumbar spine. Most of the finite element models were designed using rigid body and deformable beam elements with non-linear properties to investigate spinal stability, muscle forces and axial loadings [37]. This method also allows investigating of the influence of different levels of discs degeneration. FE models are simplified and designed to overcome the mechanical complexity of the spine. The geometry of the spine is designed or transferred from CT-scan or MRI images. This method depends on other techniques for kinematics input data to complete the simulations. These kinematics data are obtained using the optimization method; electromyography (EMG) assisted model, cost functions, or other technique. Most of the FE models have shown good agreement in comparison with “in vivo” and “in vitro” measurements for intersegmental rotation and intradiscal pressure [38, 39].

The first analytical model of the human spine was developed using spring mass model by Latham [40] to analyse the dynamic response of the pilot seat ejection under short duration of acceleration impact [40]. In 1960’s and 1970’s more complex models of human spine were developed using springs and dampers to represent vertebrae and intervertebral discs [41, 42]. More degrees of freedom were further added in the model to analyze the internal forces and bending effects [41, 42].

Pankoke, et al. [18] developed a 2-D dynamic Finite element model of sitting man to evaluate internal forces in the lumbar spine during the whole body vibration. Long term whole body vibration (WBV) can cause enormous health hazards for the lower lumbar spine (L3-L5) and to protect from the WBV, one needs to know the compression and shear forces (internal forces) of the discs. These internal forces cannot be evaluate experimentally or by physical test as force transducers cannot be introduced into living human beings because of the ethical reasons. The 2-D dynamic FE model is shown in the Figure (2-3). The model can calculate the internal forces in the spine by transferring the parameters for body height and body mass for three different postures such as straight, bent forward and relaxed.

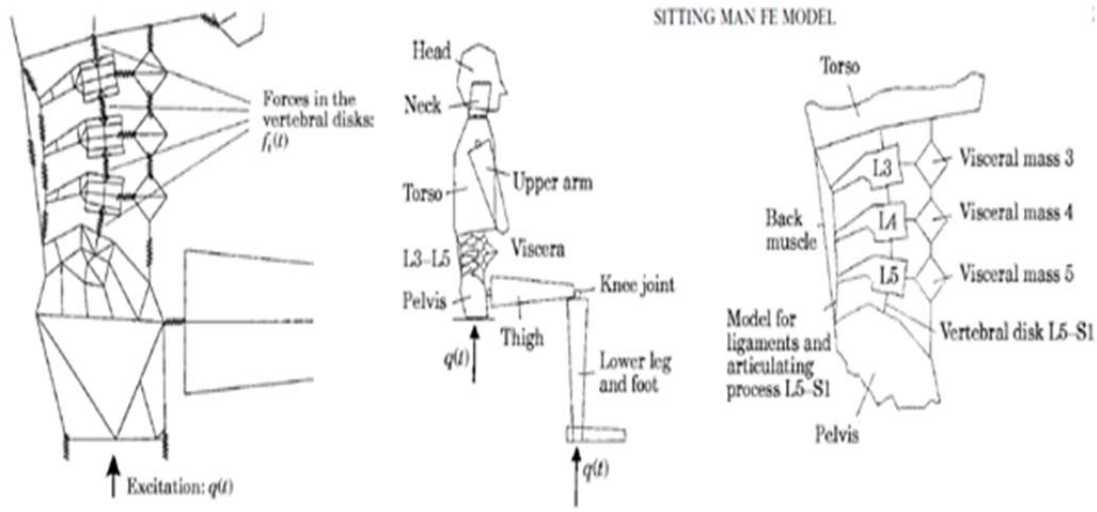

Figure 2-3: The complete model of sitting man (middle), regio lumbalis (right) and detailed lumbar model (left) [18]

Static forces were measured to be 218 N, 605 N, and 317 N, respectively while the moments were measured out to be 9 Nm, 45 Nm and 10 Nm, respectively. Later, these measurements were compared with in-vitro measurements where all results were found to be in good agreement except the data measured with higher frequency.

Similar FE models were developed by Ezquerro et al. [37] to analyze the biomechanical response of the lumbar spine in daily human activities. Initially the muscle and joint forces were predicted using an optimization algorithm and imported in the FE model. The model allows three dimensional measurements under 3D rotation between the pelvis and thorax. It also includes moment transmitted between T12 to L1 in the force predicting algorithm. Using the above

boundary condition two cases were tested for walking: considering the moment existed between T12-L1 and no moment existed between T1-L1. The results showed 21% lower compression force and 38% lower anterior shear force when the moment was consider between T12-L1. It also resulted in reduced intradiscal pressure from 0.76MPa to 0.62 MPa which was in very good agreement with results found by Wilke's group for walking activity [29, 37].

Little et al. [39] used FE modeling to show that the three-dimensional rotations in the loaded spine are due to the passive spinal anatomy alone and not because of the discs, ligaments and facet joints. A 3D osseoligamentous finite element model was generated by using the computed tomography data for the bony anatomy of the visible man lumbar spine. The external outline was interpolated for the intervertebral discs between the profiles of the endplates while the internal annulus boundary was assumed based on the external outline and center point. The ligaments were added in the middle of the each intervertebral joint. The model prediction for the loading conditions of intra-discal pressure and primary rotations was compared with the in vivo data to validate the model. The results of the coupled rotations for the flexion, axial and extension rotations showed very good agreement with in vivo results. However, the analysis of the lateral bending and couple axial rotation showed higher value compared to the in vivo results. The discrepancy in these results was due to the primary motions in the transverse and sagittal planes caused by the passive spinal anatomy. It was also indicated by the results that muscles play a vital role in the coupled response of the spine under rotational motion.

Goto et al. [43] estimated the mechanical response of the outer annulus fibrousus using three dimensional finite element model of the L4-L5 vertebrae. Using the computed tomography (CT-scan) image 4th and 5th vertebrae, intervertebral discs, and ligaments were created and compressive force of 294N in the vertical direction and flexion; and extension load of 15 N-m were applied. Results indicated that the von Mises stress was increased on the vertebral endplates, surface of the facet joints, posterior portion of the vertebral disc, and in the anterior portion of the vertebral disc. The von Mises stress was also analyzed by Wang et al. [10] for L2-L3 motion segment using finite element model. The authors have indicated that for fast loading rates, the von Mises stress at the anterior region of the outer lamellae and posterior region of the inner lamellae increases markedly.

‘M. El-Rich and A. Shirazi-Adl’ [44] expanded the non-linear finite element model developed earlier [45] to investigate the “effect of load position on muscle forces, internal loads, and spinal stability of human lumbar spine in upright posture” [44]. Using a kinematics-based approach to solve the redundancy, upright standing postures were analyzed under external loads of 195 and 380N for kyphotic posture and lordotic posture. When the loads of 195N in hands was held away from the body and close to the body, the lordotic posture showed substantial increase in moment, internal loads and muscle forces compared to kyphotic posture. The lumbar curvature for kyphotic posture remained almost the same even with load of up to 380 N. The intradiscal pressures were found to be in good agreement with in vivo measurement for load of 195N away from the body and close to the body with difference of 9% and 11%, respectively [29]. The model, however, was limited to produce motion response in sagittal plane; also any changes in muscle stiffness would influence the results.

Arjmand et al., [46] used the kinematics-based approach along with the nonlinear finite element model to study the intra-abdominal pressure (IAP) for various postures at various unloading conditions. They investigated the trunk muscle forces, spinal loads and lifting stability for various activities. The results showed that unloading action of IAP becomes more effective in forward-lifting task and the role of stabilizing disappears.

Arjmand et al. [47] used two different methods for estimating spinal loads and muscle forces; electromyography-driven (EMG) and Kinematics-driven for symmetric and asymmetric activities. The estimations of trunk muscle forces and internal loads were carried out by the balance of the external and internal moments at one particular point. The external moment was due to the lifted weight and the internal moment was the result of the trunk muscles and the passive ligamentous spine. To examine these effects electromyography (EMG) was used for single joint and Kinematics was used for multi joint models. The effect was measured for lifted weight at various heights and for the trunk flexion from neutral upright to maximum forward flexion. These two different approaches in measurements have shown differences in results of approximately 44% for trunk muscle forces and about 43% in spinal shear loads [34].

The results for symmetric flexion showed that the EMGAO model predicted less activities compared to KD model as well as the differences of the peak flexion decreases as the back muscles’ activity disappeared [34].

Bazrgari et al. [15] developed model for examination of the sudden unexpected loading conditions such as slipping, tripping, in sport activities and collision using the kinematics-driven approach. Trunk muscle forces (agonist and antagonist), internal loads, and stability were evaluated after and before releasing the sudden posterior loads. Trunk/pelvic rotation and external loads were solved using the nonlinear transient equation of motion in the finite element model. The cost function of minimum sum of quadratic muscle forces, equality equations on abdominal muscle forces and inequality equations on unknown muscle forces were calculated until the convergence was reached. Later these data were compared with the EMG activities and disc pressure measurements which indicated that muscle forces before and after release were well in the range and trunk responses were found to be very stable in both pre and post release periods. These results showed that the higher applied loads significantly increase the muscle forces, the trunk kinematics response as well as spinal loads.

Finite element models were also used to analyze degenerative disc and the influence of the disc on the mechanical behaviour of lumbar motion segment. Intervertebral discs provide flexibility as well as transmit and distribute loads of spine via gelatinous nucleus pulposus and annulus fibrosus [38]. In the degenerated discs the water content and the fibres in the nucleus pulposus are reduced which ultimately reduces the stiffness leading to a lower intradiscal pressure compared to healthy discs [48]. The disc degeneration is a biologic change associated with back pain and spinal disorders [49]; so to examine these changes and understanding the influence of the degenerated discs is greatly important.

Zhang and Teo [49], investigated the application of implants for treatment of lower back pain using the finite element model. In this study, the spinal implants, spinal motion segments, and single or multi-dimensional rotations were examined under normal healthy conditions. The healthy model was modified by removing certain parts and replacing it with implants. The effect of the implant was recorded and compared with the healthy model under various physiological loadings such as compression, flexion, extension, lateral bending, and axial rotation. The study results indicated that the pure moments are evenly distributed with minimum error when only one motion segment is modeled whereas in multi segment model, the values for the pure moments decreased. The model was not suitable for understanding of the effect of implants, especially when the disc replacement and dynamic stabilization devices were used. The same

results were achieved in the works of Goel et al. [50] and protocol proposed by Panjabi (2002) [49]. These results also indicated that loads did not change under load control protocol at the adjacent segments while the multi-segments values were decreased. The authors have concluded that compression loads are follower loads which are perpendicular to the surface and lordotic curvature of the spinal column simulating the body weight and muscle force.

Rohlmann et al. [38] studied different grades of discs degeneration by sue of simulation. Three dimensional nonlinear- finite element model of the functional spine segment of L3/L4 was created. Intersegmental rotations, intradiscal pressures, forces on joints and ligaments and maximum von Mises stress in the annulus for healthy disc, mildly, moderately and severely degenerated discs were calculated. The intersegmental rotation was higher in mildly degenerated disc in the loading plane for all cases. The intradiscal pressure was higher in healthy disc in the loading plane for all cases whereas the other degenerated discs showed very low intradiscal pressure for flexion and axial rotation and negative intradiscal pressure for extension and lateral bending. The findings indicated a difference of less than four degrees in loading directions such as flexion, extension, lateral bending and axial rotation compared to the in vitro study of Mimura [38].

A lumbar spine model was developed by Shine et al. [51] using the finite element method to study the stiffness of a dynamic stabilization device. Three spines were analyzed to investigate the effect of dynamic stabilization for spinal segment L2-L5. First, an intact model was created from the computed tomography (CT) images and was used as reference. The intact model was then modified by replacing the disc and endplates by bone graft; and ligaments by pedicle screws and flexible rigid rods to create the fused model. A dynamic stabilized model was created by further modifying the fused model by replacing the flexible rigid rods with spring elements with a stiffness value of 30 N/mm. The results for all three cases were compared with the in vivo measurements obtained by Yamamoto et al. [52] for flexion, extension and lateral bending. The results are shown in the Table (2-1).

Table 2-1: Comparison between kinematics data of present FE model and in vivo experimental study [52] for determination of three-dimensional angular motion [51]

	Flexion		Extension		Lateral bending	
	Shine et al.	Yamamoto et al.	Shine et al.	Yamamoto et al.	Shine et al.	Yamamoto et al.
L2-L3	6.3	6.5 (0.3)	4.1	4.3 (0.3)	6.4	7.0 (0.6)
L3-L4	7.2	7.5 (0.8)	4.0	3.7 (0.3)	6.3	5.8 (0.5)
L4-L5	8.5	8.9 (0.7)	6.0	5.8 (0.4)	6.4	5.9 (0.5)

These indicated that the range of motion and the disc pressures were similar for both intact and dynamically stabilized spine whereas fused spine has higher pressure on L3-L4 segment. It is also suggested by the author that stiffness is an important parameter in dynamic stabilized spine.

In conclusion, FEM has shown promise in some cases but it is not recommended for very high loadings and for higher levels of motion by many researchers. Experimental studies have shown that asymmetric geometry of the spine in FE model produces asymmetric forces for right and left facet joint which makes spine unstable and restricts it from bearing larger axial compressive loads [53, 54]. According to [55], this asymmetric behaviour is due to the limitations of FE model. Also, the muscles, which play a vital role in stabilizing the spine, were excluded from most of the FEM models for the purpose of simplifying the analysis of higher loadings and flexed postures [36, 50, 56]. In general simplifications of FE model and assumptions while creating model could diminish the accuracy of results. The dependence of the FEM model to obtain the kinematics data from other models limits the degree of accuracy of the results on the input data. Thus, using FE based dynamic modeling for measuring reaction forces, motion responses and other parameters of lumbar spine can be difficult [36].

2.5 Rigid body modeling of human lumbar spine

Rigid body modeling of lumbar spine has been used to analyze the static and dynamic motion responses and internal forces using the inverse dynamic techniques under various loading conditions. These models consider vertebrae as rigid parts in order to calculate the motion and

accompanying force for each segment of the lumbar spine and use massless springs and dampers to simulate realistic effects of discs, joints and ligaments.

Fritz [57] developed an improved biomechanical model to simulate the strain of the hand arm system under vibrational stress. The model consisted of four body components: (two) hands, forearm and upper arm as mass elements which were connected using springs and dampers. This model was further modified [58, 59] with addition of more components such as trunk, head, and neck to examine the influence of vibration stress on the human body [57-59].

The same model was further expanded [19] to analyze the response of a standing operator under vibration stress using the rigid body biomechanical model. The model consisted of 27 rigid bodies including major components such as head, thorax, lumbar spine, legs and arms as well as all other components connected by 'hinges' [19] to rotate or to translate around their neighbouring components as shown in the Figure (2-4).

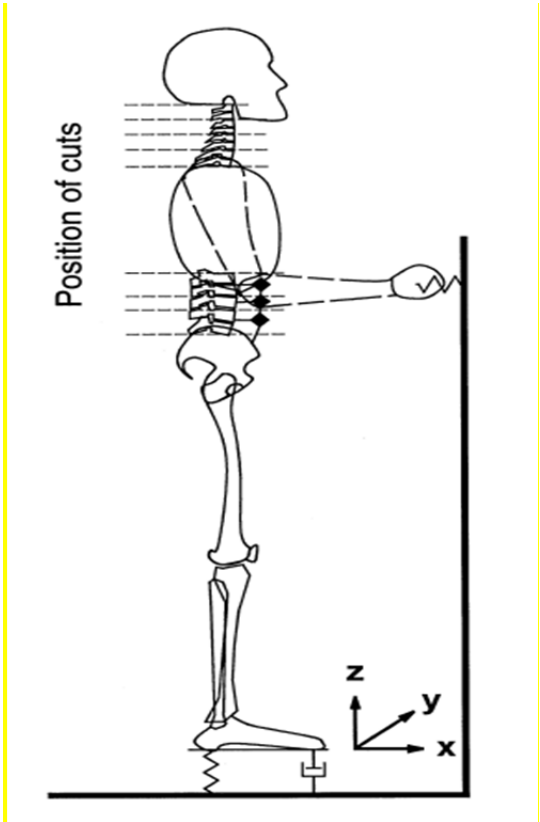

Figure 2-4: Schematic of the skeleton of the human trunk, neck, head, and legs and of the arms and the viscera (♦) in the standing posture [19]

The model was validated with the literature for the transmission of vertical seat vibration to vertical head motion, vertical ground vibration to vertical head motion and transfer function between the vertical ground vibration and compressive forces [19]. The result showed no difference between the standing and sitting posture and also showed a small difference for compressive force for lumbar spine under same vibration stress. The compressive forces on the lumbar spine were lower than the ankles, knees or hips, which is obvious since the trunk is supported by the legs and all the body weight is carried by the ankles. Thus, standing operator transmits the compression forces from leg to the head under vibration which are hardly measured because it is considered as a minor risk factor for the lumbar spine [19].

The work by Lengsfeld et al. [16] suggests that the lordotic posture of the human lumbar spine should be maintained while sitting on the chair or during any settings requiring prolonged sitting. The analysis was done using the two (mechanism of two office chairs) office chairs on sagittal curvature of the lumbar spine. The effect on the sagittal curvature of the human lumbar spine was determined by checking the three criteria such as the problem caused by the seat tilt, backrest or the direction of the synchronized mechanism of the back and seat tilt. The experiments were carried out on the sitting posture of 19 healthy adults using the adjustable seat and back lockable in either position of an office chair with and without pillow support on lumbar. The size variations of the human body were linearly scaled down by ±5% of the original size and procedure was repeated several times to collect the data. The tests were conducted on the stronger lumbar support and minor lumbar support by decreasing the backrest heights (from 95 mm to 30 mm, -45 mm and -60 mm) and segmental angles for L1/L2 to L4/L5 were measured. Figure 2-5 displays the human lumbar spine position of anterolateral (left) and posterolateral (right) view with mark (A), the upright position (left) and the maximum backrest recline position of 19˚ (right) with the mark (B) while mark (C) indicates the same position as B with 21˚ (right). The results indicated that the ergonomically designed office chair completely eliminate the lumbar lordosis problems by reducing the backrest height; so the sagittal curvature of the human lumbar spine is affected by the seat tilt, the backrest recline in stronger lumbar support and backrest height in lesser lumbar support.

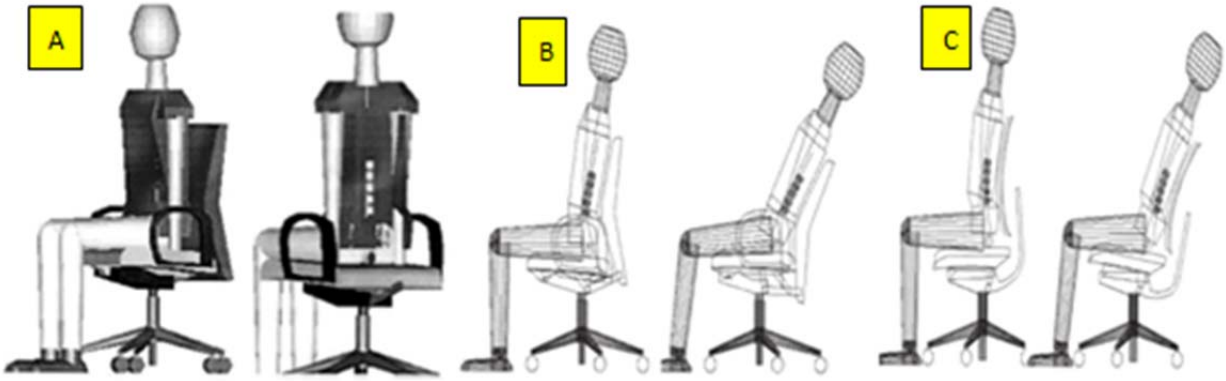

Figure 2-5: Graphical display of the office chair (A), wire-frame model of the office chair (B), wire-frame model of the entrada office chair (C) multibody interfacing the human multibody postures [16]

Another rigid body model was developed by Keller and Colloca [60] to analyze the kinematic responses of the lumbar spine by applying the static and dynamic Posteroanterior (PA) forces. To predict the motion response of the lumbar spine, a five Degrees of freedom model was designed with six flexible joints' structure as shown in the Figure (2-6). The masses of the vertebrae and surrounding tissues were considered in the model while thorax and pelvis were assumed to be immobile. Using the 2D model, PA forces such as low frequency, high velocity, very rapid impulsive thrusts and low-amplitude were applied to the spine for mobility assessment along with certain spinal mobilization and manipulation treatments. The forces were calculated using the equation of motion for three different cases: underdamped, overdamped, and critically damped. The governing equation of motion represented the inertial, dissipative and restoring forces as well as the external forces. [60]

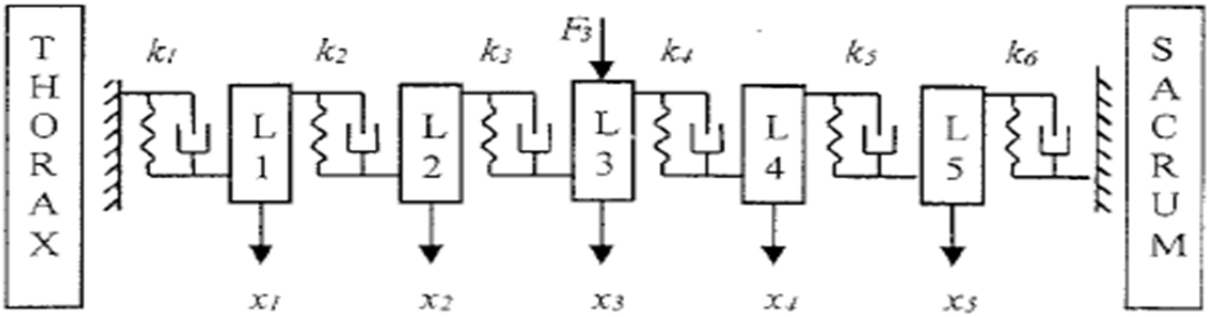

Figure 2-6: Five-DOF model of the lumbar spine with massless spring and damper [12]

Using the model, damping ratio of 0.15, spring stiffness coefficient of 50 kN/m and static force of 100N were applied to the segmental L3 and intersegmental L3-L4. The results for static and dynamic motion responses were measured for all five vertebrae. These results showed that as the stiffness coefficient increases, the damping resonant frequency increases and the displacement decreases. It was also noticed that impulsive forces produce very low segmental displacement. Furthermore, these results were compared with the reference values obtained from literature [5] which illustrated that the results are off by more than 50% for the low-force or quasi-static loading situations. This problem can be resolved by adding more DOF to the model and considering the impact of thorax and pelvis so that the prediction of transverse, axial and rotational displacements is possible [60].

The same model was expanded from 2-dimensional model to 3-dimensional model by Kassem and Sameh [61] to simulate the three dimensional motion responses as well as more degrees of freedom were added. Initially, the test was performed to estimate the sagittal-plane motion using the posterior anterior data provided by Keller et al. [12]. After seeing the capability of estimating the sagittal plane motion, the model was compared for angular stiffness and damping with data from the literature [62] and compared for force displacement curve measured by Ralph et al. [63]. The comparison for all cases showed good agreement with literature but authors have suggested that the model is limited to examine only general linear, static and dynamic mechanical responses. Another drawback is that it does not take into account the complex geometry of spine as well as the larger deformation may not be achieved.

Zee et al. [36] developed “a detailed rigid-body spine model”, to investigate the internal forces using rigid body modeling techniques. The generic lumbar spine model as shown in the Figure (2-7) below was designed with seven rigid segments with 18 DOF (degree of freedom) and 154 muscles. The main purpose of this study was to predict the muscle forces, joint reaction forces and to predict the parameters or dimensions which are very hard to measure using the other techniques.

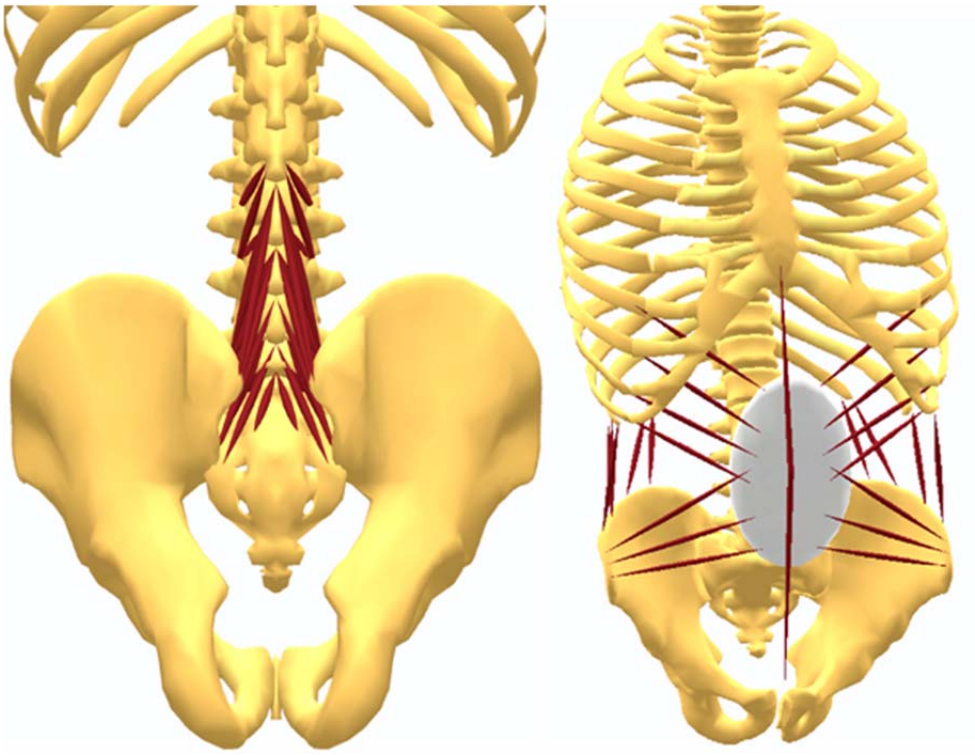

Figure 2-7: Insertion and origin of the fascicles of the multifidus in the model (right) and abdominal muscles (left) [36]

While solving for the forces, the detailed anatomy of the lumbar spine (muscles morphology) was used in the model including the three methods for simulating muscles' path. These were straight line between insertion and origin, via-points passing through segments and nonlinear wrapping muscles. In the latter path, the muscles are wrapped around their pre-defined surfaces such as cylinders and spheres.

The maximum moment of 238 Nm, shear forces of 639 N and axial forces of 4520 N were calculated at L5/S1 while maintaining the equilibrium at all levels. These results have shown that no other muscles can generate same amount of forces at lower or higher activity of the recruitment strategy. However, this work was based on many assumptions such as zero rotational inertia, muscles assumed to be recruited in an optimal way and intra-abdominal pressure was not considered (IAP). According to Daggfeldt and Thorstensson, [64] and Hodges et al. [65] IAP does contribute in back-extensor moment so the results that were found for the axial forces may not be as accurate.

2.6 Direct Vs inverse modeling of lumbar spine

Till now forward kinematics approach has not been used to determine internal forces and motion responses in lumbar spine due to the complexity of the spine [36]. Most of the lumbar spine models have been developed using the inverse kinematics approach to investigate static and dynamic motion responses as well as internal forces.

Inverse kinematics is a technique in which the desired position and orientation are given to find the set of joint angles to achieve the desired result. While acquiring the desired position and orientation, based on the number of assumptions, multiple or no results are possible. In case of multiple results, the closest result would be taken as the final result or it can be further solved using optimization, algebraic or geometric methods. While using the inverse kinematics technique many researchers have encountered problems with the final outputs. Rasmussen et al., [33] stated that for the inverse kinematics technique, there are not enough equilibrium equations available to determine all the muscle forces. According to Arjmand et al. [34] this technique is not suitable for very high loadings as well as very low loadings and is also not reliable for intervertebral translation [35].

In forward kinematics, a set of joint angles are given to find the desired position. The model is very similar to what happens in spine; a high level command, for example: pick a load, is processed through a series of controllers which activate the muscles to the appropriate level for performing the task. This eliminates the need for any assumptions and a unique solution is obtained. Forward kinematics based model also eliminates the requirements of other software for the kinematics data.

The thesis focuses on muscles forces, pressure on the intervertebral discs as well as motion response of the lumbar spine. The feasibility of this approach is demonstrated by comparison of results with data from literature.

Chapter 3: Methodology

3.1 Introduction

Human lumbar spine is a complex structure and designing a standard lumbar spine model is very difficult as well as time consuming. Although the main focus in this thesis is on lumbar spine, upper and lower body segments are also considered. To accomplish this, a 3D scanned model of the lumbar spine of a male with approximate height of 177 cm was obtained (Zygote Media Group, Inc., American Fork, USA). All other components of the human skeleton were obtained from online solid modeling libraries (Zygote Media Group, Inc., American Fork, USA), rescaled and assembled to make one whole human skeleton. The model consists of 17 rigid body segments including five vertebrae, pelvis, thighs, legs, feet, upper arm, forearm, and thorax with neck as one segment. Many experimental studies have been carried out where lumbar vertebrae were presented as rigid bodies [61, 66] while some studies have also presented pelvis and thorax as rigid body elements [33, 36]. The intervertebral discs, ligaments and joint are represented as non-linear springs and dampers with each disc representing of a six degrees of freedom (30 DOF in total).

This chapter describes the methodology to construct the 3D model of the human lumbar spine including the modeling of lumbar vertebrae, intervertebral discs, ligaments and joints, muscles attachments. After constructing the model, it was used to study the spine response for various activities such as standing straight, holding and lifting weights, squatting as well as stooping.

3.2 Structure of Human Spine

Spinal column is divided in to five sections, [1]

1. Cervical curvature
2. Thoracic curvature
3. Lumbar curvature
4. Sacrum and,
5. Coccyx

These five sections of vertebral column consist of a total of 33 bones which function to provide human body with flexibility and various postures. [1]

Lumbar curvature consists of five lumbar vertebrae and it bears the most body weight. It also allows the maximum flexion (to reach toes) and lateral flexion (sideways) with little rotation [1]. Five vertebrae are subjected to greater vertical compression forces than others and play their vital roles in human anatomy: L1 and L2 are where spinal cord ends; L3 and L4 are where lumbar puncture is performed in between and L5 joins the sacrum. [1]

Sacrum is the tail end of the spinal column which helps to protect pelvic organs (uterus/bladder) as well as supports body weight [1].

In this thesis, the focus is only on lumbar curvature and muscles that are connected to lumbar spine. However, the model does consider the internal and external forces and moments that act on the lumbar spine due to other factors. The muscles' structures and their details are briefly explained in the next section.

3.3 Lumbar Muscles

This section provides detailed explanations of the skeletal muscles that contribute to the movements of the lumbar spine by exerting forces. Skeletal muscles are the tissues in human movement; especially the ones that surround the lumbar vertebral column which are connected to spine in three different manners: straight line, via-points and wrapped around the surfaces. In the first form, muscles are connected in a straight line between insertion and origin. In second form, the muscles are rigidly fixed to the segments in which muscles pass through the segments. In the third form, the muscles are nonlinearly wrapped around their predefined surfaces such as cylindrical or spheres. This latter form is very complicated to model among all three muscle paths [36].

The muscles of the lumbar spine are divided in three different groups: intertransverse muscles (consisting of small muscles), the anterolateral muscles and the posterior muscles [48]; all three groups are explained in detailed below.

3.3.1 Intertransverse Muscles

Several different sized intersegmental muscles are attached to the transverse processes of the human lumbar vertebrae as shown in the Figure (3-1). The intertransversarii medial (ITM) and intertransversarii laterales dorsales (ITLD) are tiny slips, both of which pass from an accessory process (AP) to the mamillary process (MP) and transverse process from below, respectively, whereas the intertransversarii lateral ventrales (ITLV) pass from lower edge of the transverse process to the superior edge of the transverse process. These muscles are not responsible for the moment of the lumbar vertebrae but they do play important role in proprioception because they are densely endowed with muscle spindles [48].

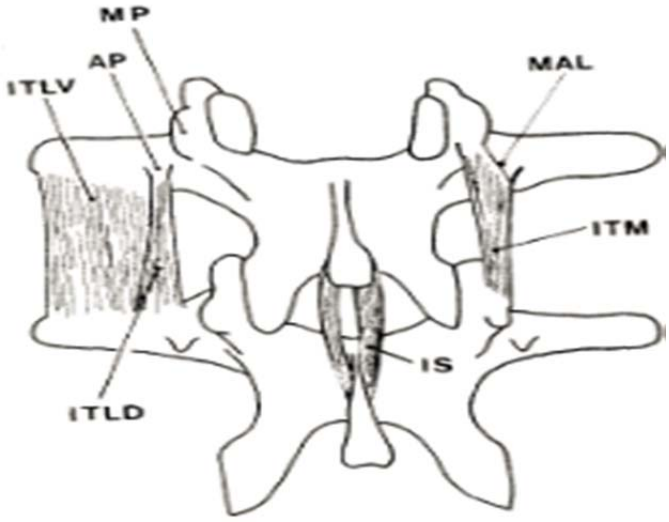

Figure 3-1: The intersegmental muscles [48]

3.3.2 Anterolateral Muscles

Anterolateral muscles consist of two types, Psoas major and Quadratus lumborum, which cover the lumbar vertebral column with anterior attachment to the transverse process and lateral attachment to the vertebral bodies. First muscles originate from the lumbar vertebral column to act on the hip without any primary action on the lumbar, whereas, the second muscles send fibres to the lumbar spine [48].

3.3.2.1 Psoas major

This muscle covers the lateral part of the lumbar vertebral bodies as shown in the Figure (3-2) and proximal quarter of the anterior part of the transverse processes. Psoas major fibres start from transverse process, intervertebral disc and the superior and inferior margins to the vertebrae adjacent to each disc. The psoas muscle can exert very large amount of forces on the lumbar disc in the action of sit ups and when it flexes the hip but it has no action on the lumbar spine [48].

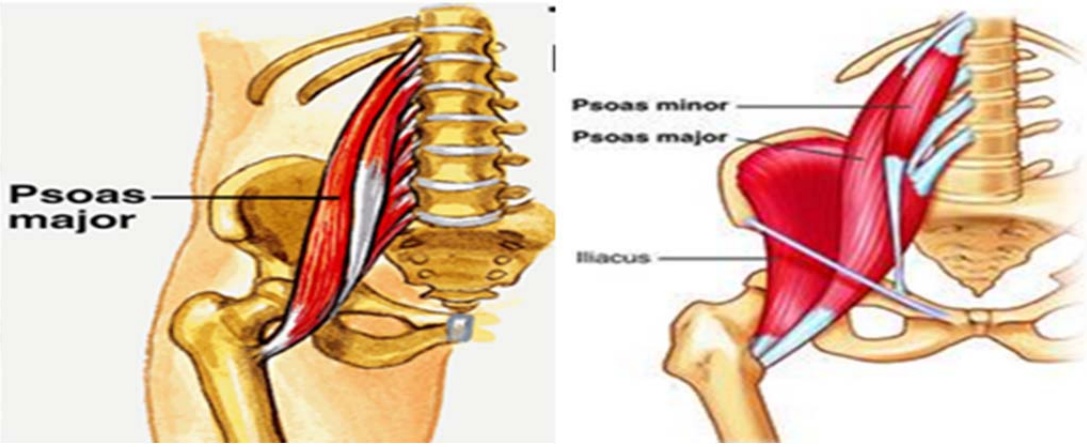

Figure 3-2: Psoas major [67, 68]

3.3.2.2 Quadratus lumborum

Quadratus lumborum muscle fibres originate from ilium and iliolumbar ligament and insert into the twelfth rib. This muscle covers the anterior surface of the transverse process by passing through the upper four lumbar vertebrae and extends beyond the tip of the transverse process. Fibres of this muscle provide steady base to the lower thoracic see Figure (3-3) [48].

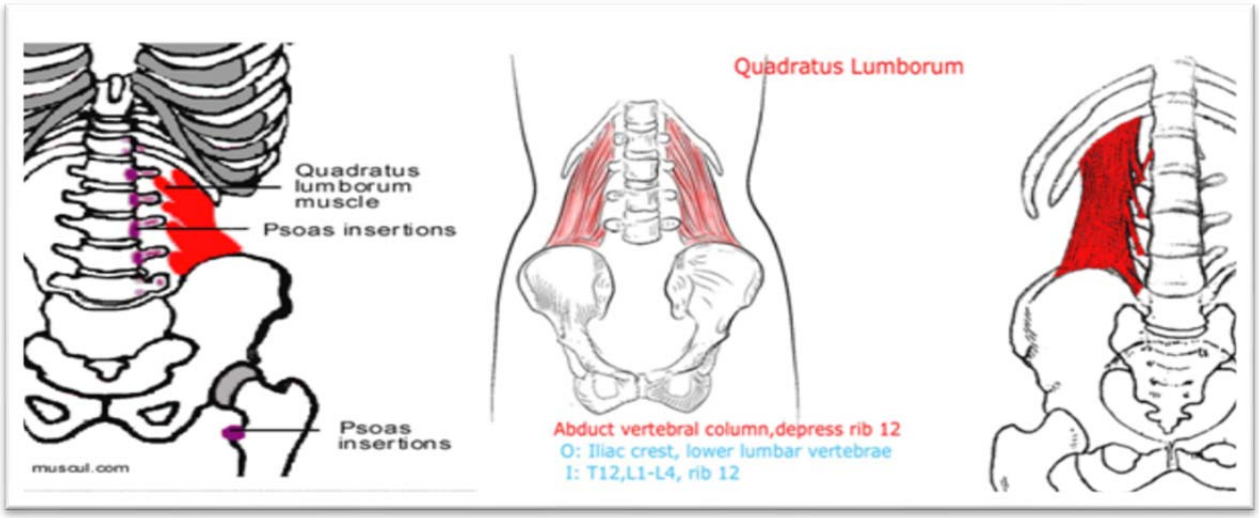

Figure 3-3: Quadratus Lumborum [69, 70, 71]

3.3.3 Posterior Back Muscles

3.3.3.1 Multifidus (MF)

Multifidus is a thin and deep muscle located parallel to the back of the spine very close to the lumbar vertebrae. Multifidus is responsible for smooth moment of the spine because it extends and rotates the vertebrae and stabilize the low back moment see Figure (3-4) [1].

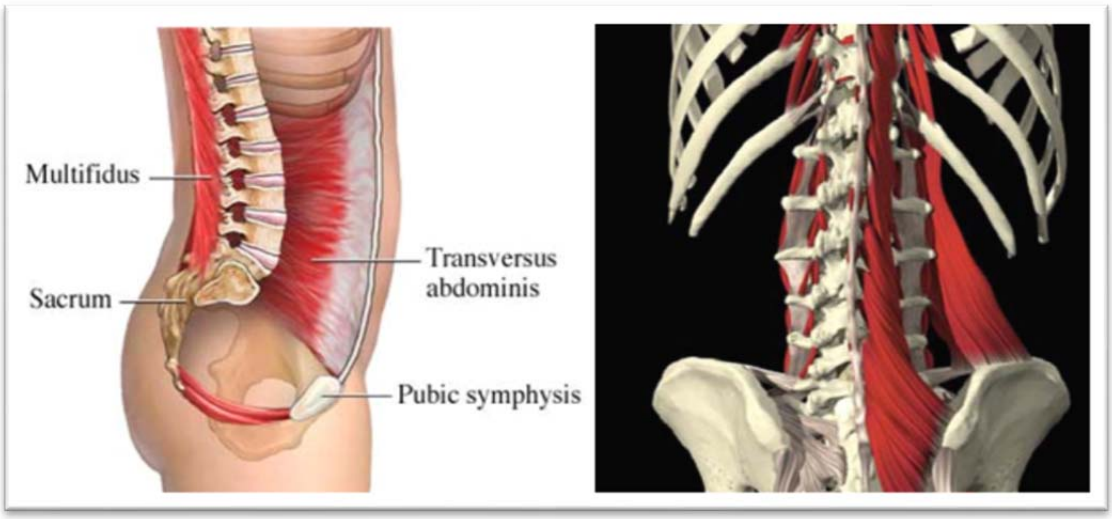

Figure 3-4: Multifidus [72, 73]

3.3.3.2 Longissimus thoracis pars lumborum

This muscle lies besides the multifidus and it is a relatively slender muscle. Its fibres arise from the tips of L1 to L4 like a branch and merge back to become a common tendon of the lumbar inter-muscular aponeurosis ending at ilium just above the iliac spine, while the fibres of L5 join the common tendon and end below L1 and L4. The main function of this muscle is to control the lateral bending of the lumbar spine (Figure 3-5) [48].

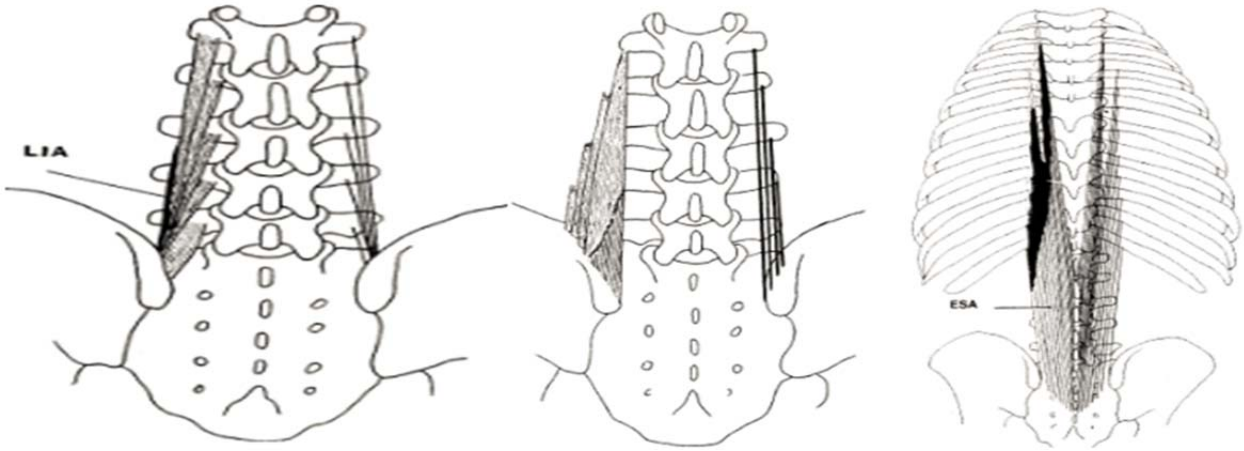

Figure 3-5: The longissimus thoracis pars lumborum (left), Iliocostalis lumborum pars lumborum (middle), longissimus thoracis pars thoracis (right) [48]

3.3.3.3 Iliocostalis lumborum pars lumborum

Fibres of this muscle arise from the tips of the first four lumbar, L1 to L4, transverse processes by covering one after the other to insert into the posterior superior iliac spine via crest of the ilium distal. The main function of this muscle is to control the flexion or extension of the lumbar vertebra [48].

3.3.3.4 Longissimus thoracis pars thoracis

This muscle consists of a series of muscle bellies that originate from T1 or T2 to T12. The tendons of the muscle bellies originate from the upper level of thorax and insert into L1 spinous process. The fibres of this muscles curve into the interspinous process space and insert into the superior border of the spinous process [48].

3.3.3.5 Iliocostalis lumborum pars thoracis

This muscle consists of small bellies arising from the lower seven or eight ribs and extending in to the lumbar region. These muscles control the forward and backward flexion of the trunk [48].

3.3.3.6 ILIOPSOAS (IP)

The iliopsoas is made up of two muscles: the iliacus and the psoas major as shown in the figure. This is a large muscle originating partly from the pelvis and partly from the lower vertebrae. These are the most powerful muscles used for walking and running. These muscles lift the knee up and forward and flex the thigh on the trunk when the pelvis is fixed (Figure 3-6) [1, 74].

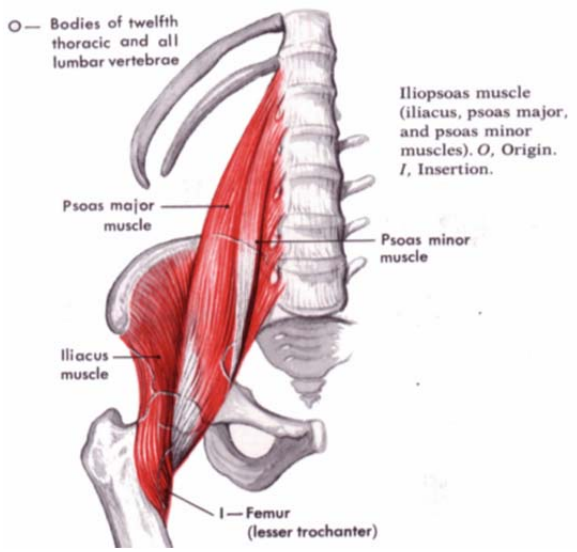

Figure 3-6: Iliopsoas [74]

3.3.3.7 Muscle Forces, Movements and Line of Action

Lumbar back muscles together act on or across each of the five lumbar vertebrae. Each muscle consists of several, individual fascicles which exert forces on a given vertebra through direct attachments or across that vertebra without attaching to it. The force exerted by an individual fascicle depends on its orientation, size and degree of activation. The degree of activation of fascicles requires knowledge of electromyographic activity of fascicles. Size and orientation of fascicles have been determined through dissection studies. These data can be applied to approximate the maximum possible force exerted by an individual fascicle since the maximum force is the product of physiological cross-sectional area of the fascicle and a force co-efficient. The physiological cross-sectional area is the volume of the fascicle divided by its length while

the force co-efficient that applies to back muscles is found to be approximately $0.46Nmm^{-2}$ [48]. Both the orientation of the fascicle with respect to the vertebra from which it arises and its line of action with respect to any vertebra that it crosses, are critically important in relation to the forces exerted by individual fascicles.

The multifidus consists of 11 fascicles on each side. One fascicle (ms) arises from the lateral aspect of the spinous process at each segmental level, and three arise from the tip of the spinous process (mt1-3). The ms fascicle from L1 inserts into L3 mamillary process and the mt fascicles insert into L4, L5 and S1 mamillary processes. The ms and mt1 fascicles from L2 spinous process insert into L4 and L5 mamillary process whereas mt2 and mt3 fascicles both insert into sacrum. The ms fascicle from L3 reaches L5 mamillary process while all three mt fascicles insert into sacrum. From L4 and L5, all fascicles insert into the sacrum. [48]

All five fascicles of the Longissimus thoracis pars lumborum arise from separate accessory processses and all reach the ilium while the four fascicles of iliocostalis lumborum pars lumborum arise from first four lumbar transverse processes and insert into ilium with fascicle lacking from L5.

There are twelve fascicles of Longissimus thoracis pars thoracis arising from thoracic levels and inserting into lumbar spinous processes across the sacrum base and posterior segment of the iliac crest. Eight fascicles of Iliocostalis lumborum originate from lower eight ribs with point of insertion into the iliac crest.

Posteriorly, the multifidus fascicles display a downward and lateral orientation. The lateral obliquity starts with a 15° for L1 and increases to 20° at L2 and L3 as the width of multifidus increases over the sacrum, but decreases to 16° at L4 and 6° at L5. The obliquity reduces the force applied by the fascicles in the sagittal plane in proportion to the cosine of its obliquity. However, the angle is so small that all of the force exerted by fascicles is in sagittal plane. [48]

Laterally, multifidus fascicles display different orientations. Fascicles from upper lumbar segments pass downwards and ventrally to their mamillary processes while from lower spinous processes pass downwards and dorsally to reach the sacrum. Their orientation varies from 11° ventral to long axis of originating vertebra to 23° dorsal to same axis. [48]

The fascicles of Longissimus thoracis pars lumborum in posterior view go in increasing obliquity from top to bottom, with L1 and L2 fascicles orientated at 5° to the sagittal plane and L5 fascicles at 27° to sagittal plane. Iliocostalis lumborum pars lumborum fascicles are all orientated at about 5° except L4 fascicles which are orientated at 15°. [48]

Laterally, the L2-L4 fascicles of longissimus thoracis pars lumborum are oriented at about 30° to their vertebral origin. L1 fascicle is inclined about 10° less while L5 fascicles are about 10° more. Iliocostalis lumborum pars lumborum fascicles are all oriented at about 20° to their vertebral origin.[48].

The thoracic fascicles of longissimus thoracis and Iliocostalis lumborum run along a sagittal plane while lateral projection of these fascicles displays parallel run to the lumbar spine with force exerted parallel to lumbar vertebrae.

Table (3-1) highlights the physiological cross-sectional areas (PCSA) of the fascicles of lumbar back muscles, their maximum force in the sagittal plane (F_{sag}), their moment arms, and the maximum applied moments on individual segments. Maximum force generated by unit cross-sectional area of muscle is expressed in terms of a force co-efficient – K. A value of 0.46 or above for K indicates that the fascicles are acting on the segment in question. [48]

Table 3-1: Moment for all muscles acting on each segment on each side [48]

Muscle and fascicle	PCSA (cm^2)	F_{avg} (N)	Moment arm (cm) by segment					Maximum moment (Nm) by segment				
			L1–2	L2–3	L3–4	L4–5	L5–S1	L1–2	L2–3	L3–4	L4–5	L5–S1
Multifidus												
L1ms	0.40	39.5K	4.4	4.2	3.5	–	–	1.7K	1.7K	1.4K	–	–
L1mt1	0.42	41.6K	5.5	5.1	4.2	2.8	–	2.3K	2.1K	1.8K	1.2K	–
L1mt2	0.36	35.7K	5.5	5.6	5.2	4.0	2.5	2.0K	2.0K	1.8K	1.4K	0.9K
L1mt3	0.60	59.4K	5.3	6.4	7.0	6.8	6.0	3.1K	3.8K	4.2K	4.1K	3.6K
L2ms	0.39	38.2K	–	4.6	4.2	3.0	–	–	1.7K	1.6K	1.2K	–
L2mt1	0.39	38.4K	–	5.6	5.2	4.0	2.5	–	2.2K	2.0K	1.5K	0.9K
L2mt2–3	0.99	97.1K	–	5.3	6.3	6.5	6.0	–	5.2K	6.2K	6.4K	5.8K
L3ms	0.54	52.0K	–	–	4.5	3.9	2.8	–	–	2.4K	2.4K	1.4K
L3mt1–3	1.57	151.8K	–	–	5.2	6.0	5.9	–	–	7.9K	9.0K	8.9K
L4 all	1.86	179.2K	–	–	–	4.9	4.7	–	–	–	8.7K	8.5K
L5 all	0.90	88.5K	–	–	–	–	4.2	–	–	–	–	3.7K
TOTAL								**9.1K**	**18.7K**	**29.3K**	**35.9K**	**35.9K**
LTpL												
L1	0.79	78.8K	3.3	4.8	5.8	6.1	5.6	2.6K	3.8K	4.6K	4.8K	4.4K
L2	0.91	90.7K	–	3.6	4.9	5.5	5.2	–	3.2K	4.4K	4.9K	4.7K
L3	1.03	102.7K	–	–	3.5	4.6	4.8	–	–	3.6K	4.7K	4.9K
L4	1.10	108.6K	–	–	–	3.3	4.2	–	–	–	3.5K	4.5K
L5	1.16	115.7K	–	–	–	–	2.8	–	–	–	–	3.3K
TOTAL								**2.6K**	**7.0K**	**12.8K**	**17.9K**	**21.8K**
ILpL												
L1	1.08	107.4K	3.5	5.0	6.2	5.7	5.7	3.8K	5.6K	6.7K	6.7K	6.1K
L2	1.54	153.8K	–	3.6	4.6	4.8	4.2	–	5.6K	7.1K	7.4K	6.5K
L3	1.82	181.8K	–	–	3.5	4.1	3.8	–	–	6.4K	7.4K	7.0K
L4	1.89	188.6K	–	–	–	3.2	3.5	–	–	–	6.0K	6.6K
TOTAL								**3.8K**	**11.2K**	**20.3K**	**27.5K**	**26.2K**
LTpT												
T1	0.29	28.7K	5.3	–	–	–	–	2.0K	−2.1K	–	–	–
T2	0.57	56.4K	5.3	–	–	–	–	3.9K	−4.1K	–	–	–
T3	0.56	55.4K	5.3	4.7	6.2	–	–	3.8K	4.0K	−4.0K	–	–
T4	0.45	44.6K	5.3	5.7	6.2	–	–	3.1K	3.2K	3.2K	−3.0K	–
T5	0.44	43.6K	5.3	5.7	6.2	–	–	3.0K	3.1K	3.2K	−3.0K	–
T6	0.64	63.4K	5.3	5.7	6.2	5.7	–	4.4K	4.6K	4.6K	4.3K	−3.8K
T7	0.78	77.2K	5.3	5.7	6.2	5.7	4.5	5.3K	5.5K	5.6K	5.3K	4.6K
T8	1.25	123.8K	5.3	5.7	6.2	5.7	4.5	8.5K	8.9K	9.0K	8.5K	7.4K
T9	1.46	144.5K	5.3	5.7	6.2	5.7	4.5	9.9K	10.3K	10.4K	9.9K	8.6K
T10	1.60	160.0K	4.6	5.7	6.2	5.7	4.5	10.4K	11.2K	11.8K	11.7K	10.3K
T11	1.67	167.0K	3.8	4.9	6.2	5.7	4.5	10.4K	11.7K	12.5K	12.5K	11.6K
T12	1.38	138.0K	3.1	4.0	5.2	5.7	4.5	8.2K	9.6K	10.5K	10.4K	9.9K
TOTAL								**72.9K**	**65.9K**	**66.8K**	**58.6K**	**48.6K**
ILpT												
T5	0.23	22.8K	5.3	5.7	6.2	5.7	6.8	1.5K	1.6K	1.7K	1.6K	1.6K
T6	0.31	30.7K	5.3	5.7	6.2	5.7	5.7	2.1K	2.2K	2.3K	2.2K	2.1K
T7	0.39	38.6K	5.3	5.7	6.2	5.7	4.5	2.5K	2.7K	2.8K	2.8K	2.6K
T8	0.34	33.7K	5.3	5.7	6.2	4.6	3.6	2.2K	2.4K	2.5K	2.4K	2.3K
T9	0.50	49.5K	5.3	5.7	5.2	4.6	2.6	2.9K	3.1K	3.3K	3.2K	2.8K
T10	100	99.0K	5.3	4.9	5.2	4.6	2.6	5.8K	6.3K	6.6K	6.4K	5.6K
T11	1.23	121.8K	3.1	4.0	5.2	4.6	2.6	5.7K	6.7K	6.7K	6.4K	5.1K
T12	1.47	147.0K	3.1	3.0	4.3	3.6	2.6	4.7K	5.3K	5.6K	5.3K	3.8K
TOTAL								**27.4K**	**30.3K**	**31.5K**	**30.3K**	**25.9K**
TOTAL for all muscles acting on each segment (on each side)								**116K**	**133K**	**161K**	**168K**	**158K**

3.3.4 Muscles in the dynamic model

The model presented in this thesis is a direct kinematics representation. As such, muscle forces are applied to vertebrae to produce the desired motion. For this reason, the muscles were included in the model. These muscles were generated using the "Virtual Muscle" 4.0.1 [75]. First, the fibres types of the muscles were generated. These fibres were later used to create muscle blocks. The optimal sarcomere lengths [76] and the physical cross sectional area of the muscles were taken from the literature [48]. The lengths of the muscles were directly measured from the two segments of the body where the muscles are connected in the real human body. The "Virtual muscle" [75] was used to simulate the input-output relationship between muscle activation, the length and the corresponding forces. Figure (3-7) shows the block diagram of rectus abdominis muscle and the force generated given a specific length and activation level.

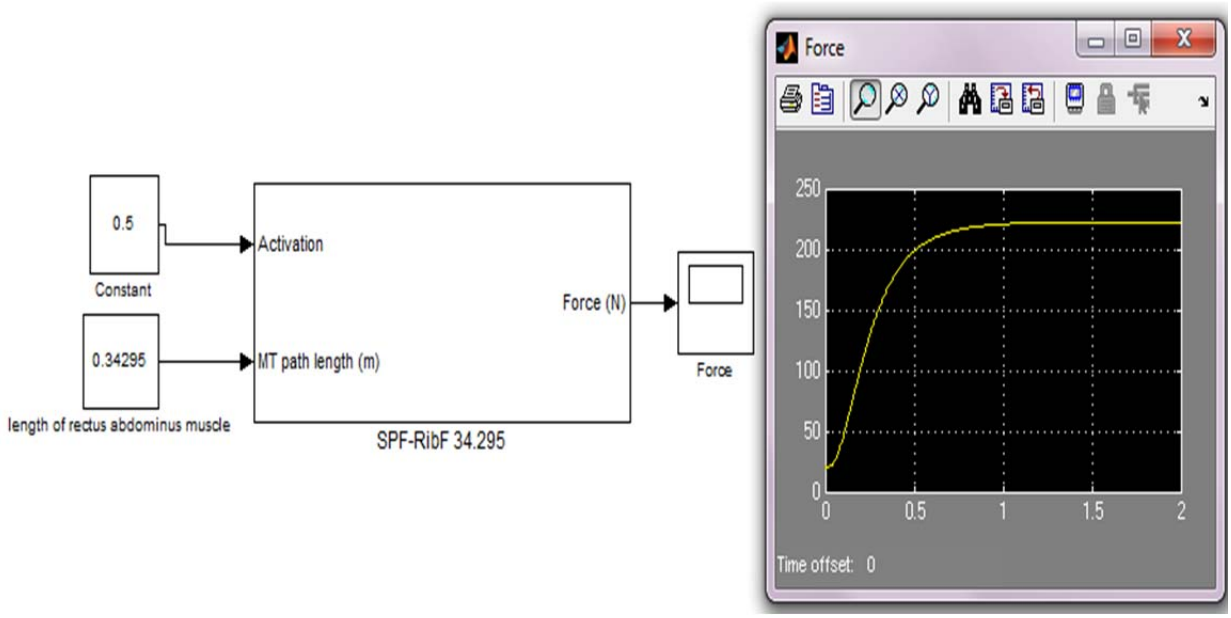

Figure 3-7: Rectus abdominis muscle with muscle force curve

In this thesis, two types of dynamic models have been proposed: (1) simplified model and (2) full model to analyse lumbar forces and moment using forward kinematics. The difference in these two models is that the simplified model consists only of 17 muscles in total including 15 local back muscles and two global muscles (one front and one back). The full model consist of 46 muscles in total including 28 local, six global back muscles; and ten local and two global

front muscles. The lengths of the muscles were approximated by connecting two segments of the lumbar spine.

3.3.5 Simplified model

The simplified model was created by reducing the number of muscles and increasing the physiological cross sectional area of the muscles. Local muscles were connected from transverse processes of each vertebra to iliac crest and spinous processes of each vertebra to the sacrum (10 and 5, respectively). The global front muscle was connected from 12th rib of the spine to the pelvis while the global back muscle was connected from 8th rib of the spine to the sacrum. All local muscles and global front muscle were connected straight whereas global back muscles were connected using via-point to reflect the realistic muscle path. For each muscle, "the physiologic cross section area (PCSA) determines the force-producing potential" [77]. In the model the PCSA of the global back muscles, longissimus thoracis pars lumborum (LGPL), was taken as 12.10 cm^2 [34]. The PCSA of the global front muscle, rectus abdominis (RA), and local muscles were considered larger to produce enough muscle force for all required motion. Figure (3-8) shows the structure of the whole lumbar spine model with the front and back muscles.

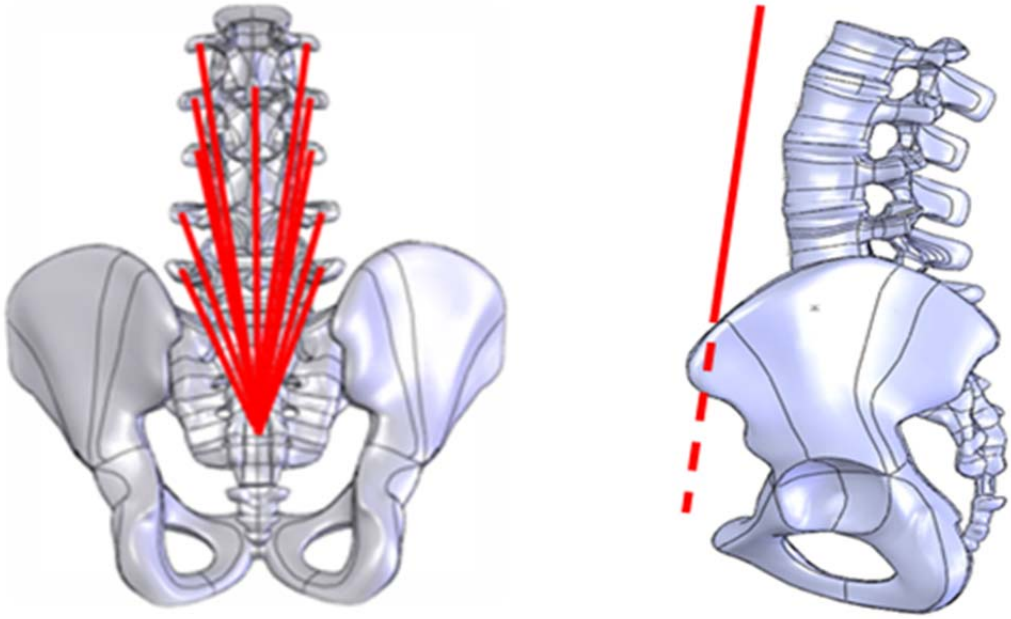

Figure 3-8: Lumbar spine model with front, back and side muscles attached

3.3.6 Full Model

Full model consists of 38 local muscles attached to the vertebrae and eighth global muscles attached to the thoracic cage [6, 15, 34, 46, 47]. As described by Zee et al., [36] lumbar muscles are connected in three different paths, straight line, via-point and non-linear wrapping. In order to create real effect of the muscles as close to the real human, muscles were attached following the same approach. In this study, the local muscles' path was considered as straight line and via-points, while global muscles' path was considered as non-linear wrapping in order to follow a curve path. The global muscles included in to the model are rectus abdominis (RA), longissimum thoracis pars thoracis (LTPT), ilicostalis lumborum pars thoracis (ILPT), whereas the local muscles include multifidus (MF), iliopsoas (IP), quadratus lumborum (QL), ilicostalis lumborum pars lumborum (ILPL), and longissimum thoracis pars lumborum (LTPL) [34, 48]. Physiological cross-sectional areas (PCSA) for the trunk muscles on each side are shown in the Table (3-2) [34] while the insertion points of the global and local muscles were followed as described by the [48].

Table 3-2: Physiological cross-sectional areas (PCSA, mm^2) for front and back trunk muscles on each side of the spine at different insertion levels [46]

Local muscles	Physiological cross sectional area (mm^2)				
	ILPL	MF	LTPL	MF	IP
L1	108	96	79	88	252
L2	154	138	91	80	295
L3	182	211	103	75	334
L4	189	186	110	70	311
L5		134	116		182
Global Muscles	RA	ILPT	LTPT		
	567	660	1210		

3.4 Lumbar Spine Intervertebral Discs

Intervertebral discs are complex structures designed to provide six degree of freedom including rotation and translation in X, Y, and Z directions by creating a potential space in between the two

vertebral bodies. The intervertebral discs are named numerically according to vertebral bodies, i.e. L1-2, L2-3, L3-4, L4-5 and the fifth disc is known as the lumbosacral (L5-S1). These vertebral bodies are separated by the tissue because the tissues of the discs are flexible to accommodate movements; and at the same time are stiff and strong enough to sustain large amounts of compressive loads. The basic structure of the intervertebral disc shown in the Figure (3-9) highlights the three components of the disc: superior and inferior endplates, nucleus pulposus in the centre and the anulus fibrosus which is surrounded by the nucleus pulposus [78]. These tissues provide some degree of movement between the vertebral bodies by restricting their limitations (radial expansion of nucleus pulposus is resisted by anulus fibrosus which ultimately prevents anulus fibrosus from buckling inwards and losing its stiffness). The nucleus pulposus is a hydrated gel and expands in a radial fashion under compression while anulus fibrosus consists of 10-20 lamellae packed together in a circumferential fashion. These lamellae are very stiff and are able to sustain large compressive loads. The third component, superior and inferior vertebral endplates of the intervertebral disc cover almost the entire surface of the vertebral bodies except for the ring apophysis (narrow rim of bone).

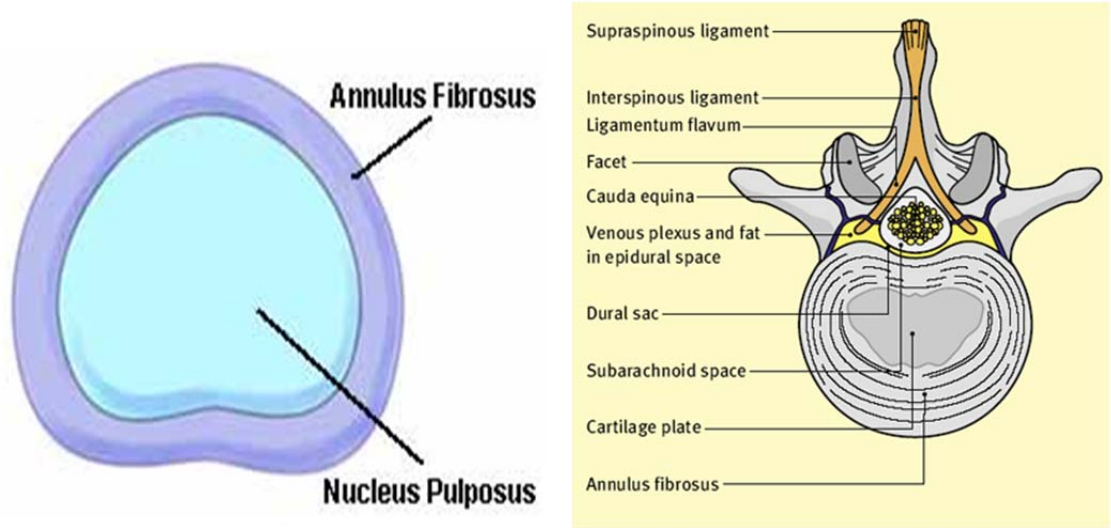

Figure 3-9: Axial view of intervertebral disc [78, 79]

The height of each lumbar intervertebral disc is 10 mm and total height for all five lumbar vertebrae is 5 cm. During the daily activities, such as standing upright, lifting, twisting or bending, an individual squeezes the water (gel) out of the lumbar discs and loses height. This

height is restored in recumbent position in other words when the water is re-imbibed during the sleep at night.

In the proposed model, the non-linear springs and dampers were used in place of intervertebral discs between the two vertebrae. This represented disc as a six degree of freedom joint and was used to model the dynamic characteristic of these discs along their axes. Similar approach was also used in rigid body modeling of lumbar spine [12]. Under the external loads, during the normal physiological motion and due to the upper body weight, disc sustains compression, shear and bending. Therefore, the determination of spring stiffness of the intervertebral discs of the lumbar spine is important while modeling the lumbar spine. Keller et al. [12] have used stiffness coefficient ranging from 75-700 N.m/rad for the springs between thorax and pelvis while in proposed model, a stiffness coefficient of 570 N.m/rad was used for all springs. Figure (3-10) shows the compression spring and damper placed in between the disc after cutting it into two halves.

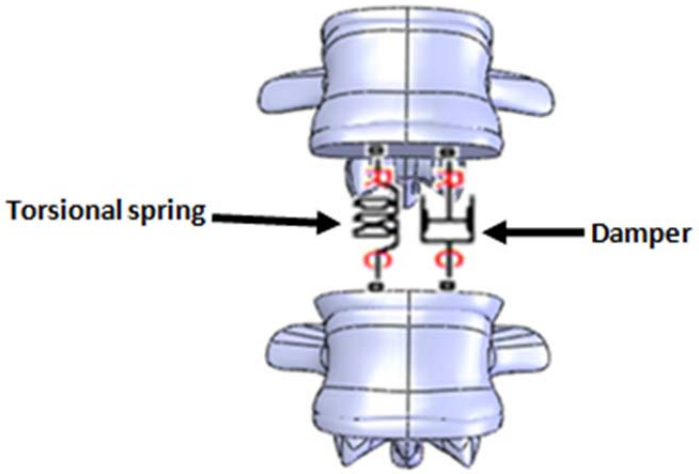

Figure 3-10: Intervertebral discs with torsional springs and damper

As described by Eberlein et al. [66] intervertebral disc consists of water with solutes, gelatinous nucleus pulposus, annulus fibrosus and macromolecules such as collagens, proteoglycans (PGs) and cells. To obtain accurate material parameters, homogeneous stiffness and geometric dimensions of these contents are very difficult. For this reason, the scanned model of lumbar spine was obtained from Zygote Media Group to avoid discrepancy in results. The cross

sectional areas of the discs measured from the model were 1747.76 mm^2, 1969.77 mm^2, 1830.92 mm^2, 1790.17 mm^2, and 1805.54 mm^2 from L1 to S, respectively (Zygote Media Group, Inc., American Fork, USA).

3.5 Lumbar Vertebrae

The five lumbar vertebral bodies are the essential components of the lumbar vertebral column. They are named numerically in sequence as lumbar one to five i.e. L1, L2, L3, L4 and L5. These vertebrae support and protect spinal cord as well as consist most of the body weight. Lumbar vertebral bodies can resist larger amounts of compressive forces acting down the long axis of the spine but these forces vary from posture to posture, loading history and the age of the individuals. These vertebral bodies lose their strength at the age in which a fracture can easily occur during an individual's normal daily activities or due to the hormonal changes (mostly in women).

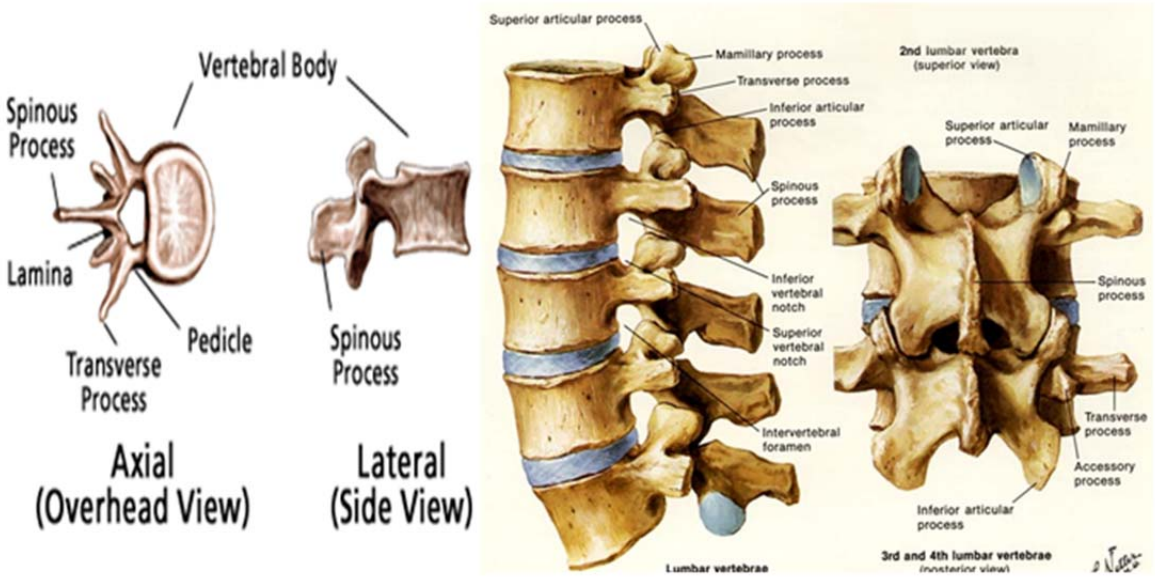

Figure 3-11: Lumbar vertebrae with axial and lateral views [1]

The Figure (3-11) shows the axial and lateral view of the vertebrae which consist following elements:

Vertebral body: the largest part of the vertebra with somewhat cylindrical shape which is thicker at the end and thinner in the middle covered with cortical bone. Both upper and lower surfaces are cushioned by the vertebral disc. [1]

Pedicles: the slender and bony part that forms back wall of the vertebrae. [1]

Processes: there are main three processes: spinous, transverse and articular. Spinous processes are positioned centrally and projects backward in the thoracic region rather than downward while transverse processes project laterally and are attached to large back muscles and strong ligaments. The four articular processes; two inferior and two superior are linked with the articular process of the adjacent vertebrae and form facet joints to allow motion in the spine. [1]

Endplates: endplates cover almost the entire surface of the vertebral bodies except for the ring apophysis (narrow rim of bone) [1].

Intervertebral foramen: the place between the adjacent pedicles in which the spinal nerves enter and leave; visible from the side view of the vertebrae [1].

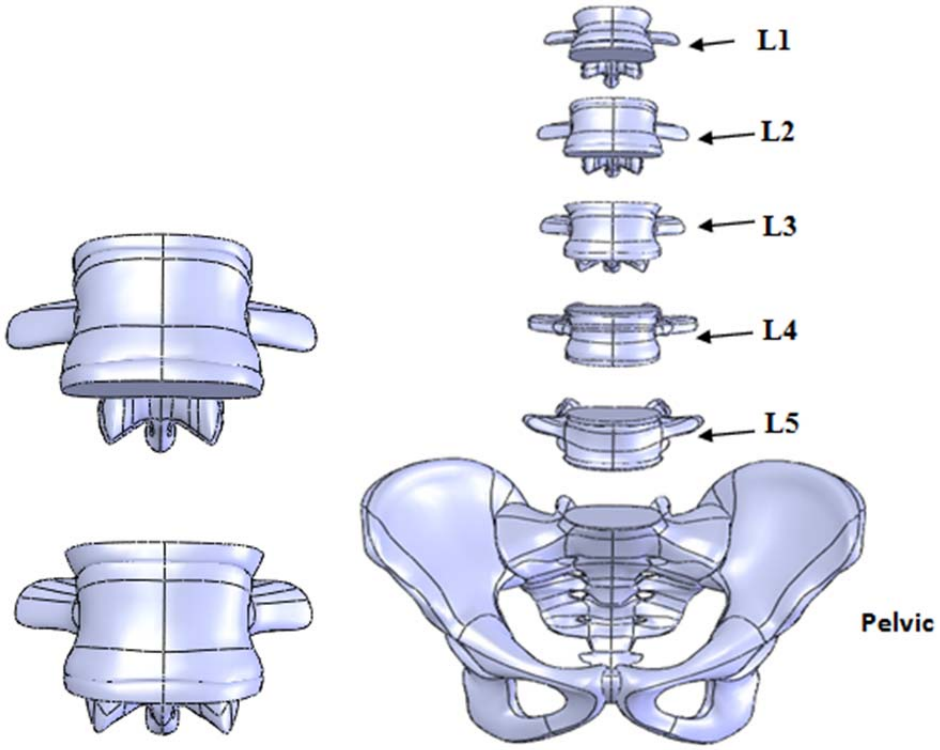

Figure 3-12: CAD model of Lumbar vertebrae and pelvic

In proposed model, vertebrae were considered as rigid bodies same as in FE models and rigid body models developed in literature [12, 36, 34, 40, 60, 46]. Most of the lumbar muscles are attached to the vertebral bodies; and muscle strength and forces mainly depend on muscle's length and physiologic cross sectional area (PCSA). In order to establish accurate location for attaching muscles, scanned model of vertebrae were obtained from Zygote Media Group. The lumbar spine model consists of five lumbar vertebrae, from L1 to L5 and five intervertebral discs attached to the pelvis. Each disc has six degree of freedom (30 DOF in total). Each vertebra was restricted to rotate no more than five degrees with respect to base vertebra starting from pelvis. This means L1 moves 25 degrees in total with respect to pelvis. Figure (3-12) shows the scanned model of lumbar vertebrae.

3.6 Joints

Joints provide the important locking mechanism to the vertebrae. They are designed to block forward sliding of the vertebrae and prevent dislocating of vertebral bodies. Also by blocking axial rotation they protect the intervertebral disc from torsion. Axial rotation occurs around the longitudinal axis of the spinal cord. To block this rotation, joints create locking mechanism and block lateral displacement of the posterior elements.

3.7 Ligaments

The vertebrae are joined by the two ligaments, anterior longitudinal (interspinous ligament) and posterior longitudinal ligaments (superspinous ligament) to form a spinal column. Connecting ligaments and vertebral discs supports the bones of the spinal column and act as shock absorber. Ligaments restrict the excessive flexion and extension of the vertebrae under excessive shear loading. [48]

Interspinous ligaments are connected to the adjacent posterior spine and create large angle of obliquity. These ligaments protect against the posterior shearing of the superior vertebra by creating oblique line of action. Superspinous ligament is connected to the tip of the posterior spine and is also aligned with the compressive axis of the spine to provide resistance against excessive forward flexion.

Spine is surrounded by six ligaments: anterior (ALL), posterior (PLL) longitudinal ligaments, intertransverse (ITL), Flavum (FL), capsular (JC), and intertransverse (ITL) ligaments [80]. Ligaments behave similar to visco-elastic and hyper-elastic material; so the failure of the ligaments is based on strain criteria [81].

In proposed model, joints and ligaments were modelled using the torsional springs and dampers. These torsional springs and dampers were placed between the two vertebrae (Figure 3-13). The spring rate of the rotational spring was assumed to be 570 N.m/rad, whereas damping coefficient of the rotational damper was taken to be 150 N.m/ (rad/s) which is in the range in literature [12, 60]. To see the realistic effect of the ligaments and joints, a third component placed along with the springs was the rotational hard-stop, implemented as a stiff spring.

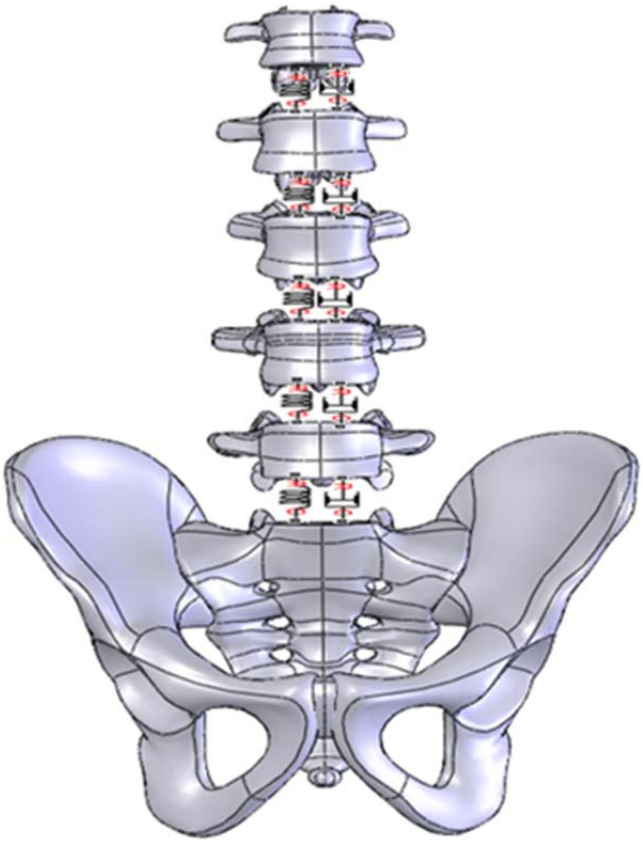

Figure 3-13: The whole model of Lumbar spine including springs and dampers

The rotational hard-stop was also placed in between two vertebrae and used to restrict the motion of the vertebrae by limiting the upper bound and lower bound. The hard-stop spring creates

linearly proportional force to oppose the slider into stop. Each joint in the model was set to follow the base of the relative body component such that the movement of the end effector (thorax) would be the total movement of the body.

Figure (3-14) shows the structure of the whole lumbar spine model with the front and back muscles. The model was first tested for balancing the weight of the body (standing straight) and later, it was tested for holding and lifting 20 kilograms of weights, respectively. The second test was performed to evaluate the thorax rotations, compression forces, and moments between the discs L1-S1 for squat and stoop lifts with and without loads.

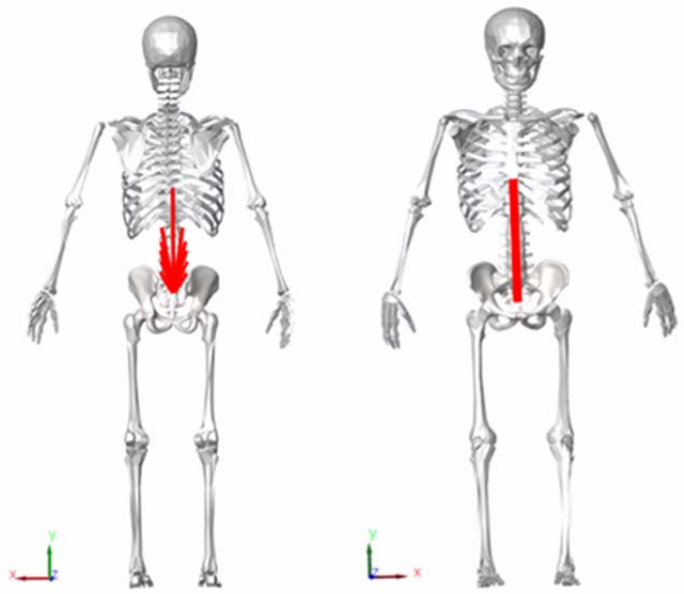

Figure 3-14: Structure of whole human skeleton with front and back muscles

3.8 PID Controller

PID (proportional integrator and derivative) controller was used to control the activation of the muscles. Controlled activation of the muscles made it possible to regulate the force being produced by the muscle. The in-built saturation function of the PID controller was used to limit the output of the activation between 0 and 1. In addition to the PID input, the 'Muscle' block requires the instantaneous muscle length. The force produced by the muscle is applied on the

lumbar vertebrae, which causes rotation of the vertebrae. This rotation is compared with the desired lumbar spine position and the difference between the current and desired position is calculated as error. This error is fed in to the PID controller, which adjusts the muscle accordingly until the desired lumbar spine position is achieved. While running the simulation, the tune function of the PID controller was used to tune the gain, integral and derivative to achieve the best possible activation input.

There are seven such feedback controllers in the model; five of the controllers are connected to a lumbar vertebra in sequential order while the other two controllers are connected to the back and front of the thorax to control the upper body position in simplified model. Figure (3-15) shows the structure of sub system for lumbar vertebra L1 only while the Figure (3-16) shows the five sub systems for five lumbar vertebrae for the feedback controller block, each with 'n' number of muscles. The rotation caused to respective vertebrae by each sub system is collectively stored in the form of an array of current configuration. This array is compared with the desired position of the lumbar spine; also in the form of an array. The difference between the two is obtained as an array of error vector and fed back into the controller block, to re-adjust the position of the lumbar spine to match the desired position.

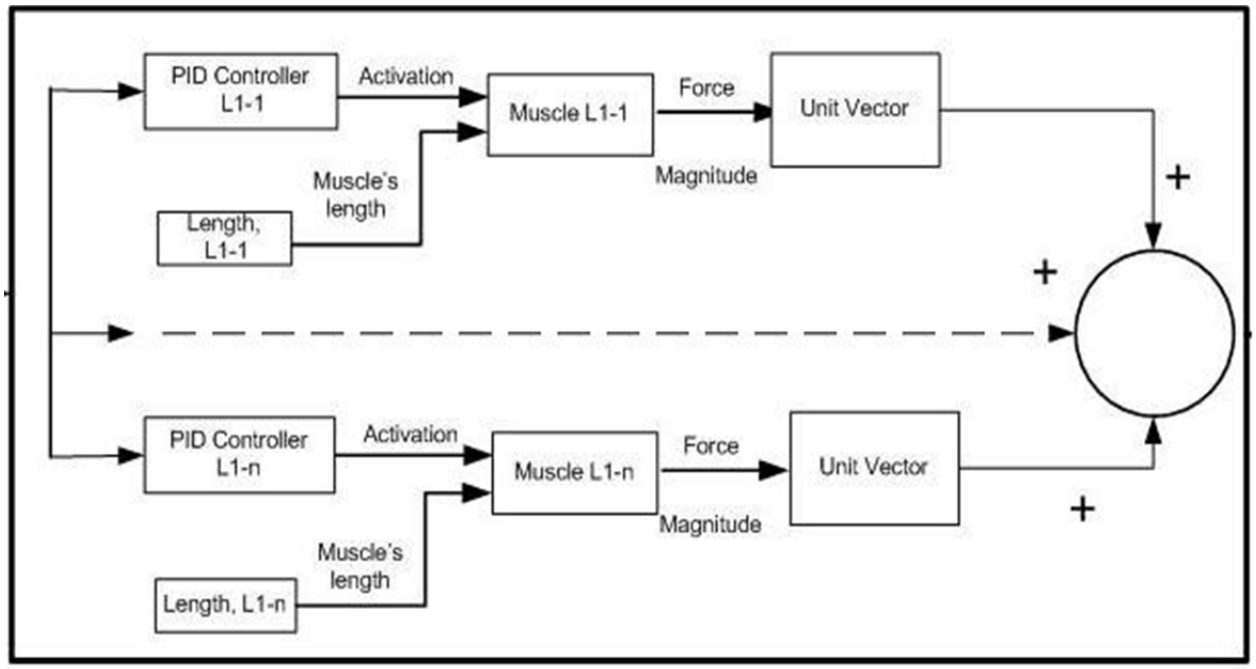

Figure 3-15: Sub system of Lumbar vertebra L1

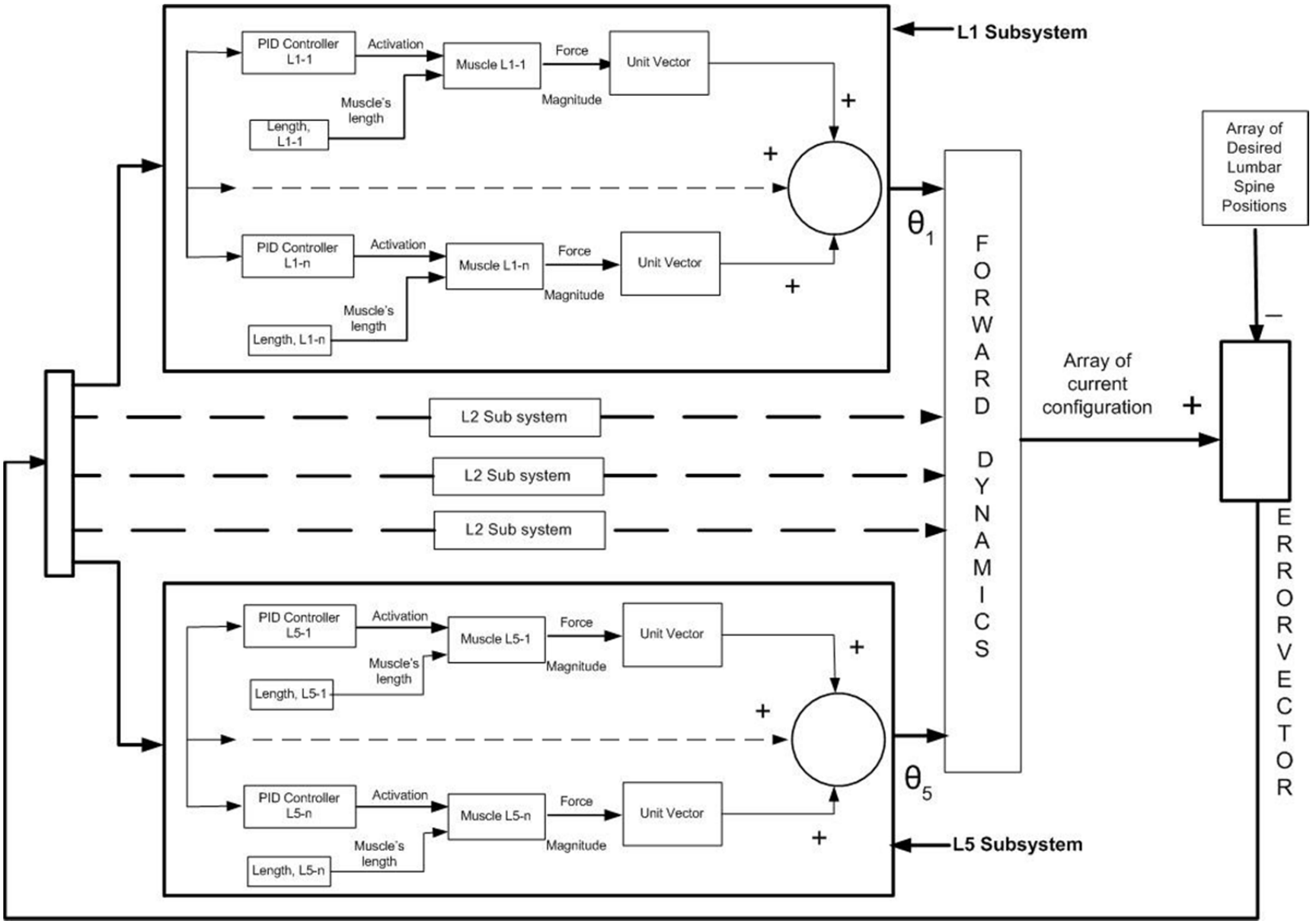

Figure 3-16: Sub systems of feedback controller block

3.9 Forward kinematics model of lumbar spine

The mechanical model of spine can also be represented as forward kinematics of a robot manipulator, in which the manipulator is composed of a set of nearly rigid links connected with various joints. These joints allow relative motion (translation and rotational motion) of connecting links. This similarity can be used to derive the dynamic equations required for representing the lumbar spine dynamics. A robot manipulator with n joints will have n+1 links where each joint connects link i-1 and link i. The base link (i.e. link i) will stay at its fixed position with respect to link i-1 when the joint i is actuated. The position and orientation of the end-effector can be found by the transformation matrix relating two frames starting from the base frame to the end frame, i.e., ${}^{i-1}\mathbf{T}_i$ where i = 1, 2, 3, 4 and 5. In the current model, pelvis and all five lumbar vertebrae (L1-L5) are considered as links and the five intervertebral discs as joints (see Figure 3-17). The pelvis represents the base frame (link 0). The relative motion between vertebrae can be represented using Denavit-Hartenberg (D-H) transformation matrix [82].

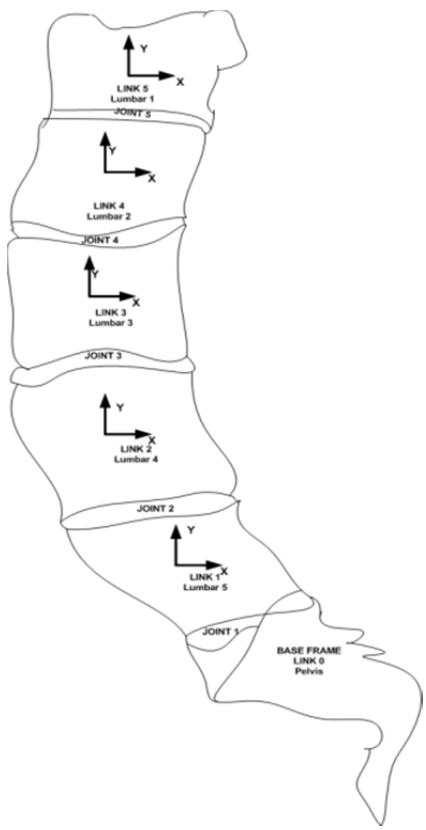

Figure 3-17: Mathematical representation of lumbar spine

The general form of the transformation matrix is shown below [82].

$$\boldsymbol{T_i^{i-1}} = \begin{pmatrix} \mathrm{C}\,\theta_i & -\mathrm{S}\,\theta_i & 0 & \mathrm{a}_{i-1} \\ S\theta_i\, C\alpha_{i-1} & \mathrm{C}\,\theta_i C\alpha_{i-1} & -S\alpha_{i-1} & -S\alpha_{i-1} d_i \\ S\theta_i\, S\alpha_{i-1} & \mathrm{C}\,\theta_i S\alpha_{i-1} & C\alpha_{i-1} & C\alpha_{i-1} d_i \\ 0 & 0 & 0 & 1 \end{pmatrix} \qquad \textbf{Equation 1}$$

Where a_i = the distance from Z_i to Z_{i+1} measured along X_i, α_i = the angle between Z_i and Z_{i+1} measured about X_i, θ_i = the angle between X_i to X_{i+1} measured about Z_i, and d_i = the distance from X_i to X_{i+1} measured along Z_i. Newton's law for motion can be written as [83]:

$$\overline{\boldsymbol{F}}_{\mathbf{res\ i}} = \boldsymbol{m_i}\ \overline{\boldsymbol{a}}_{\boldsymbol{i}\mathbf{G}} \qquad \textbf{Equation 2}$$

$$\boldsymbol{M_{res}} = \dot{\overline{\boldsymbol{H}}}_{\boldsymbol{G}} + \overline{\boldsymbol{w}} \times \overline{\boldsymbol{H}}_{\boldsymbol{G}} \qquad \textbf{Equation 3}$$

Where, $\bar{F}_{\mathrm{res\,i}}$ is the resultant forces and $\bar{M}_{\mathrm{res\,i}}$ is the resultant moment acting on vertebra i and $\bar{H}$ is angular moment [83].

In expanded form these equations can be written as follow [83]:

$$\sum \boldsymbol{F_x} = \boldsymbol{m}(\boldsymbol{a_G})_x \qquad \textbf{Equation 4}$$

$$\sum \boldsymbol{F_y} = \boldsymbol{m}(\boldsymbol{a_G})_y \qquad \textbf{Equation 5}$$

$$\sum \boldsymbol{F_z} = \boldsymbol{m}(\boldsymbol{a_G})_z \qquad \textbf{Equation 6}$$

$$\sum \boldsymbol{M_x} = \boldsymbol{I_{xx}}\dot{\boldsymbol{w}}_{\boldsymbol{x}} - (\boldsymbol{I_{yy}} - \boldsymbol{I_{zz}})\boldsymbol{w_y}\boldsymbol{w_z} - \boldsymbol{I_{xy}}(\dot{\boldsymbol{w}}_{\boldsymbol{y}} - \boldsymbol{w_z}\boldsymbol{w_x}) - \boldsymbol{I_{yz}}(\boldsymbol{w_y^2} - \boldsymbol{w_z^2}) - \boldsymbol{I_{zx}}(\dot{\boldsymbol{w}}_{\boldsymbol{z}} + \boldsymbol{w_x}\boldsymbol{w_y}) \qquad \textbf{Equation 7}$$

$$\sum \boldsymbol{M_y} = \boldsymbol{I_{yy}}\dot{\boldsymbol{w}}_{\boldsymbol{y}} - (\boldsymbol{I_{zz}} - \boldsymbol{I_{xx}})\boldsymbol{w_z}\boldsymbol{w_x} - \boldsymbol{I_{yz}}(\dot{\boldsymbol{w}}_{\boldsymbol{z}} - \boldsymbol{w_x}\boldsymbol{w_y}) - \boldsymbol{I_{zx}}(\boldsymbol{w_z^2} - \boldsymbol{w_x^2}) - \boldsymbol{I_{xy}}(\dot{\boldsymbol{w}}_{\boldsymbol{x}} + \boldsymbol{w_y}\boldsymbol{w_z}) \qquad \textbf{Equation 8}$$

$$\sum \boldsymbol{M_z} = \boldsymbol{I_{zz}}\dot{\boldsymbol{w}}_{\boldsymbol{z}} - (\boldsymbol{I_{xx}} - \boldsymbol{I_{yy}})\boldsymbol{w_x}\boldsymbol{w_y} - \boldsymbol{I_{zx}}(\dot{\boldsymbol{w}}_{\boldsymbol{x}} - \boldsymbol{w_y}\boldsymbol{w_z}) - \boldsymbol{I_{xy}}(\boldsymbol{w_x^2} - \boldsymbol{w_y^2}) - \boldsymbol{I_{yz}}(\dot{\boldsymbol{w}}_{\boldsymbol{y}} + \boldsymbol{w_z}\boldsymbol{w_x}) \qquad \textbf{Equation 9}$$

Where, I_{xx}, I_{yy}, and I_{zz} are moments of inertia of vertebra (with respect to centre of gravity).

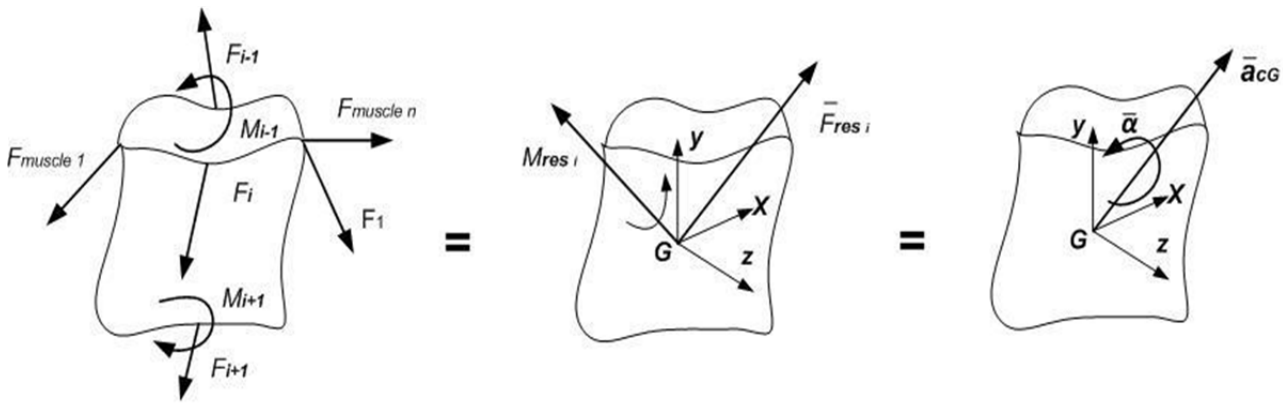

Figure 3-18: Resultant forces and moment and angular acceleration acting on to vertebrae

Figure (3-18) shows how the resultant force and moment are calculated for each vertebra. $\bar{F}_{\mathbf{i\ -1}}$, $\bar{M}_{\mathbf{i\ -1}}$, $\bar{F}_{\mathbf{i\ +1}}$, and $\bar{M}_{\mathbf{i\ +1}}$ represent reaction forces and moments transmitted through (i-1), i, (i+1) discs respectively. $F_{\text{muscle 1}}$ represents forces applied by muscles.

These forces and moments can be simplified and represented by $\bar{F}_{\text{res i}}$ and $\bar{M}_{\text{G res}}$. In each iteration during modeling process, the resultant forces and moments are calculated and used to update linear and angular acceleration of each vertebra.

Chapter 4: Case studies

4.1 Introduction

The main objective of this investigation was the development and validation of a forward kinematics lumbar spine using Simulink model. To show the feasibility of the direct kinematic modeling of lumbar spine, simulation methods have been conducted for both simplified and full model. Three sets of case studies were undertaken including static and dynamic loading to study the behaviour of the lumbar spine. Loadings considered were free standing, lifting a load away and close to the chest, stooping, squatting and gym squatting. Model predictions were compared with in vivo measurements and other dynamic model.

Intervertebral pressures were calculated using relevant disc cross sectional areas while anterior shear forces were calculated by projection of muscle forces. Compression forces, net external moments and passive ligamentous moments were directly measured from the model, whereas the moments generated by muscle forces were calculated by taking the difference between the net external moment and passive ligamentous moments. Both simplified and full models were validated by comparing the results with in vivo measurements and dynamic model results in literature [6, 29].

The total body weight of 70 kg with external load of 195N was considered while comparing the results with in vivo measurements [29], whereas the total body weight of 74 kg (mean value of 11 subjects) with external load of 180N was used while comparing with other dynamic models [6]. The body weight of each segment was calculated using the anthropometric data (see Appendix D) [84].

4.2 Case study I: Sanding and lifting weights

In the first case study, the model was used to measure compression force acting on the lumbar spine for three different scenarios; a) standing, b) lifting the total load of 195 N close to the chest and c) lifting a total load of 195N at a distance of 60 cm from the chest.

In free standing, the simplified model was used to determine posterior and anterior muscle force required for equilibrium force from surrounding posterior and anterior muscles. Basic posture of standing was considered as described in the literature [29] and as shown in the Figure (4-1). The pelvis and spine were stretched tight in upright posture. The forearms and upper arms were extended and kept parallel at the sides of body and thigh and legs were also straight with no movement such that the body weight was distributed equally on both feet. Constant upright erect posture was maintained by muscles in the model during the simulation.

Figure 4-1: Free standing posture

In lifting the load away from and close to the chest, initial positions were same as in free standing (as described above). In both cases, the load of 97.5N was applied in each hand as soon as the body reached equilibrium and then forearms and upper arms were moved to achieve the final position shown in Figure (4-2) by rotating the forearms and upper arms.

In Figure (4-2b), forearms were kept at an angle of 62.5 degrees and upper arms to an angle of 30 degrees with the rate of 25 and 12 degrees per second, respectively. On the other hand, for lifting the total load of 195 N close to the chest, forearms were brought to an angle of 112.5 degrees and upper arms to an angle of 20 degrees with the rate of 45 and 8 degrees per second,

respectively (Figure 4-2c). The above angles and external loads were used in accordance with the literature for close proximity of the results to the literature [29].

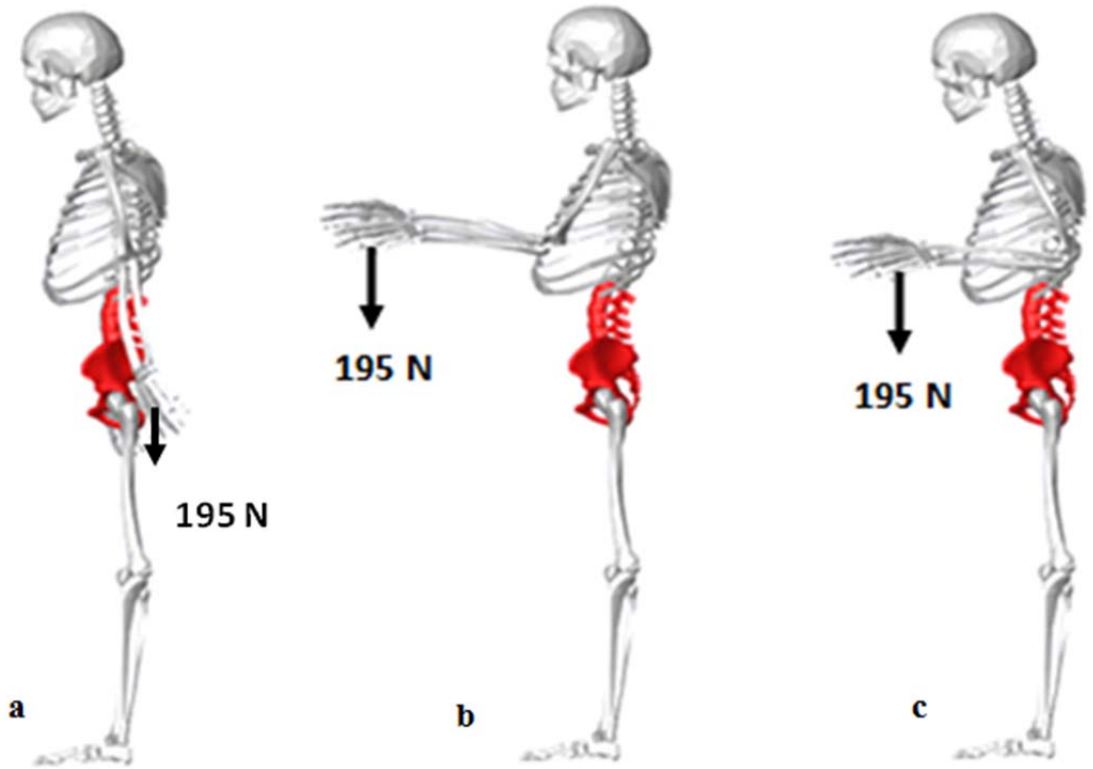

Figure 4-2: Lifting activities: (a) holding weight in each hand, (b) lifting load away from the chest, (c) lifting load close to the chest

While standing straight, the muscle activation in the model was very low because trunk and pelvis were supported by the legs. Front and back muscles' forces rapidly increased as simulation started and became constant as body stabilized (Appendix A, Figure A1). Same trends were found for lifting activities but in lifting load away from the chest, the activation and muscle forces were much higher as compared with lifting loads closer to the chest. All three activities indicate that the maximum compression force happens at L5-S1 disc in comparison to other four discs.

The compression force for disc L5-S1 in simplified model for all three activities was measured to be 893N, 2438N, and 3860N for free standing, lifting the load of 195 N close to the chest and

lifting a load of 195N at a distance of 60 cm from the chest, respectively. The maximum compression forces for all three activities for all five intervertebral discs are shown in the Figure (4-3). Figure (4-3) shows that lifting the load of 195N close to the chest increases the compression force on L5-S1 disc by approximately three times compared to free standing. Lifting the same amount of load away from the chest increases the compression force by ~50% as compared with lifting the load closer to the chest. This shows that the large moment arms can significantly increase the compression forces on the discs. As it can be seen in Figure (4-2b) the body is tilted backward, which also replicates the expected posture, when lifting a heavy load. This helps to prevent instability in spine. In both lifting activities, both hands rotate from vertical to horizontal axis. The compression forces increase linearly for all five discs. The rate of increase in compression forces are higher for first 30˚ compared to later 60˚ (Figure 4-4 and Figure 4-5).

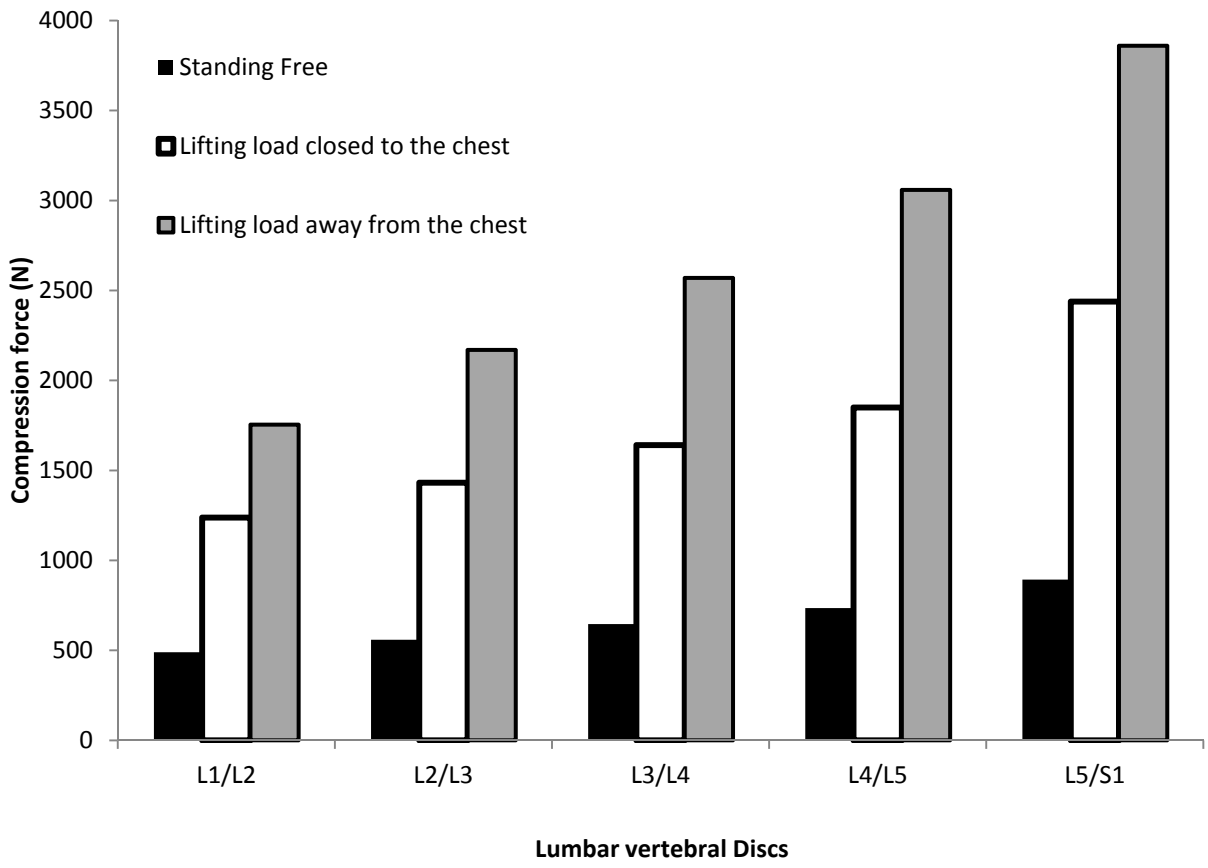

Figure 4-3: Compression forces on the lumbar discs during relaxed standing and isometric lifting the loads close to the chest and away from the chest.

The maximum intradiscal pressures were determined by dividing the normal reaction forces with cross sectional areas of the intervertebral disc. The area of the disc L4-L5 was directly measured from the scanned CAD model of lumbar spine (17.9 cm^2). In free standing, the intradiscal pressure was measured to be 0.41 MPa; for lifting the total load of 195N, the pressures were measured as 1.05 MPa and 1.85 MPa for close to the chest and 60 cm away from the chest, respectively. The maximum compression forces and intradiscal pressure for all five lumbar vertebral discs are shown in Table (4-1).

Table 4-1: Maximum compression forces and pressure measured on the lumbar discs for different cases

Compression forces/pressure on Lumbar discs	Standing Free		Lifting load of 195N close to the chest		Lifting load of 195N away from the chest	
	(N)	(MPa)	(N)	(MPa)	(N)	(MPa)
L1/L2	490	0.28	1238	0.71	1755	1.00
L2/L3	559	0.28	1432	0.73	2170	1.10
L3/L4	646	0.35	1641	0.90	2570	1.40
L4/L5	735	0.41	1850	1.03	3059	1.71
L5/S1	893	0.49	2438	1.35	3860	2.14

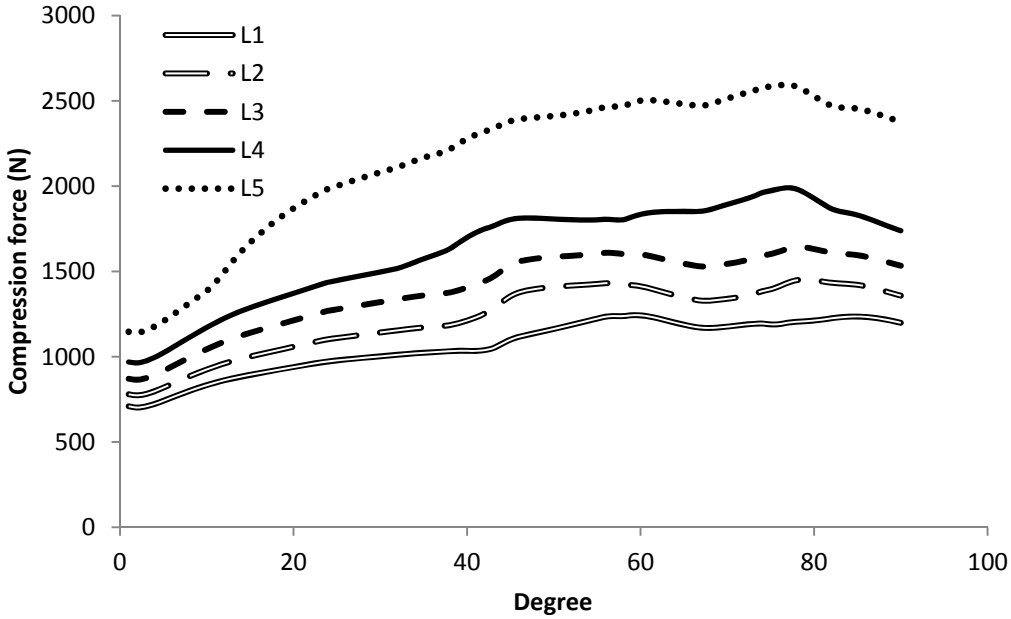

Figure 4-4: Compression forces on the discs during lifting close to the chest

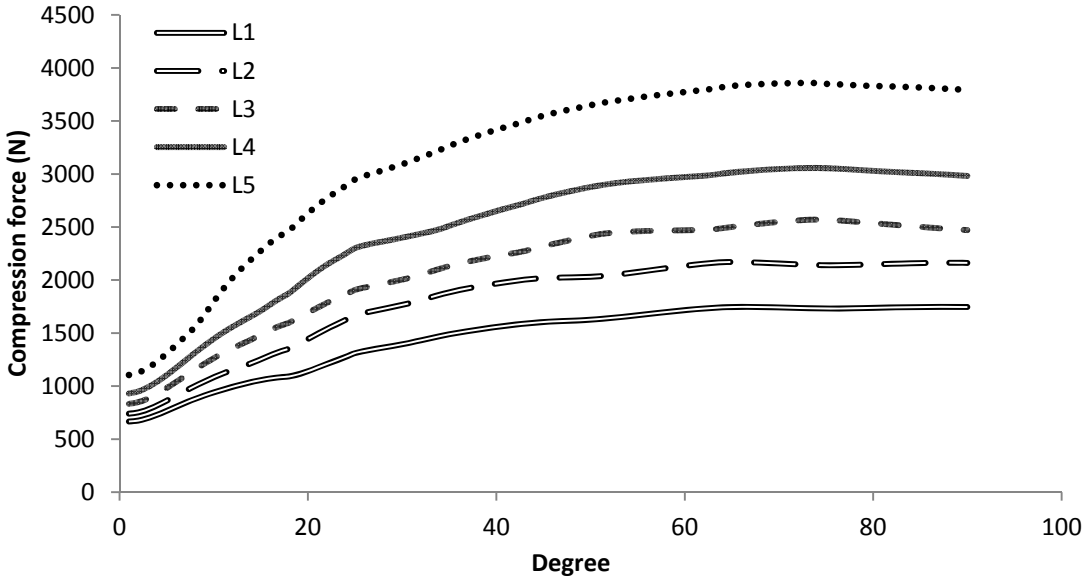

Figure 4-5: Compression forces on the discs during lifting away from the chest

4.3 Case Study II: Stooping and squatting

To examine more dynamic loading situations, the model was made to lift a load from a height of ~53 cm (certain height) by squatting and stooping. Stoop lift and squat lift were carried out without load and with loads of 180N and 195N. Simulation was performed for five seconds and four types of data were obtained: thorax rotation, compression forces, shear forces and bending moments. In stooping with load and without load, hip, knee and ankle joints were stabilized during the lift while rotating the pelvis to 45 degrees and lumbar spine at its maximum rotation. The upper body of the model was considered rigid so there were no discs from L1 to the neck. To create rotation between the upper body and lumbar spine, a custom joint was placed between L1 and thorax to rotated six degrees more in the forward direction. In squatting, hip was rotated 30 degrees, knees 90 degrees and ankles 60 degrees. The pelvis rotation was limited to 45 degrees for stooping and 26.3 degrees in squatting in forward direction based on literature (see Figure 4-6). For the lumbar rotation in stooping, the allowable rotation for each disc was around five degrees during the running of the model; the disc between L1 and L2 rotated slightly more than five degrees whereas the other four discs rotated less than five degrees. Trunk rotation for the squatting with load of 195N and stooping with load of 0N and 195N is shown in the Figure

(4-7) whereas Figure (4-8) shows the same type of movements with load of 0N and 180N for both squat lift and stoop lift.

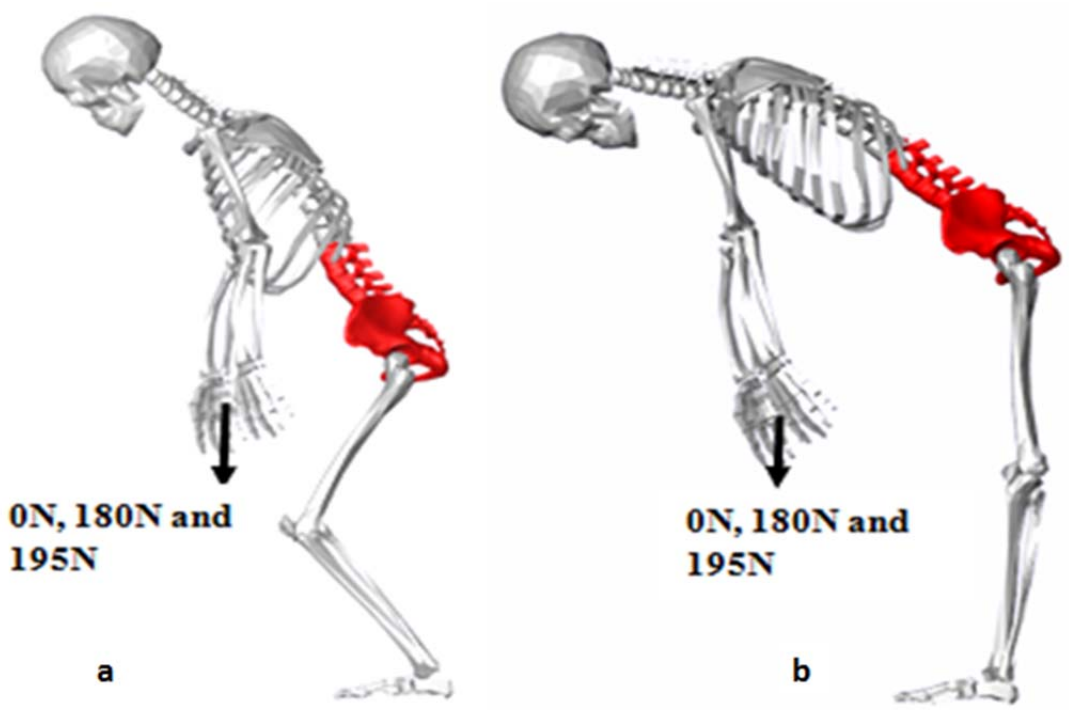

Figure 4-6: Lifting activities: (a) Squat lift, (b) stoop lift with load of 0N, 180N, and 195N

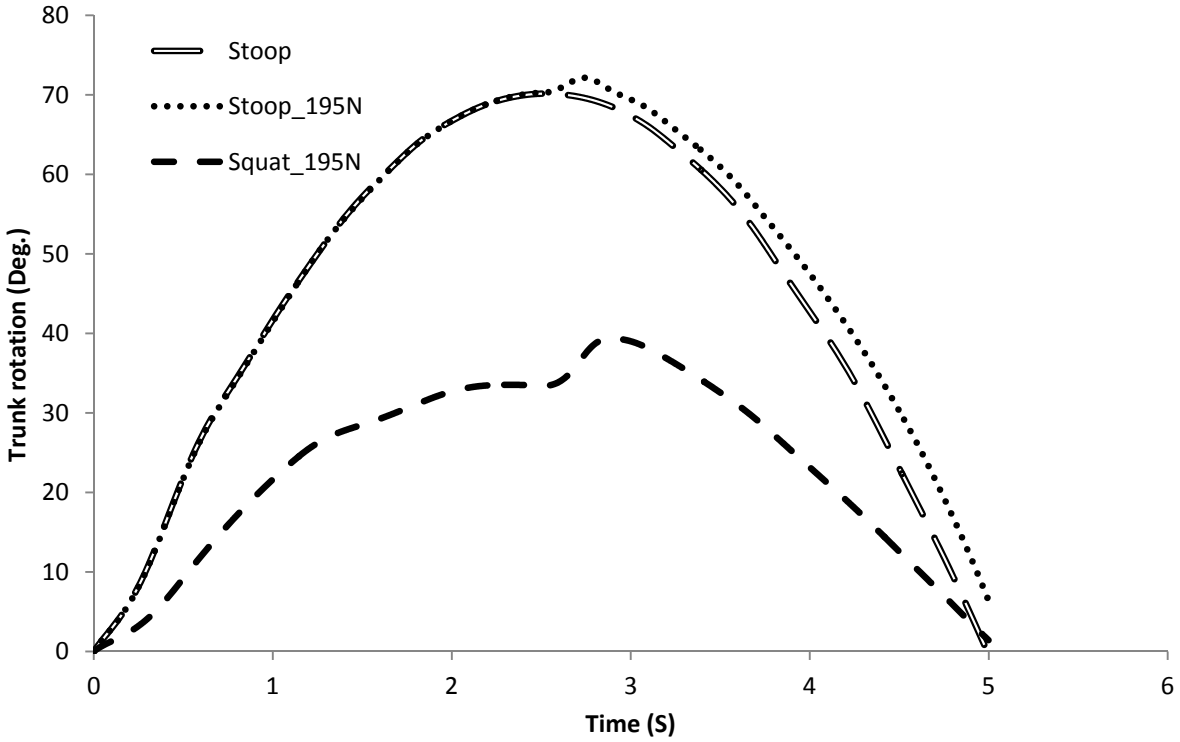

Figure 4-7: Trunk Rotation for squat 195 N and stoop lift with load of 0 N and 195 N

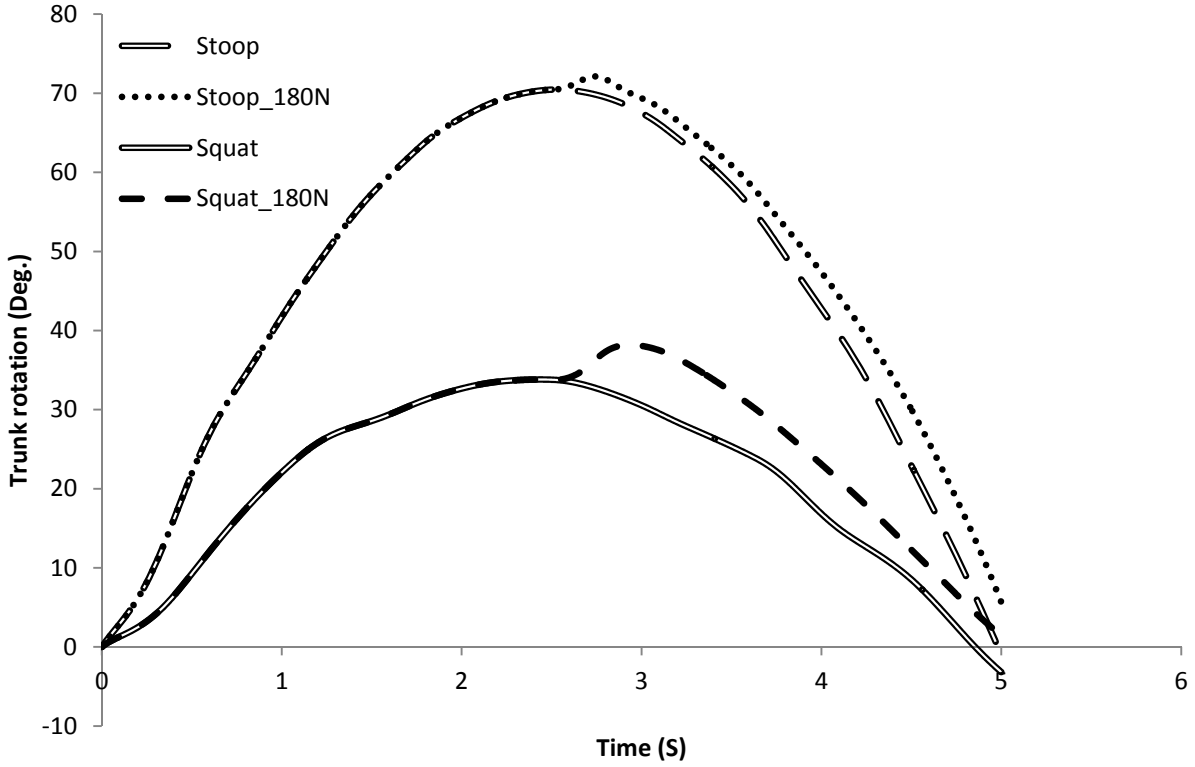

Figure 4-8: Trunk Rotation for squat and stoop lift with load of 0 N and 180 N

In stooping, the figure shows the maximum thorax rotation of 70 degrees at 2.5 seconds with or without load. In squatting, the trunk rotation for lifting the load is higher than the one without lifting the load. This can be explained this way: as the model lifted the load, the gravitational force pulled the body forward and allowed the trunk to rotate about five degrees further until muscles' force balanced the spine. This kind of major change was not observed in the stoop movement but a rather subtle change was observed in the trunk rotation as can be seen in the Figure (4-7 and 4-8). For stooping movement, all five lumbar discs were allowed to rotate a maximum of five degrees, allowing the whole trunk to be fully extended. This is why after lifting a load of 180N the trunk rotated only a few additional degrees. Another change observed for the graphs of both stooping and squatting after picking up the load, was an upward shift as compared with the movements without the load. These changes observed between the two curves were due to the gravitational force applied on the body which requires more force to pull the body from the fully extended position to standing straight. Same types of curves were observed for the cases with 195 N external loads in hands. The only change observed was with squat lift with a load of

195N where the trunk rotated close to two degrees more compared to the squat lift with a load of 180N. In both stoop and squat lifts with and without loads, the half cycles were the same for the trunk rotations which predicted the same compression forces for both activities.

The effect of these two movement patterns is clearly indicated in intradiscal loadings shown in Figures (4-9 and 4-10). The maximum compression forces were recorded on disc L5/S1 for all the activities. The maximum compression force on same disc for squat lift and stoop lift with load of 180 N were measured to be 4119N and 4909N, respectively. The compression forces on disc L4/L5 for stooping and squatting with load of 195N were measured to be 3886N and 3390N. Compression forces for all discs are shown in the Table (4-2 and 4-3) for both stoop lift and squat lift for all three loading condition (0N, 180N, and 195N). The compression forces for squat and stoop lifts without load and with loads of 180N and 195N for all lumbar vertebral discs are shown in the Appendix (A).

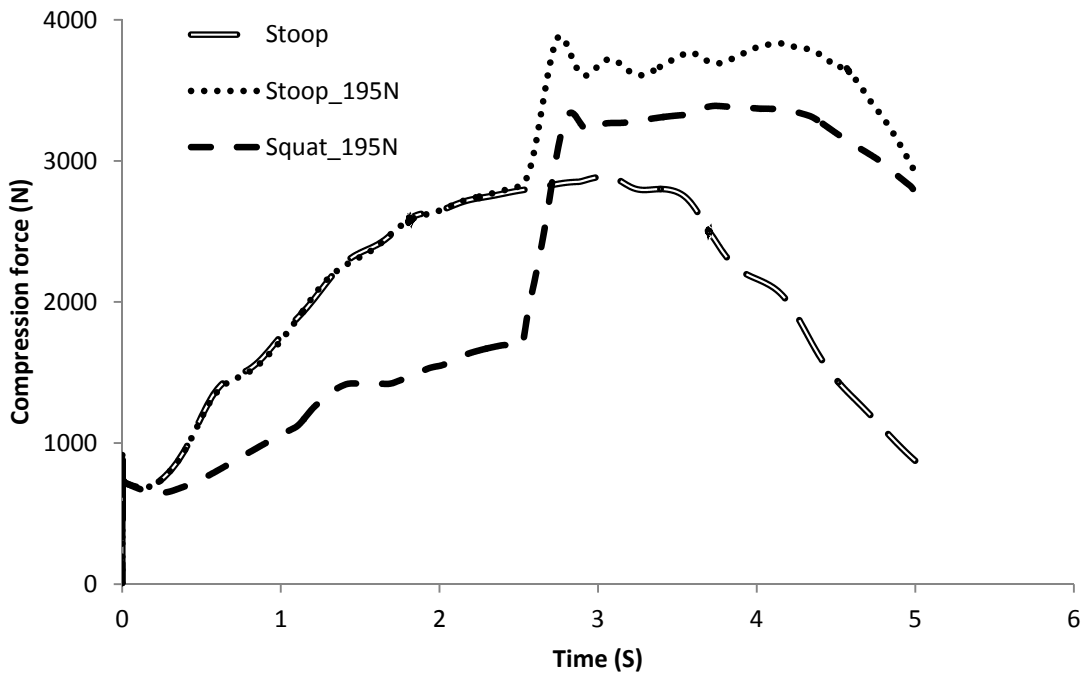

Figure 4-9 : Compression force on discs between L4-L5 for squat 195 N and stoop lift with load of 0 N and 195 N

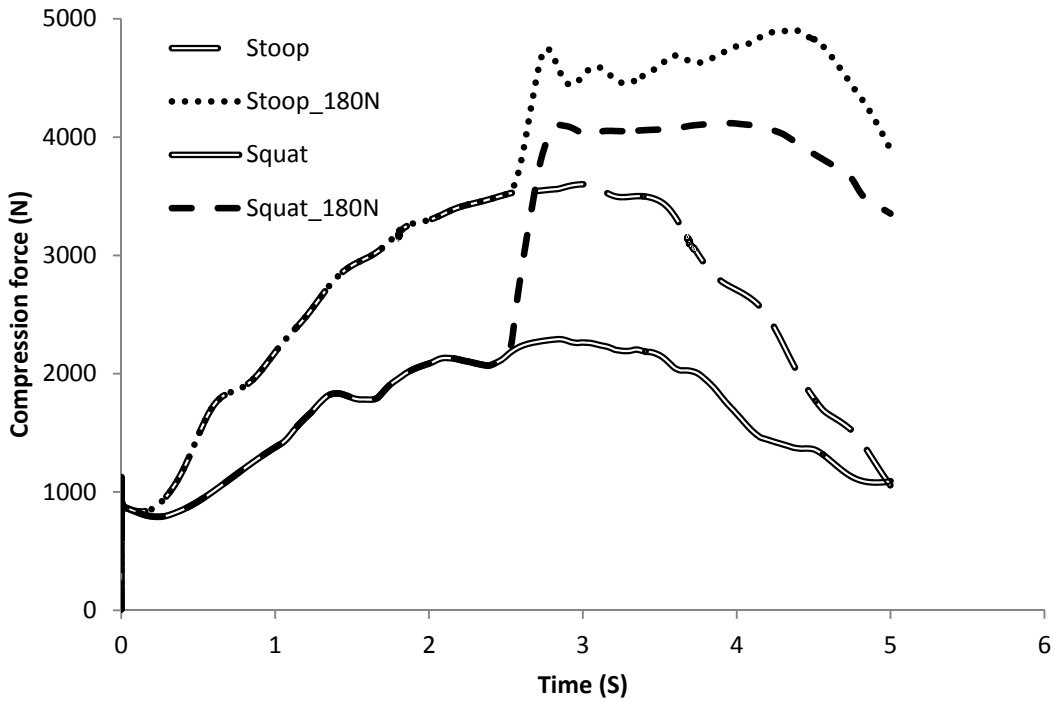

Figure 4-10: Compression force on discs between L5-S1 for squat and stoop lift with load of 0N and 180N

Table 4-2: Maximum internal loads measured in spine for different cases at various level; Compression force, C (N), local anterior shear force, S (N), and Passive ligamentous moment, M (N.m)

Lumbar discs	Squat (0 N)			Stoop (0 N)			Squat (180 N)			Stoop (180 N)		
	C	S	M	C	S	M	C	S	M	C	S	M
L1/L2	1088	138	23	1627	222	66	2003	233	46	2150	328	86
L2/L3	1326	34	13	2074	76	36	2404	106	23	2693	107	48
L3/L4	1517	56	10	2587	119	22	2870	95	18	3402	166	31
L4/L5	1820	134	12	2953	259	23	3325	225	20	3889	358	31
L5/S1	2292	262	20	3602	453	42	4119	430	38	4909	612	56

Table 4-3: Maximum compression forces and pressures on the lumbar for different cases with load of 0N and 195N

Compression forces/Pressures on Lumbar discs	Stoop (0 N) 30.52kg		Squat (195 N) 30.52kg		Stoop (195 N) 30.52kg	
	(N)	(MPa)	(N)	(MPa)	(N)	(MPa)
L1/L2	1590	0.91	2058	1.18	2179	1.25
L2/L3	2027	1.03	2467	1.25	2688	1.36
L3/L4	2529	1.38	2935	1.60	3399	1.86
L4/L5	2889	1.61	3390	1.89	3886	2.17
L5/S1	3520	1.95	4180	2.31	4980	2.76

The difference in compression forces for both loadings (180N and 195N) was very low except for disc L5-S1. The main reason for these little changes in the compression forces was thought to be due to difference in upper body weight and external loads. As stated in earlier chapter that in lifting the load of 180N for both activities, 74 kg of a total body weight was considered (mean value of the subject from the literature by Bazrgari et al. [6] whereas for lifting a load of 195N, the total body weight was considered as 70 kg according to the literature review by Wilke et al. [29]. Using the anthropometric data, the upper body weight was calculated to be 32.26 kg and 30.52 kg for lifting 180N and 195N, respectively. Therefore the external load of 195 N compared to 180N did not create much difference in compression force. However, the external load increased the compression forces in stoop lift as compared to squat lift with maximum difference reaching ~800N for disc L5-S1 (in both cases of 195N and 180N).

As apparent from the graph, the compression force increases gradually after picking up the load. When a person lifts the load, brain sends a signal to the nervous system to activate, the muscles and as the muscles get activated the nervous system varies the muscle forces by varying the simulation frequency or changing the number of motor units that are activated at a given time [84]. This process may take up to one third to half a second depending on the load. In present case study, time duration of 0.2 second was used to lift the load of 180N and 195N. A similar rate has been used in the literature [6]. Also the compression forces for both stoop and squat lifts without loads were higher for later half of the cycle (from forward flexion to upright position) compared to first half of the cycle (from upright position to forward flexion). This is a depiction

of real human body scenario according to which body requires more gravitational force to pull the trunk from forward flexion to upright position.

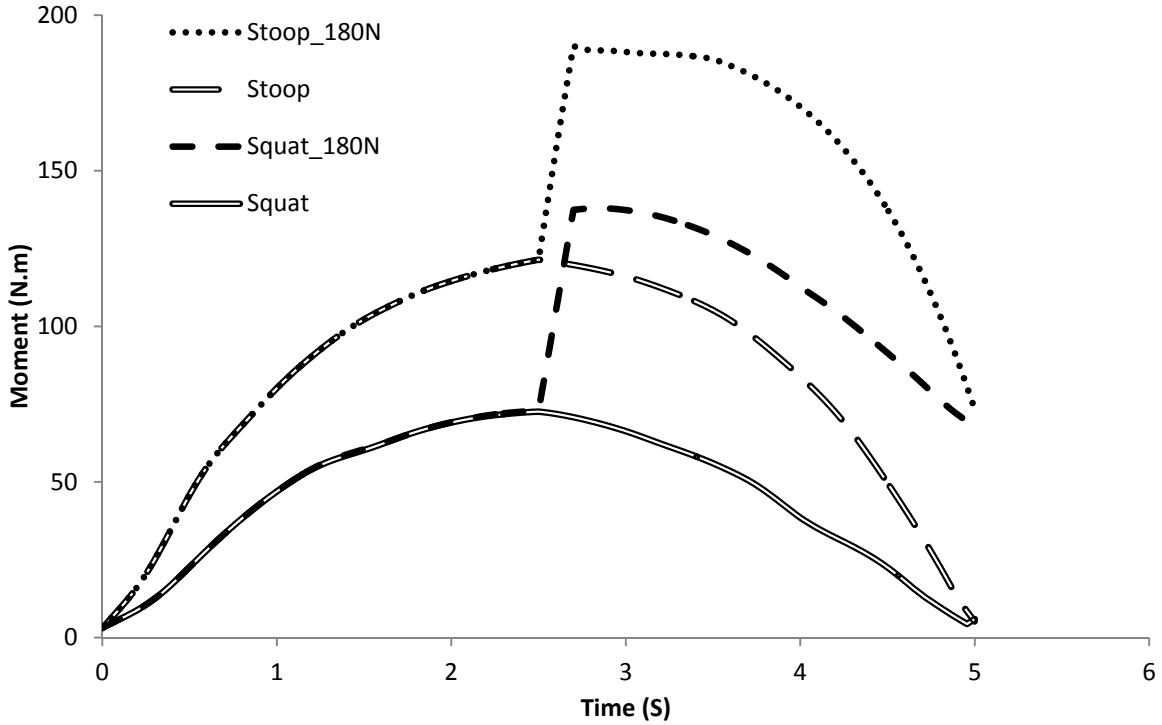

Figure 4-11: Net external moment at the L5-S1 level for stoop and squat lift without load and with load of 180N

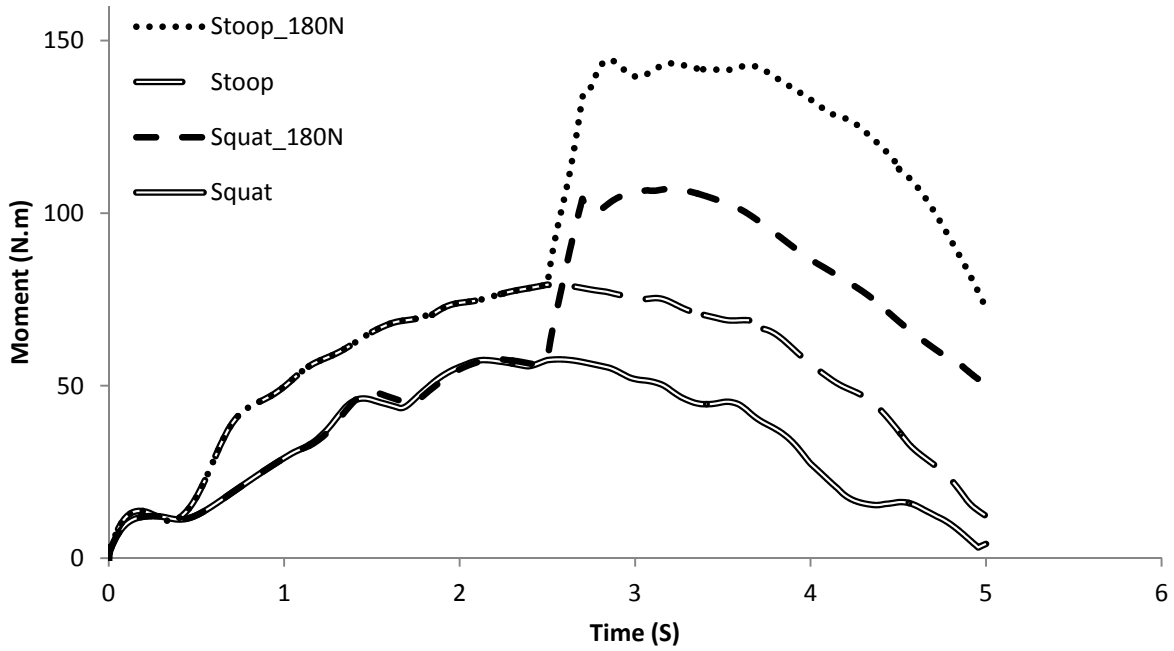

Figure 4-12: Portion of the moment resisted by the muscles on disc L5-S1 during lifting

For zero loads, the maximum passive ligamentous moments at L1-L2 was recorded as 66Nm and 23Nm for stoop and squat lift, respectively. At the same disc, moments for stoop and squat lifts with load of 180N were obtained to be 86Nm and 46Nm respectively. These occurred at time of maximum trunk rotation. The maximum external moments were measured on the disc between L5-S1, where stoop lift showed greater moment compared to squat lift. Same trend was observed even with carrying the load of 180N for both movements (stoop and squat lifts). The net external moments were higher by ~40% and ~26% in stoop lift as compared with squat lift while carrying the load of 0N and 180N, respectively. Similar results were obtained for passive ligamentous moments where the moments were higher by ~52% and ~34% in stoop lift compared to squat lift for no load and a load of 180N. Furthermore, the muscle moments were higher for stoop after lifting the load of 180N (higher by 3%) compared to squat lift. This indicates that the moments were primarily carried by passive ligamentous spine but after applying the external loads, some portions of the moments were resisted by the muscles. Figure (4-11 to 4-13) shows the predictions of the external moments, muscle moments, and passive ligamentous moments. The passive ligamentous and muscle moments were higher in stoop lift due to the larger intersegmental rotation of the lumbar spine. In both stoop and squat lift cases with load in hands, the passive ligamentous, muscle and external moments were increased abruptly as the load reached its maximum value of 180 N. After reaching its peak point, external moments and muscle moments curve decrease gradually while the passive ligamentous moments decrease abruptly. The passive ligamentous moments for squat and stoop lifts without load and with loads of 180N and 195N for all lumbar vertebral discs are shown in the Appendix (B).

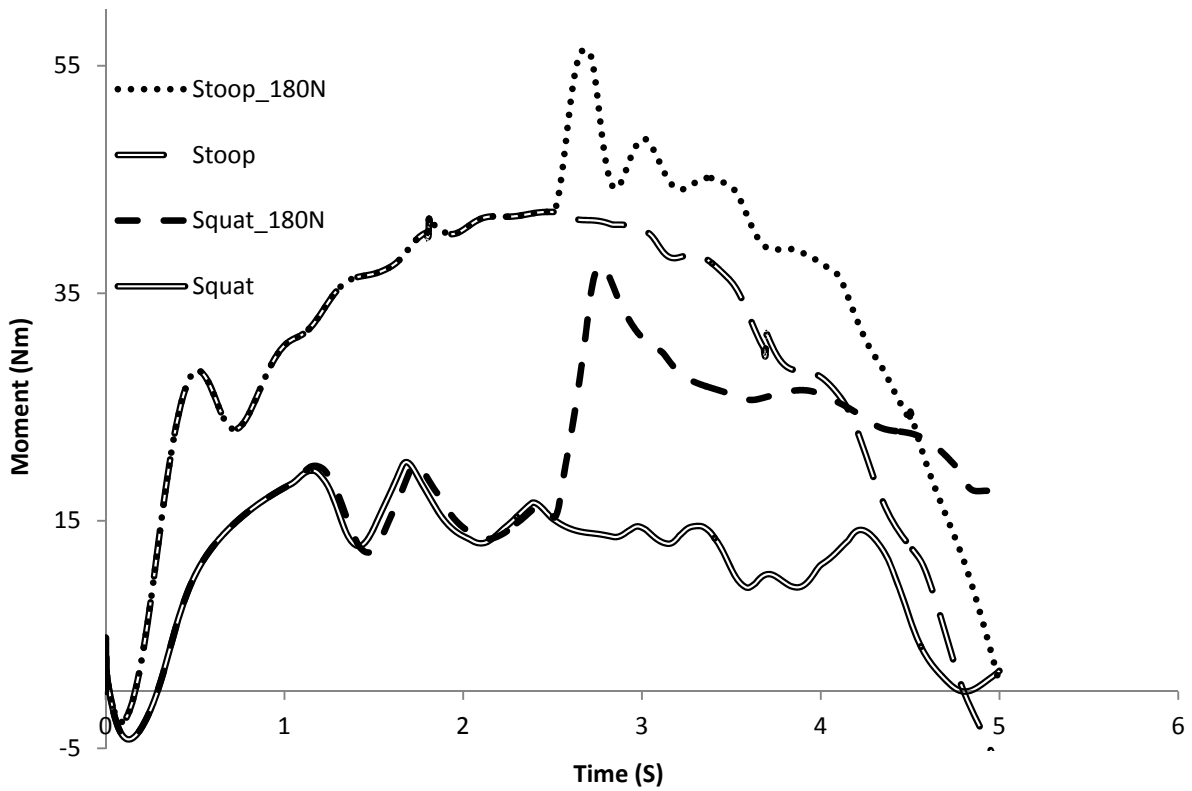

Figure 4-13: Passive ligamentous moment during squat and stoop lifts with load of 0N and 180N

The maximum shear forces were also measured on the disc between L5-S1 for all activities. Stoop lifts showed greater shear forces as compared to squat lifts, in a pattern similar to moment curves. Shear forces were increased by ~73% and ~43% in stoop lifts as compared to squat lifts without load and with load of 180N for disc L5-S1 (see Figure 4-14). As the external loads were applied to the hands, the difference in shear forces was reduced by ~30% for disc L5-S1. These can be interpreted as some portion of shear forces being resisted by the muscle forces. Anterior shear forces were higher in stoop lift due to the larger trunk rotation resulting in larger lever arm with respect to S1 as compared with the squat lift. The calculated shear forces showed sudden increase from L4-L5 level to L5-S1 level for both cases when loads in hands were applied. Also, as the simulation progressed, shear forces from L4-L5 level increased and L5-S1 level decreased so the difference became smaller in between the two levels for squat lifts while this changed was not seen in stoop lift. The lowest shear force was found on disc between L2-L3 for stoop and disc between L3-L4 for squat lift. The shear forces for squat and stoop lifts without load and with load of 180N for all lumbar vertebral discs are shown in the Appendix (C).

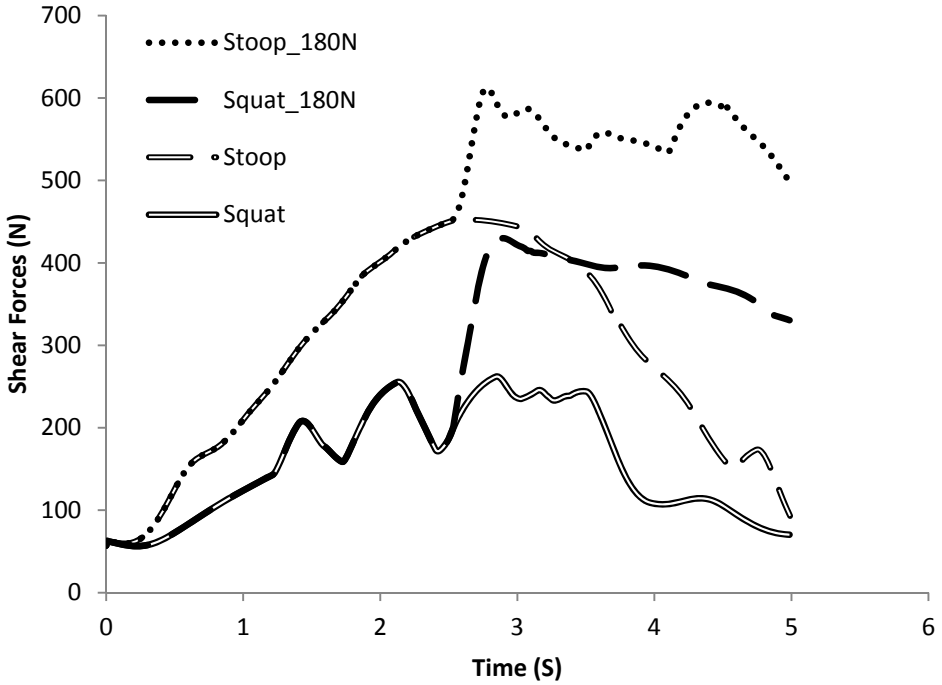

Figure 4-14: Anterior shear forces at the L5-S1 level for different cases

4.4 Gym Squat (Improper and proper squatting)

This case study was carried out to evaluate the risk of lower back injury by not using the proper techniques to lift a load. To examine these kinds of activities, barbell squat lifts were considered. In proper squatting, thighs, knees and ankles are rotated while keeping the back as straight as possible with both hands vertically folded from the elbow to carry the load. Load of 20kg was placed on the shoulder supported by two hands as the spine goes down without further bending. In improper squatting same process is repeated with the same rate while going down but during lift ankles and knees come faster than the thighs which causes spine to tilt forward. Figure (4-15) shows the improper and proper barbell squatting postures.

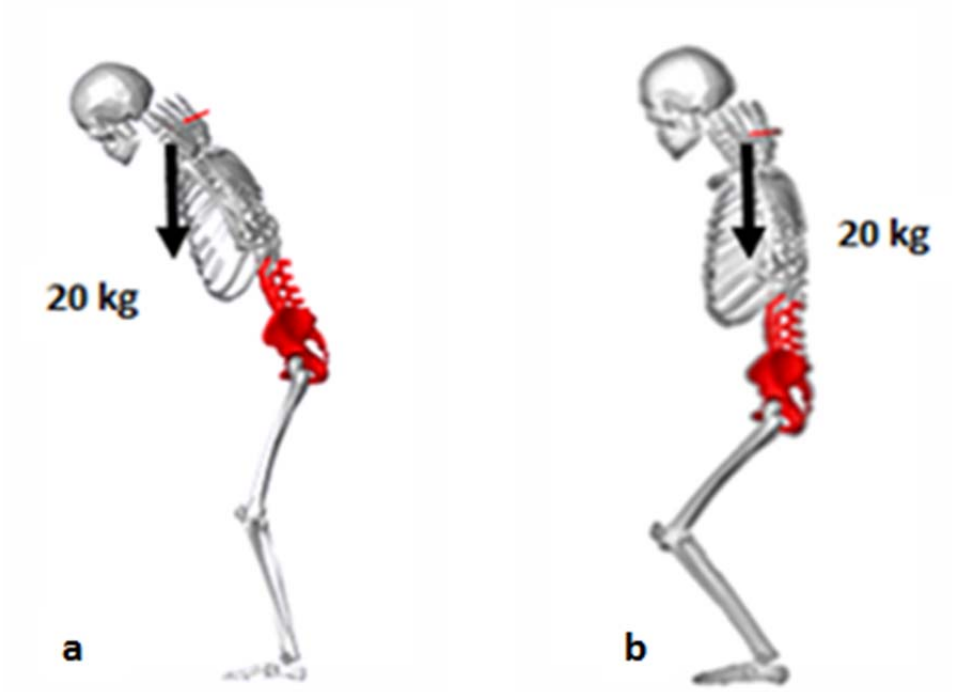

Figure 4-15: (a) Improper and (b) proper gym squatting

The differences in compressive forces experienced by intervertebral disc for the two cases are shown in Figure (4-16). The maximum reaction forces recorded on disc L5/S1 for proper and improper squatting were 5168N and 6688N, respectively. Figure (4-16) indicates the change of these compressive forces as squatting progresses. Difference between the compression forces as knees and ankles increase the rate of squatting as compared to the thighs.

As shown in Figure (4-17) after roughly five seconds, the compression forces in improper squatting increase by ~30% compared to proper squatting. This is due to the extra pelvis rotation in improper squatting compared to proper squatting. To find the pressure between the discs, same procedure was applied as described in section 4.2.1. The maximum intradiscal pressures for proper and improper squatting were calculated as 2.86 MPa and 3.70 MPa in the disc L5-S1 while lowest maximum pressures were calculated as 1.31 MPa and 1.41 MPa on disc L1-L2.

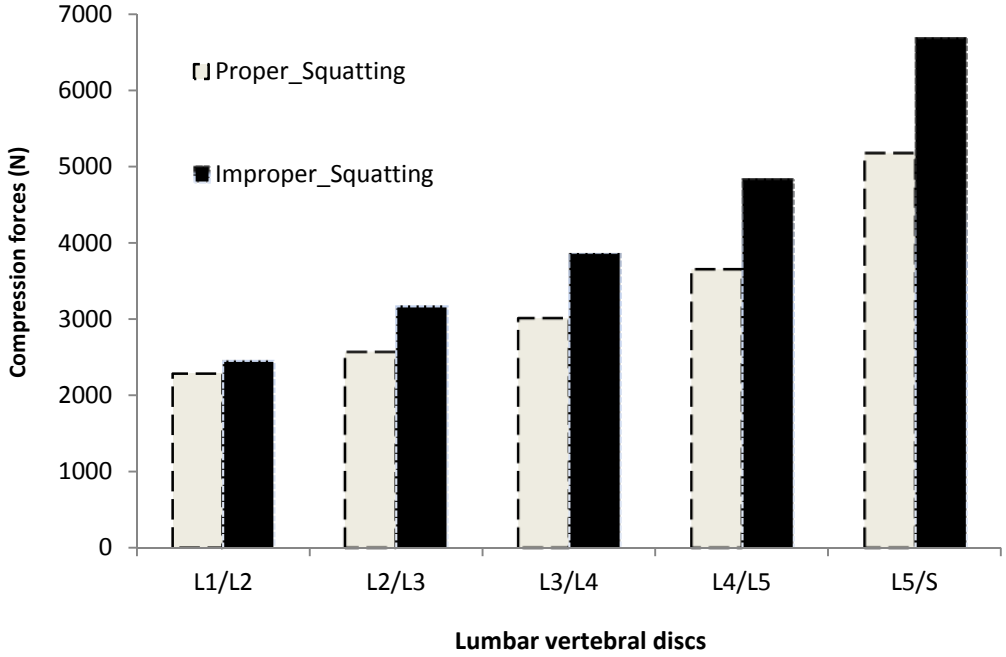

Figure 4-16: Maximum compression forces measured on lumbar discs during good and bad squatting

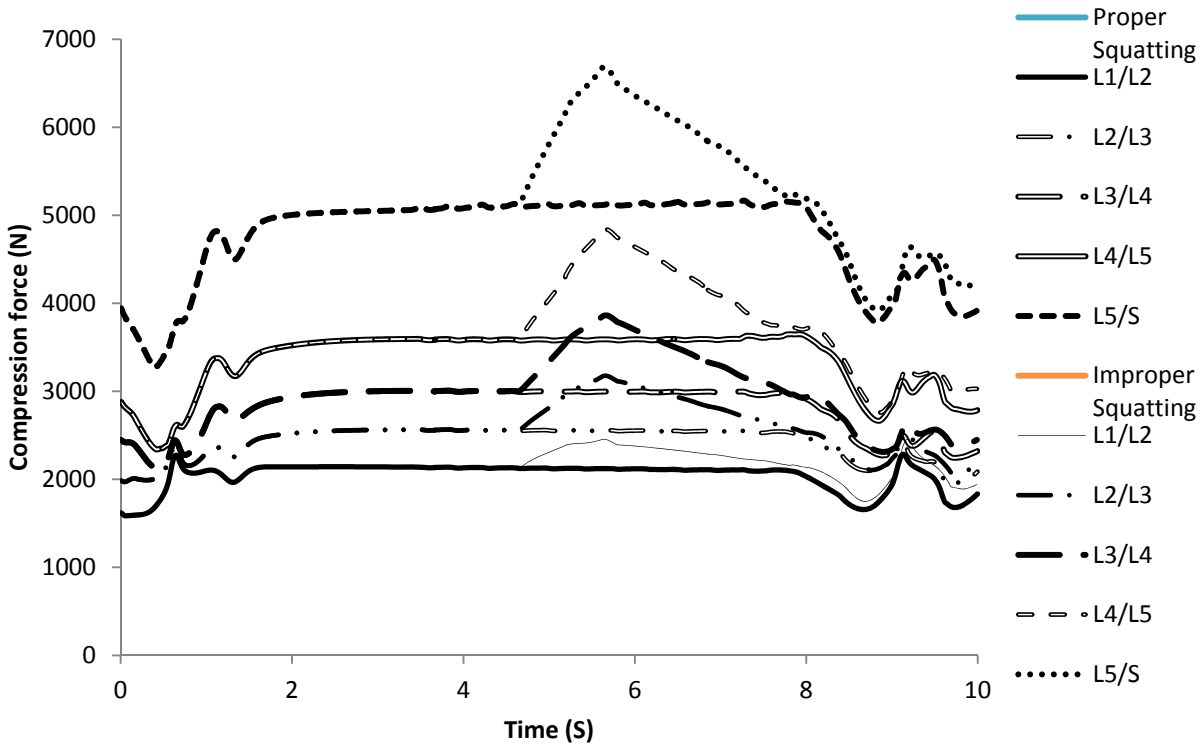

Figure 4-17: Comparison in compression forces between proper and improper (gym) squatting

4.5 Case study III: Full model

As described in section 3.3.6, the full model consists of 38 local muscles attached to the vertebrae and eighth global muscles attached to the thoracic cage. In this case study some of the activities from case study I and II were repeated to analyze the mechanical behaviour of the full lumbar spine model. Only compression forces were measured due to the time constraints. For free standing and lifting the load of 195 N close to and away from the chest, the full model predicted similar results for disc L4-L5 when compared with simplified model. The differences were 7%, 8% and 9%, respectively (see Figure 4-18). The maximum compression force in both full and simplified model was observed at L5-S1.

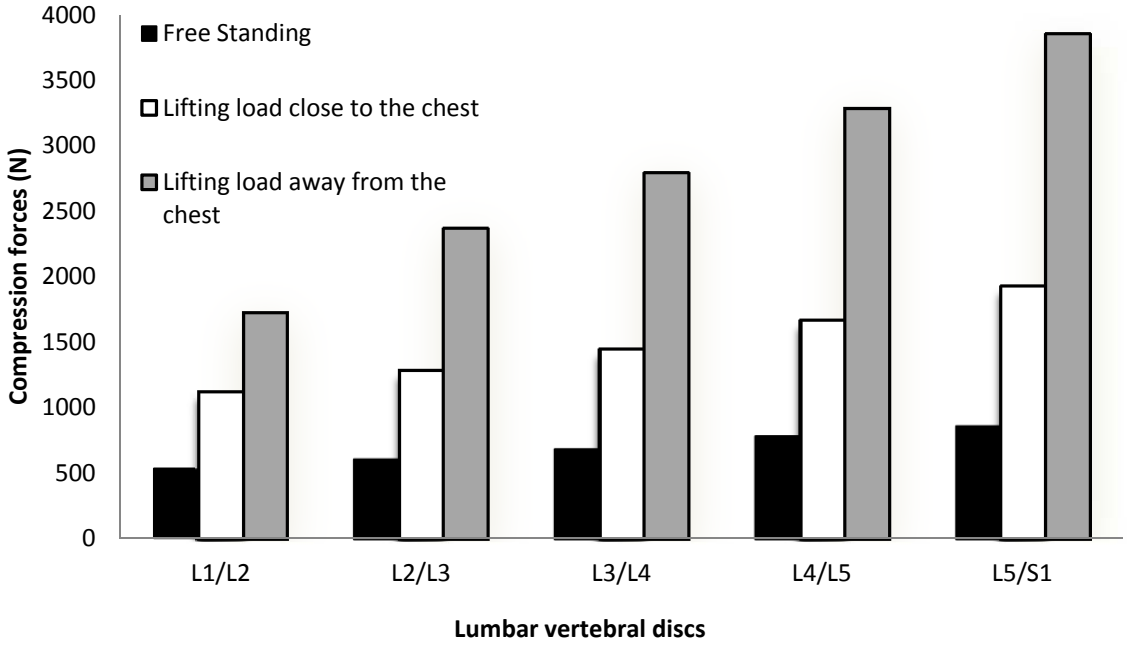

Figure 4-18: Compression forces on the lumbar discs during relaxed standing and isometric lifting the loads close to the chest and away from the chest by full model

In full model the intradiscal pressures for all three activities, free standing and lifting load away from and close to the chest were found to be 0.39 MPa, 0.95 MPa, and 1.72 MPa, respectively.

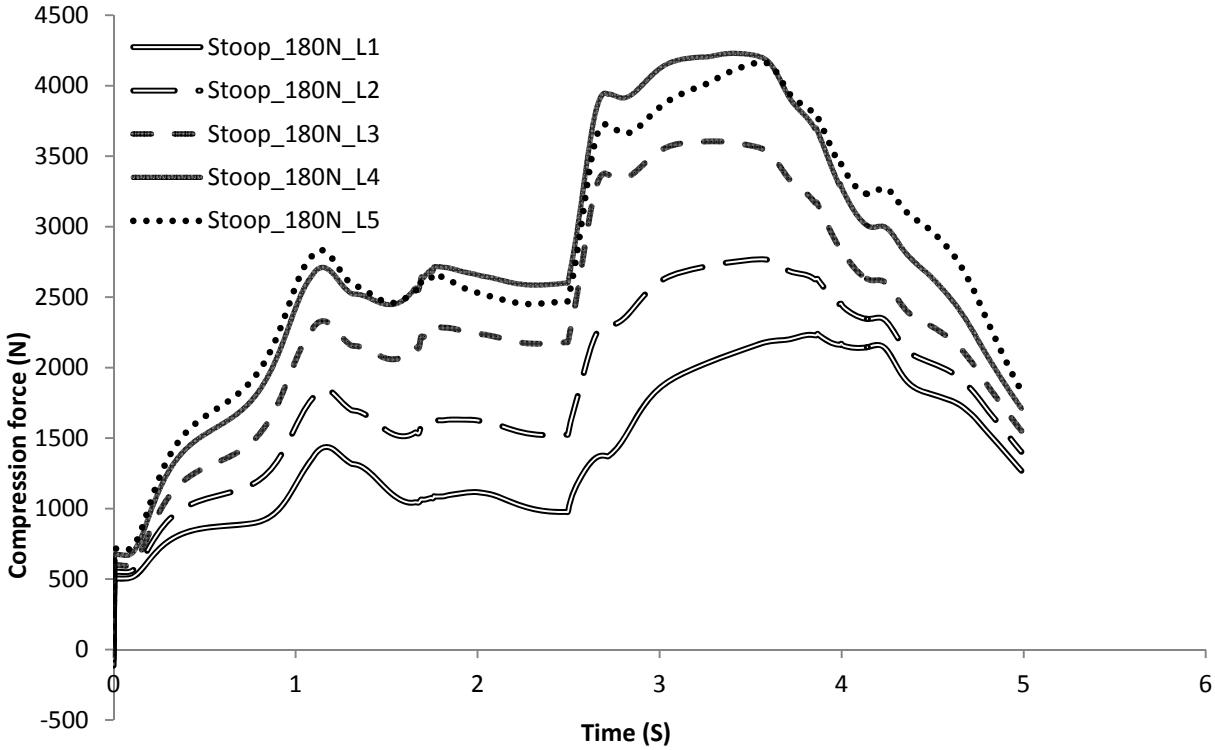

Figure 4-19: Compression forces on the discs for stoop lift with load of 180N

Stooping with load of 180N was performed using full model to obtain the effect of the muscles. Same anthropometric data and pattern of lumbar and thorax movement was used as described in section 4.3. The results obtained for the thorax rotation and compression forces were similar to those obtained by the simplified model expect for the compression force result for disc L5-S1 (Figure 4-19). The main reason for the difference in result was due to the inclusion of greater number of muscles. The inclusion of more muscles might have caused the segments L4-L5 and L5-S1 to behave as a single segment and hence similar values were obtained for both.

Chapter 5: Discussion

5.1 Introduction

The main purpose of the case studies presented in previous chapter was to validate the forward kinematics model by comparing the results with *in vivo* intradiscal pressure measurements and the results from dynamic model provided in the literature [6, 29]. Dynamic model is in which the task is dependent of time whereas in static model the task is independent of time. The proposed model is capable of measuring both static and dynamic tasks and the results predicted by this model could also be useful in understanding the significance of postures while lifting loads.

5.2 Case study I:

In the simplified model the intradiscal pressures were measured for three different postures at disc L4-L5; free standing with no load and lifting the total load of 195 N closed to the chest and 60 cm away from the chest. Using the disc area of 17.9 cm^2, the intradiscal pressure was calculated between the discs L4-L5 and compared with the *in vivo* intradiscal pressure measurements [29]. The results of the intradiscal pressures were in good agreement with those in the literature with the difference of 15%, 5% and 9% as compared with in vivo intradiscal pressures of 0.48 MPa, 1.0 MPa and 1.8 MPa, respectively [29]. Some of this discrepancy can be attributed to the fact that the forearms and upper arms angles were not specified in the literature [29].

Also, the effect of the loads on the thorax rotation was not shown in the work of Wilke et al. [29]. In the proposed model, thorax moved in forward direction while lifting the load close to the chest and the thorax was tilted backward while lifting the load away from the chest.

There are other factors which would have created minor differences in the results such as the centre of gravity of load and the fact that instead of point loads the subjects in literature carried a full crate of beer. The intradiscal pressure and compression forces for all five discs for all three activities are shown in the Table (4-1).

5.3 Case study II:

For the second case study, the results of the compression forces and moments on the discs between L5-S1 and thorax rotation for stoop and squat lifts with load of 180N and 0N were compared with Bazrgari et al. [6]. The same activities were repeated with load of 0N and 195N with different body mass and compared with in vivo intradiscal pressure measurement provided by the literature for the disc between L4-L5 [29].

The trunk rotations were found well within the range except for squat lift with 0 N loads as well as some minor differences in stoop lifts. Rotation obtained for the thorax was lower compared to the prescribed thorax rotation in the literature for squat lift with load of 0 N Bazrgari et al [6]. The difference in thorax rotation for squat lift with 0 N was mainly due to the lumbar rotation. The proposed model encountered ~50% lower lumbar rotation while the pelvis rotations were predicted approximately same as prescribed rotations in the literature. The trunk rotation in the squat lift was increased by approximately five degrees after lifting the load which was not seen in the literature. In stoop lifts and squat lifts the thorax and pelvis rotations with load and without load for first half cycle were over lapping in proposed model whereas in vivo measurements of the thorax and pelvis rotations were shifted toward left after lifting the load. The main reasons for the shift in curves in Figure (4-5,4-6) for the prescribed rotations were due to the lack of instructions in lifting the load as well as the measurements were based on the mean values of 11 subjects; and the data was smoothed by a sixth order polynomials filter.

The compression force on the disc L5/S1 was found higher in all activities for load 0N and 180N whereas other discs reported lower compression forces except for stoop lift with 0N (see Table 4-2) compared to the Bazrgari et al. [6]. The maximum passive ligamentous moments in the proposed model were measured on disc L1-L2 and were found higher compared to literature for all activities whereas the net external moments, moments resisted by the muscles and anterior shear forces were measured higher on disc L5-S1 but were found to be lower compared to the Bazrgari et al. [6] data.

Both the proposed model and reference literature showed sudden increase in compression forces, shear forces and moments after lifting the load in both activities (stoop lifts and squat lifts). In the literature, the compression forces, shear forces, and moments increased sharply to their

maximum values and decreased suddenly while in the proposed model, the compression forces increased sharply to a point and then gradually reached their maximum value. In the results for proposed model, shear forces and moments also increased sharply and reached its maximum point but decreased gradually. Recent model showed higher difference for compression forces between the stoop lift and squat lift without load with maximum difference reaching 1310 N compared to the reference value of ~200N for disc L5-S1, while in stoop lifts and squat lifts with load of 180N the maximum difference in compression forces was measured as ~790N compared to the reference value of ~800N for same disc. For net external moments, the maximum difference was calculated to be 15% or lower for all activities in current model but shear forces made dramatic decrease for all activities in proposed model for disc L5-S1 compared to reference data. The compression forces, anterior shear forces and passive ligamentous moments are shown in the Table (4-2).

The difference in compression forces and moments could be attributed to differences in lumbar rotation at each segment as well as shoulder and forearm rotation.

Similar studies were also carried out by Wilke et al. [29] for stoop lift with no load; and stoop and squat lift with a load of 195 N. The proposed model predicted pressures of 1.61 MPa, 2.17 MPa and 1.89 MPa for the same activities with difference of 0.9%, 6% and 11% compared to the in vivo intradiscal pressure measurements from Wilke et al. [29]. The results obtained by current model were in close agreement taking into account the difference in the load applied in the two studies and the rigidity of the upper body of the subjects. In the current only the pelvis and discs between L1-L5 were allowed to rotate. Wilke et al. [29] only provides anthropometric data for subject but no such information regarding lumbar rotations or upper and forearm movements during lifting. The compression forces and intradiscal pressures for all levels of discs for stoop lifts and squat lift are shown in the Table (4-3).

5.4 Case study III:

In third case study, activities from the case study I and II were repeated using the full model to evaluate the muscle behaviour on the lumbar spine. Results of the compression forces on the disc between L5-S1 for free standing, lifting load of 195N close to the chest and away from the chest and stoop lifts with load of 180N were compared with results from literature [6, 29]. Full model

showed similar results for disc L4-L5 in comparison with Wilke's data for free standing, lifting load close to the chest and away from the chest with intradiscal pressure differences of 8%, 6% and 2%, respectively. Stoop lifts with load of 180N were also found well within the range with maximum compression force difference of 15% for disc L5-S1 in comparison with results from [6]. The results for full model were in good agreement in comparison with the literature and the results obtained by simplified model. Irrespective of the number of muscles, results of the simplified model and full model for all activities were in close agreement with each other. The compression forces, shear forces, moments and lumbar motion can be predicted easily using the simplified model. There is no need for a full model. However, when evaluating the muscle forces; the full model would be preferred due to the use of actual cross section area of the muscles and inclusion of the greater number of muscles in the model as compared to simplified model.

Chapter 6: Contribution, Conclusion and Future work

6.1 Contributions

The main contributions of this research are:

- Development of a lumbar spine model using forward kinematics
- Using widely available software instead of specialized and much more expensive customized software to create the model.
- Elimination of redundancy problem and the need for simplifying assumptions.
- Capability to predict forces, moments and lumbar motions.

6.2 Conclusion

The model presented in this thesis can be used to determine the compression forces, shear forces, moments and motion responses of the lumbar spine using the forward kinematics technique which eliminates the need of optimization based on loading assumptions. The model can easily be modified to evaluate different postures such as standing, lifting, sitting or bending in either direction. Muscles play a vital role in stabilizing the spine so it will be appropriate to include all muscles in a complete model of spine. In the present study, two models of lumbar spine including simplified model and full model were used. Simplified model included fewer numbers of lumbar muscles with larger physiological cross section areas to make model simple without reducing the required muscle force to perform a particular activity. On the other hand, full model included more muscles with actual cross section areas of the muscles to observe the real effect and behaviour of the muscles at each segments of lumbar spine. Results for the free standing, lifting loads and stoop and squat lifts were found in good agreements with experimental results from literature for both models. According to the model, in lifting of loads, lifting load closer to the chest is preferred over lifting load away from the chest in order to reduce compression forces due to the larger lever arm of lordotic posture. Adopting an isometric lifting load close to the chest can reduce muscle forces and internal loads; and increase spine stability. The dynamic models have advocated squat lifts over stoop lifts in reduction of compression forces, shear forces and moments. The forces and moments were larger in stoop lifts compared to squat lift

mainly due to the larger thorax rotation not because of larger lever arm. Model also illustrated that the same rate of change in thighs and knees is required during the gym squatting to lower the compression forces on lumbar spine.

6.3 Future work

To complete the model, thoracic and cervical spine should be included to predict the forces and moments on thoracic and cervical discs as well as to examine the change in present results through modeled lumbar spine. The model should also be examined for twisting and linear translation in all three directions. The model could also benefit from developing adaptive PID controllers which would be more robust and require less tuning effort.

Appendices

Appendix A: Compression forces on discs L1to S1 for all activities

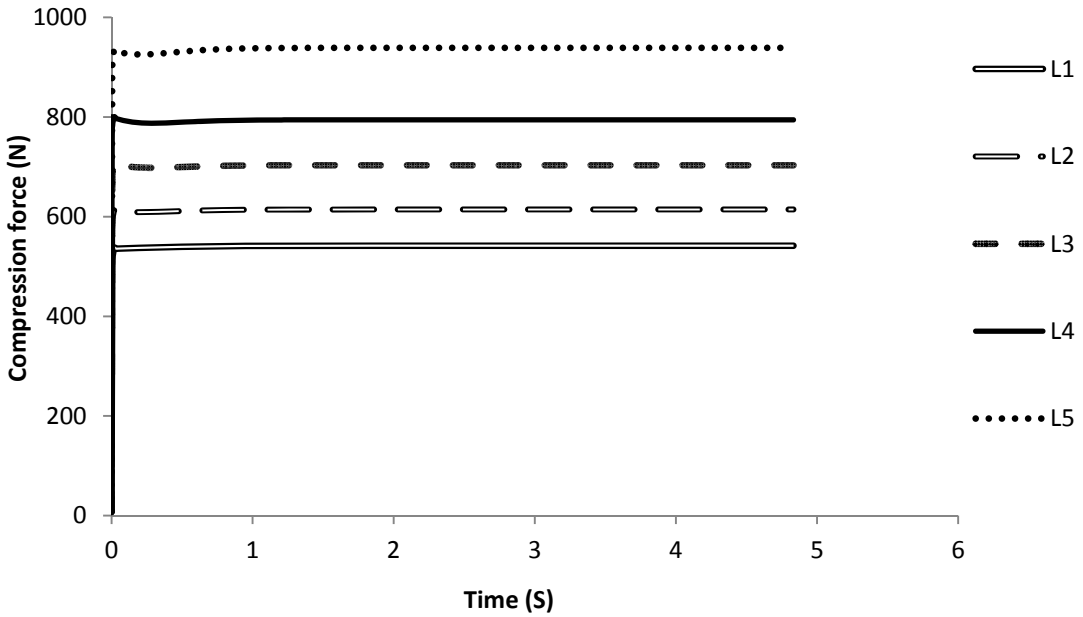

Figure A1: Compression force on discs L1 to S1 for standing free.

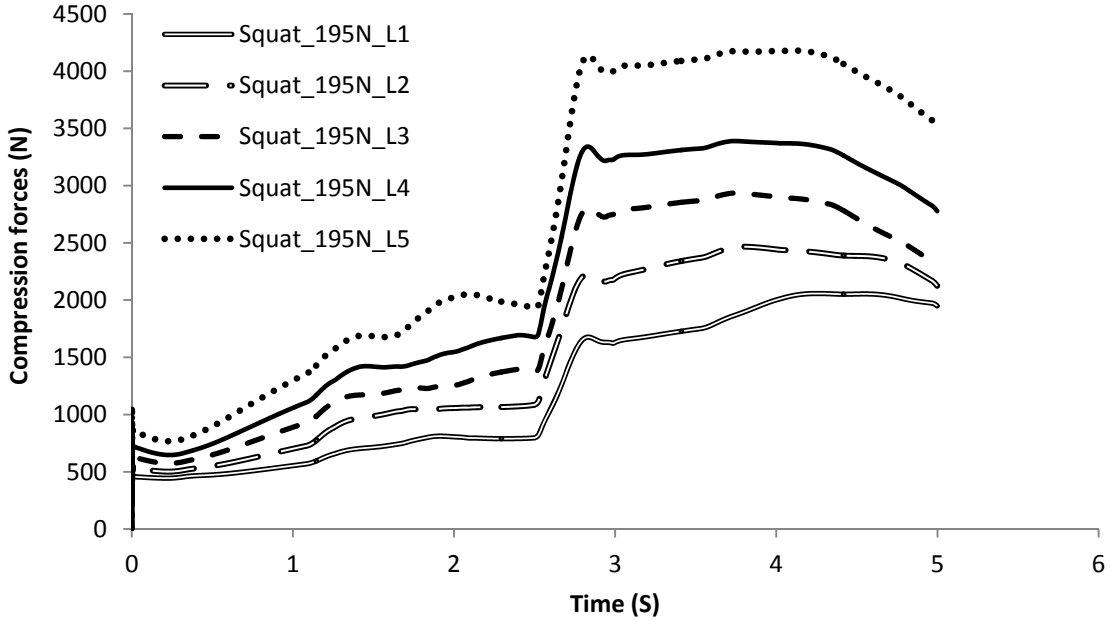

Figure A2: Compression force on discs L1 to S1 for squatting with load of 195N.

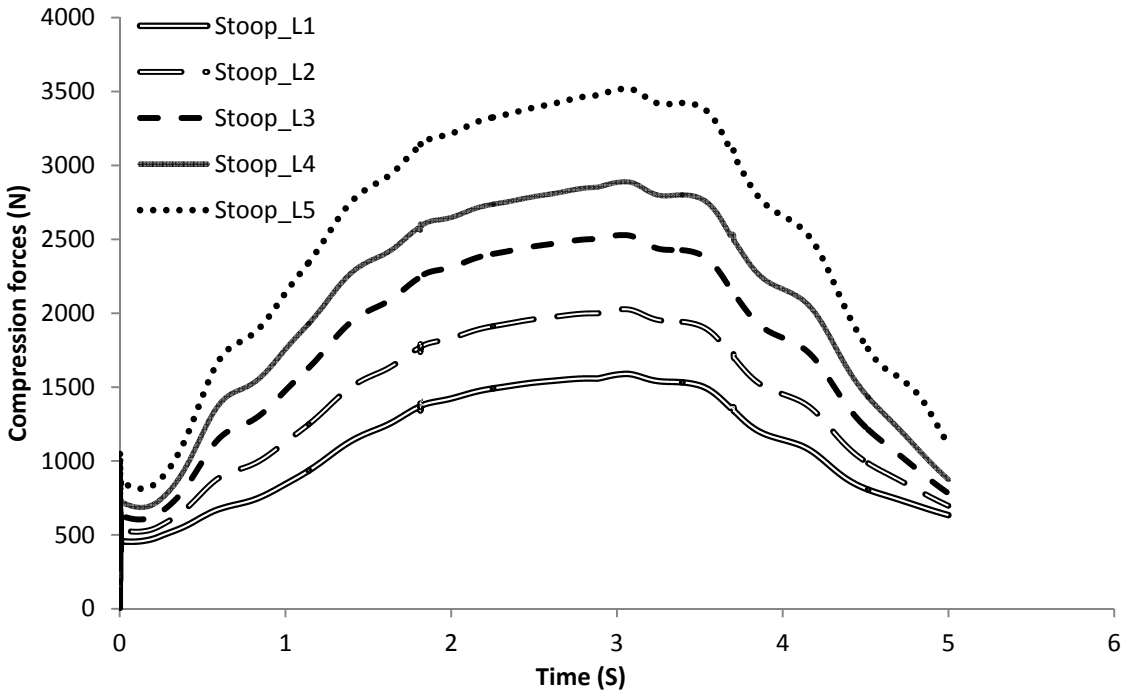

Figure A3: Compression force on discs L1 to S1 for stooping without load.

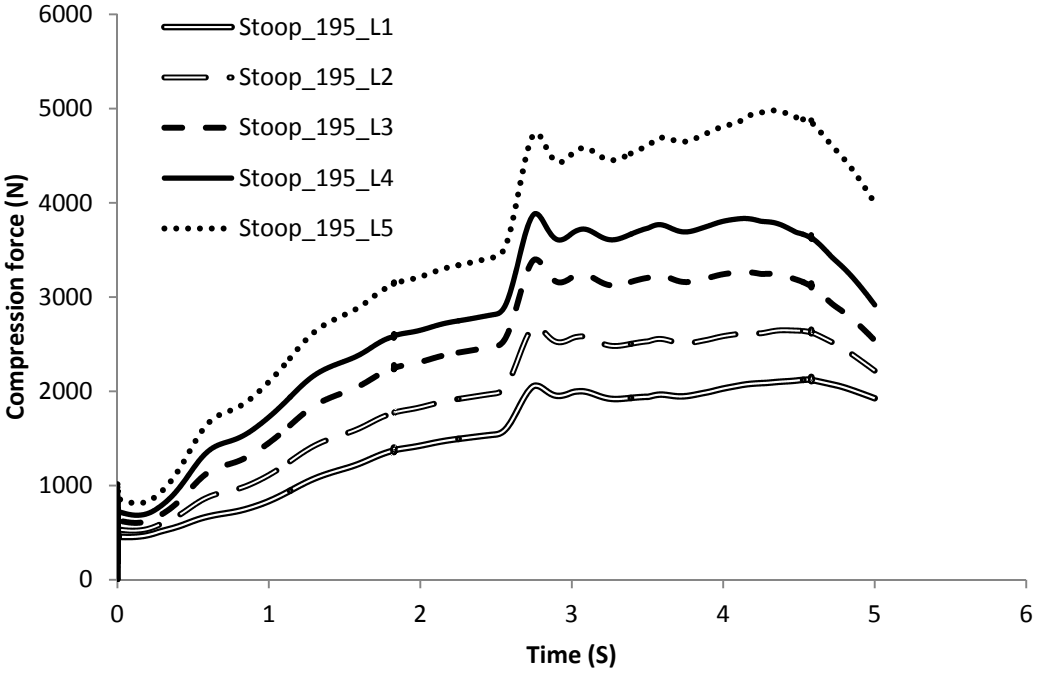

Figure A4: Compression force on discs L1 to S1 for stooping with load of 195N.

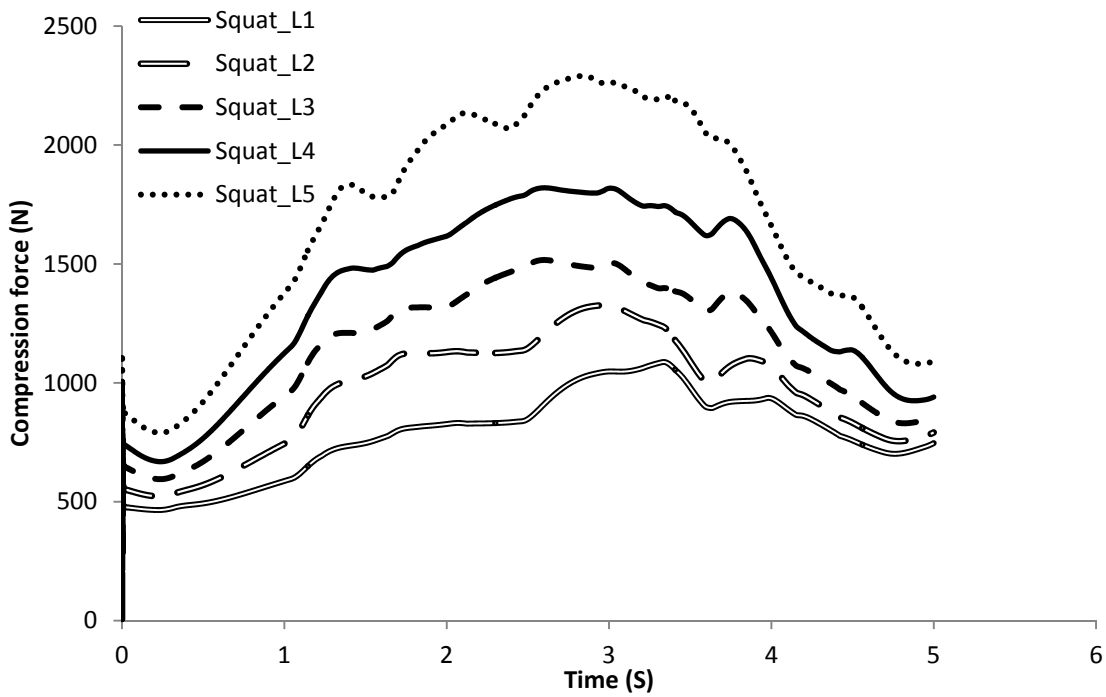

Figure A5: Compression force on discs L1 to S1 for squatting without load.

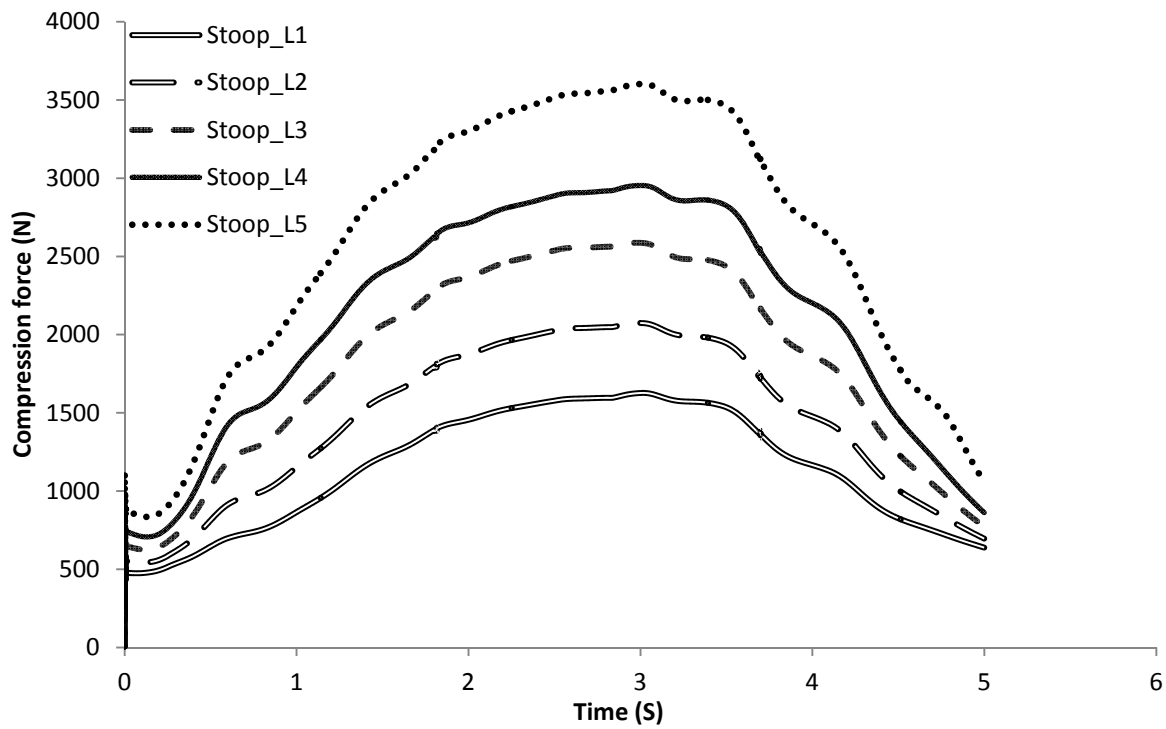

Figure A6: Compression force on discs L1 to S1 for stooping without load.

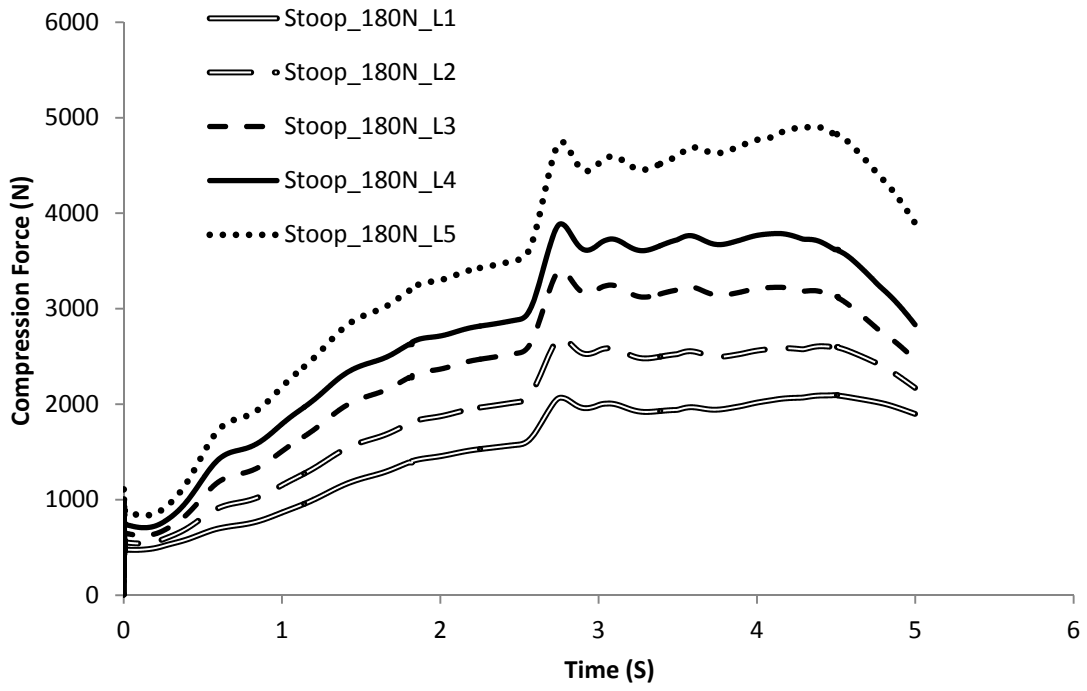

Figure A7: Compression force on discs L1 to S1 for squatting without load.

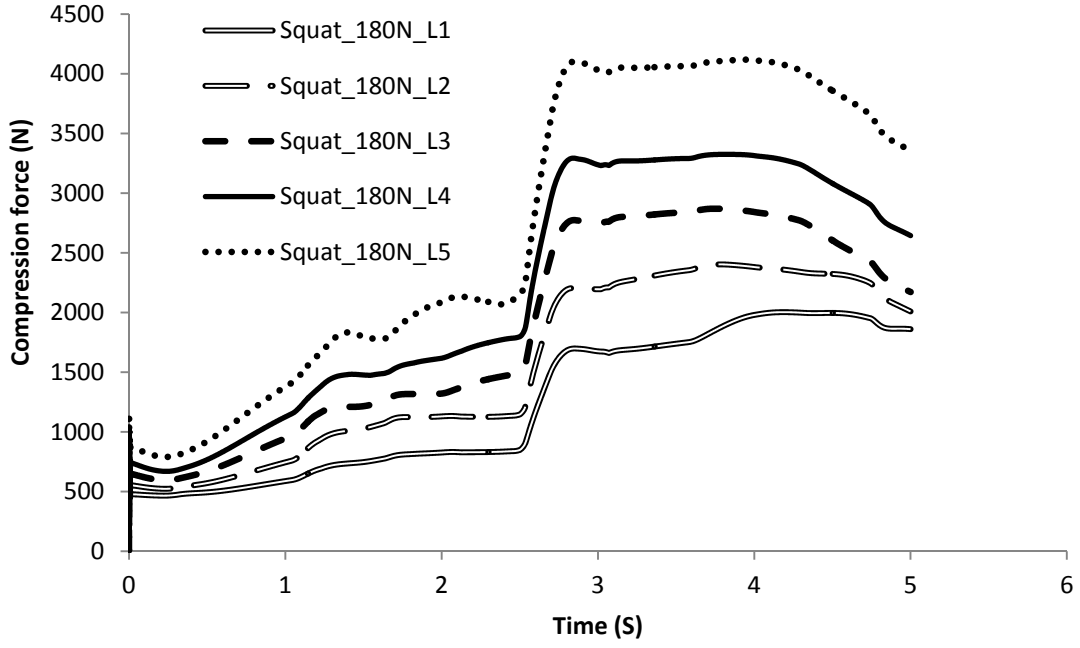

Figure A8: Compression force on discs L1 to S1 for squatting with load of 195N.

Appendix B: Moments on discs L1 to S1 for stooping and squatting

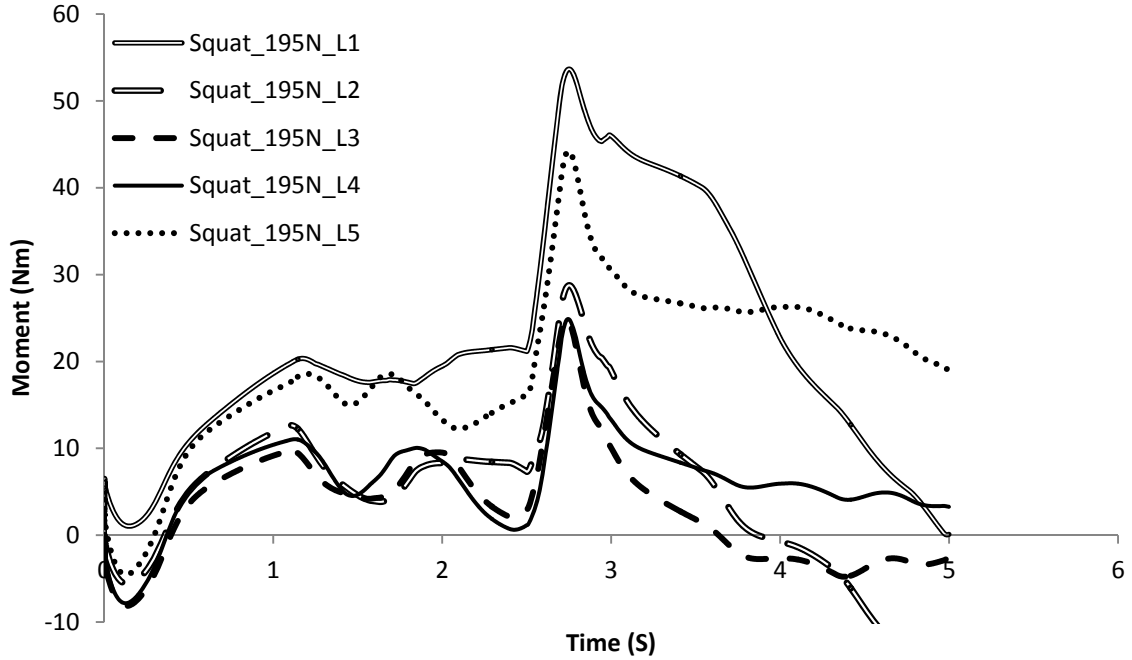

Figure B1: Passive ligamentous moment on discs L1 to S1 for squatting with load of 195N.

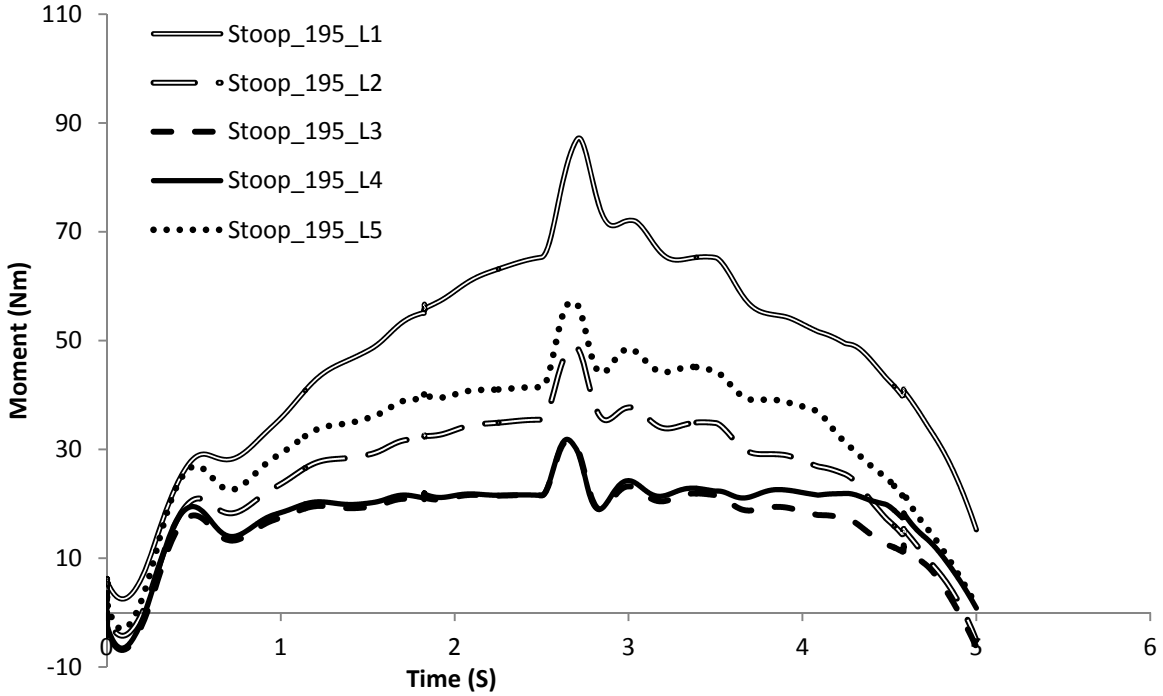

Figure B2: Passive ligamentous moment on discs L1 to S1 for stooping with load of 195N.

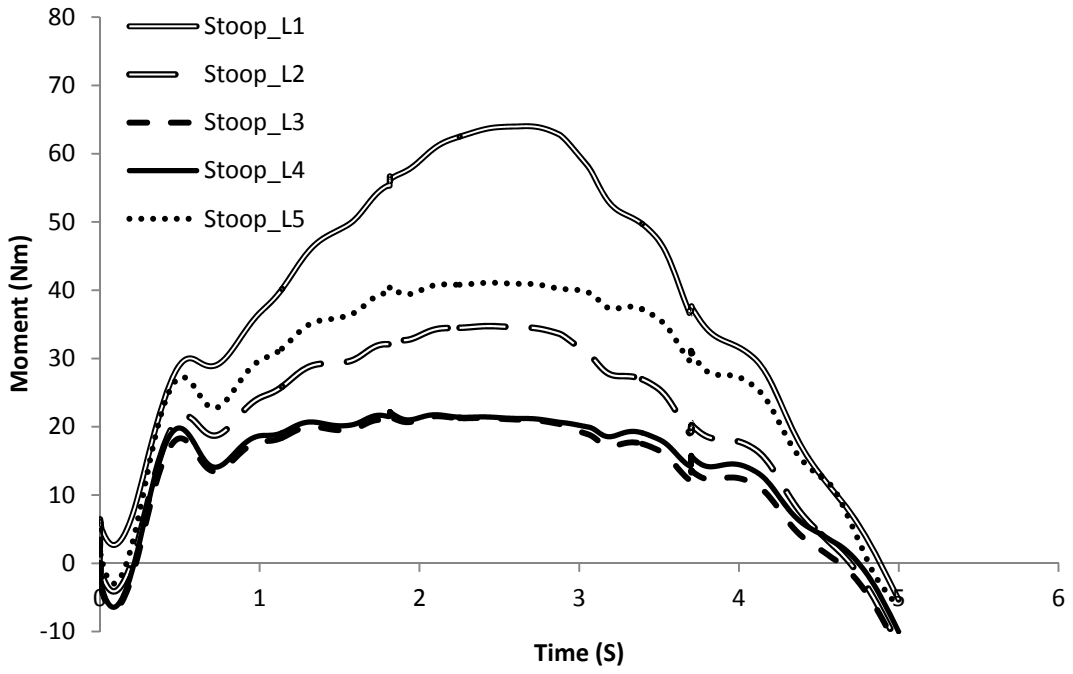

Figure B3: Passive ligamentous moment on discs L1 to S1 for stooping without load.

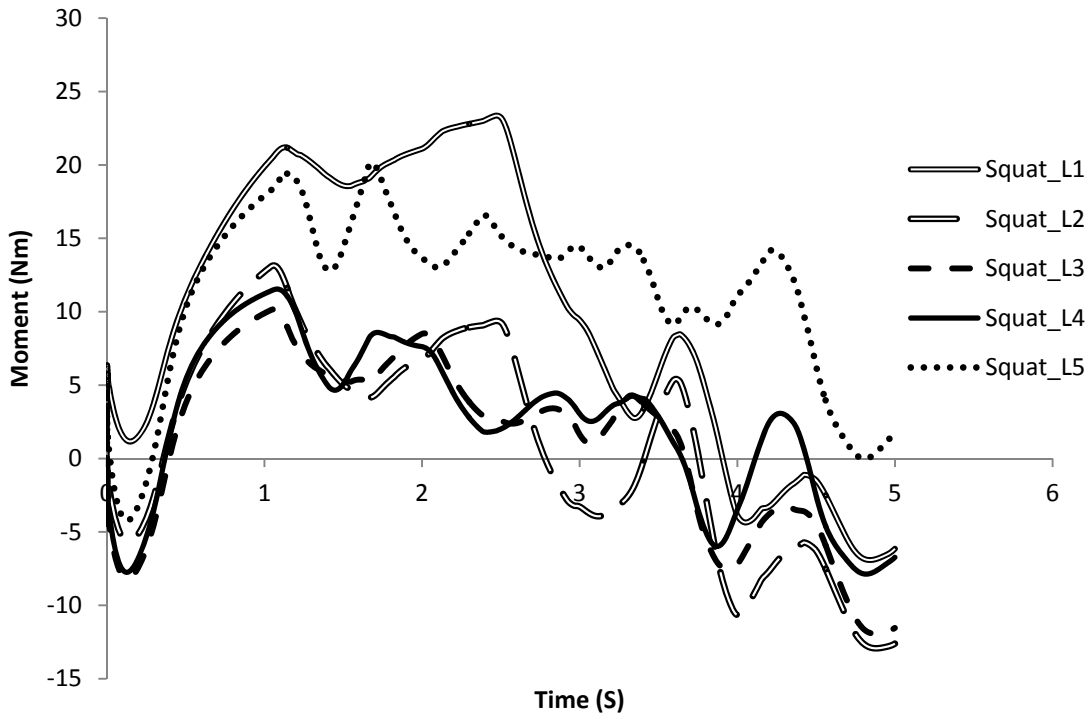

Figure B4: Passive ligamentous moment on discs L1 to S1 for squatting without load.

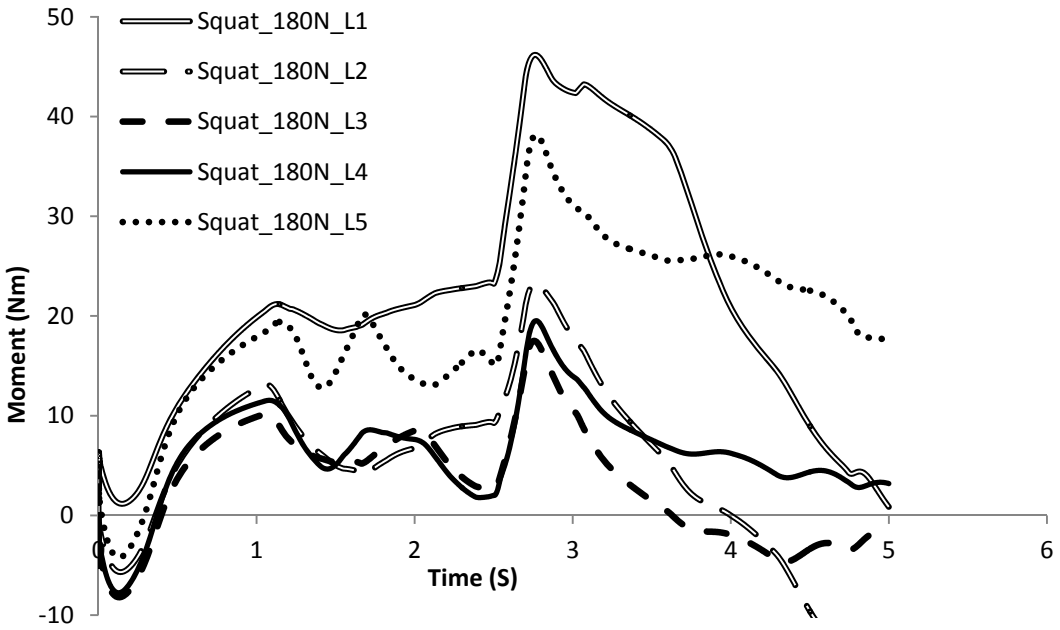

Figure B5: Passive ligamentous moment on discs L1 to S1 for squatting with load of 180N.

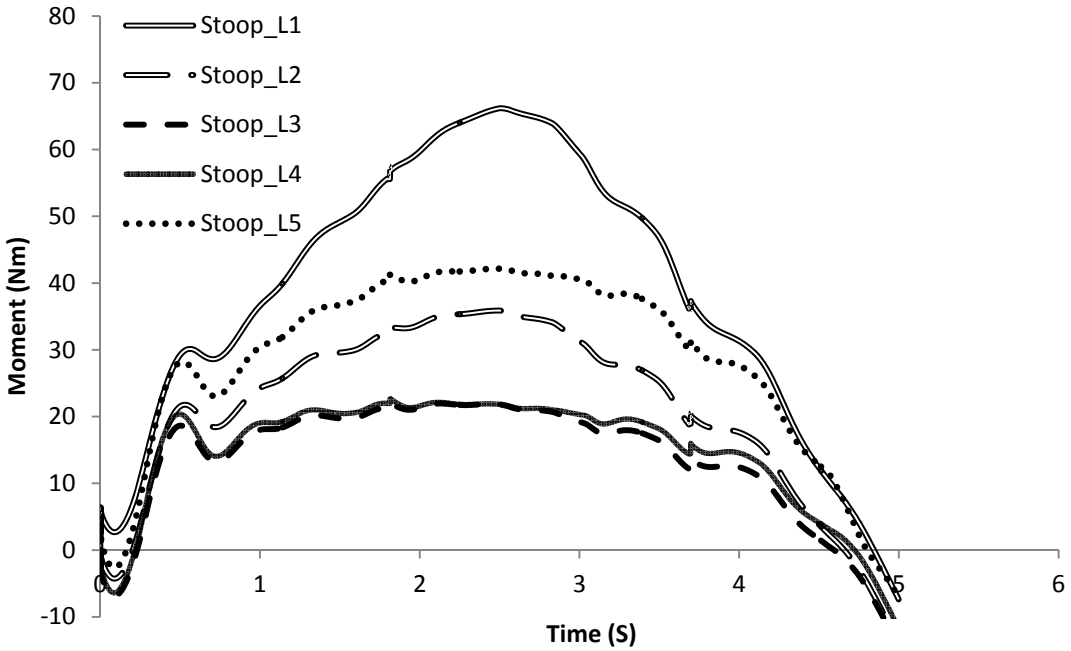

Figure B6: Passive ligamentous moment on discs L1 to S1 for stooping without load.

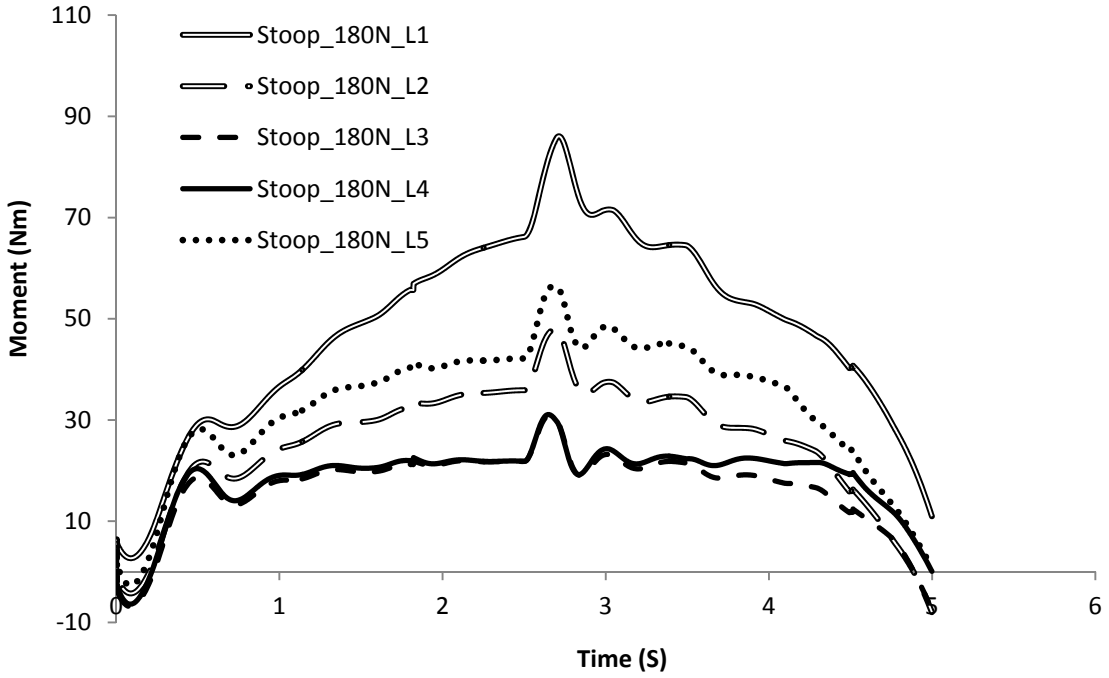

Figure B7: Passive ligamentous moment on discs L1 to S1 for stooping with load of 180N.

Appendix C: Shear forces on discs L1 to S1 for stooping and squatting

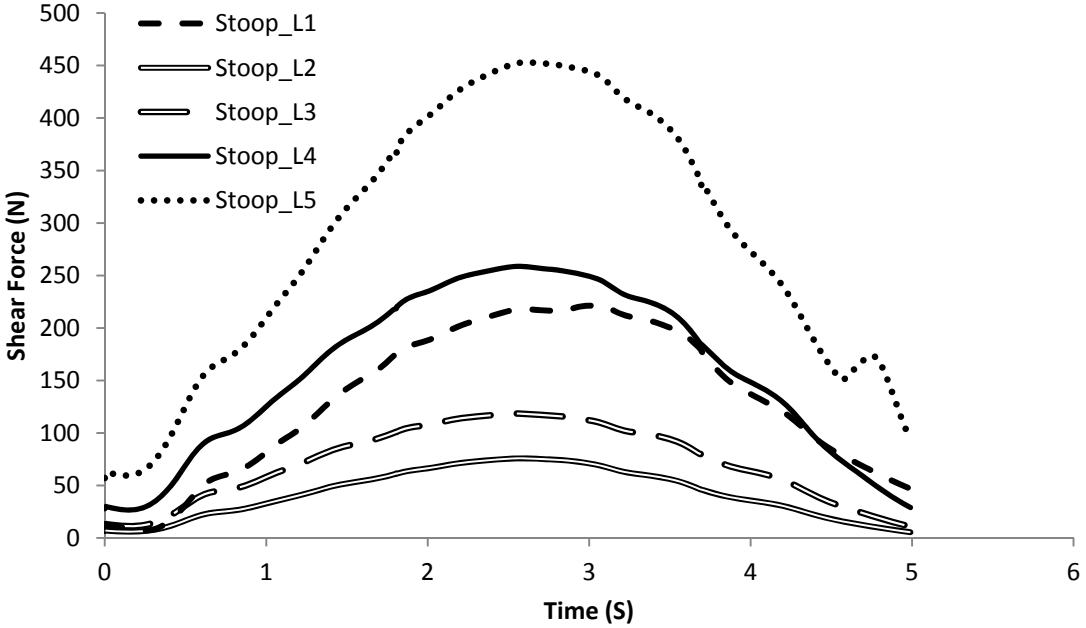

Figure C1: Shear forces on discs L1 to S1 for stooping without load.

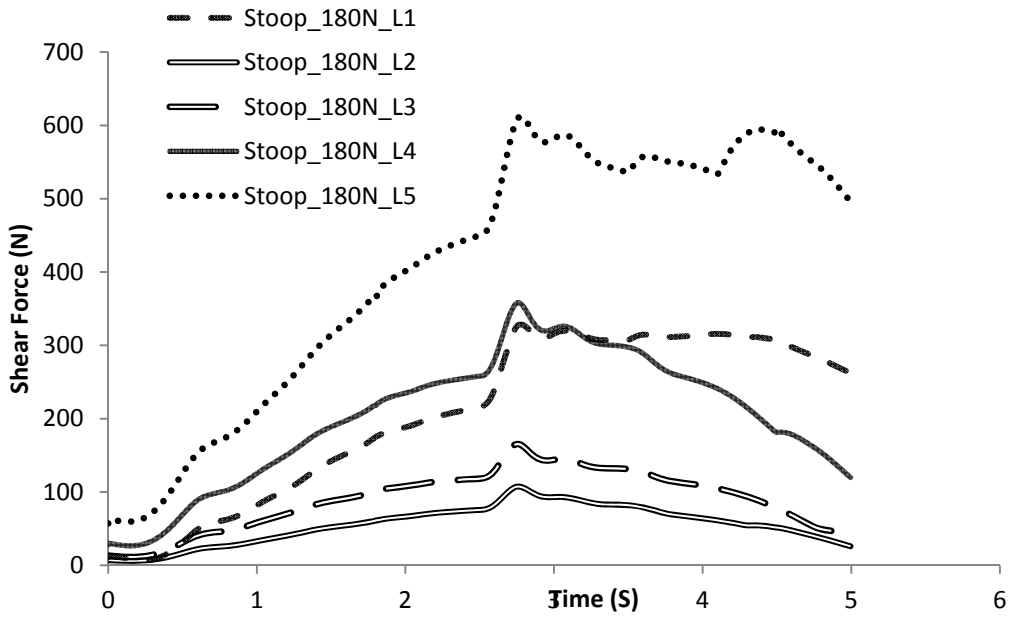

Figure C2: Shear forces on discs L1 to S1 for stooping with load of 180N.

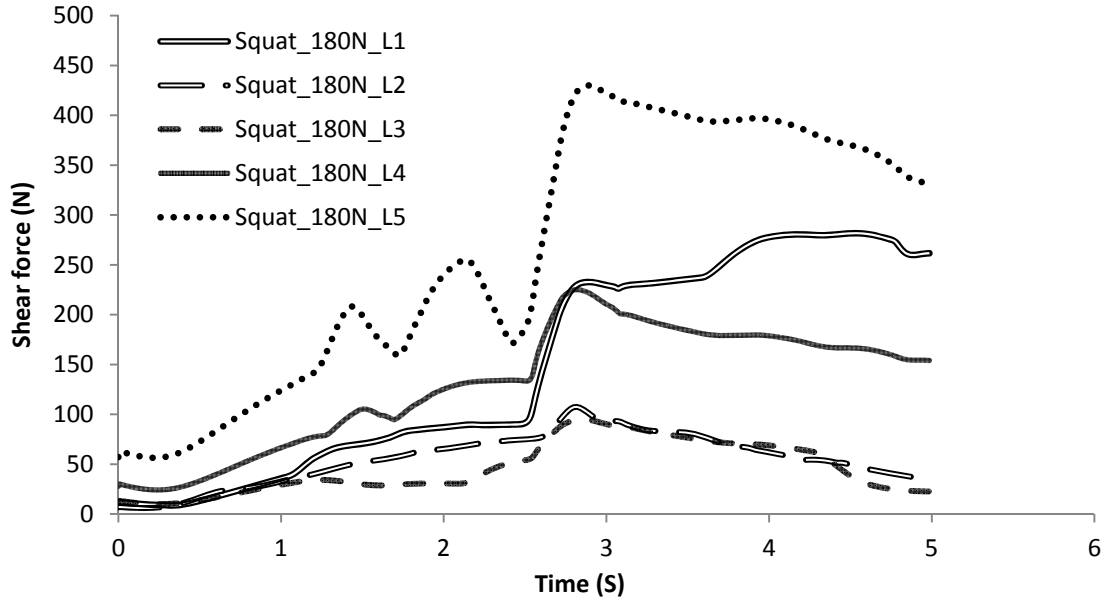

Figure C3: Shear forces on discs L1 to S1 for squatting with load of 180N.

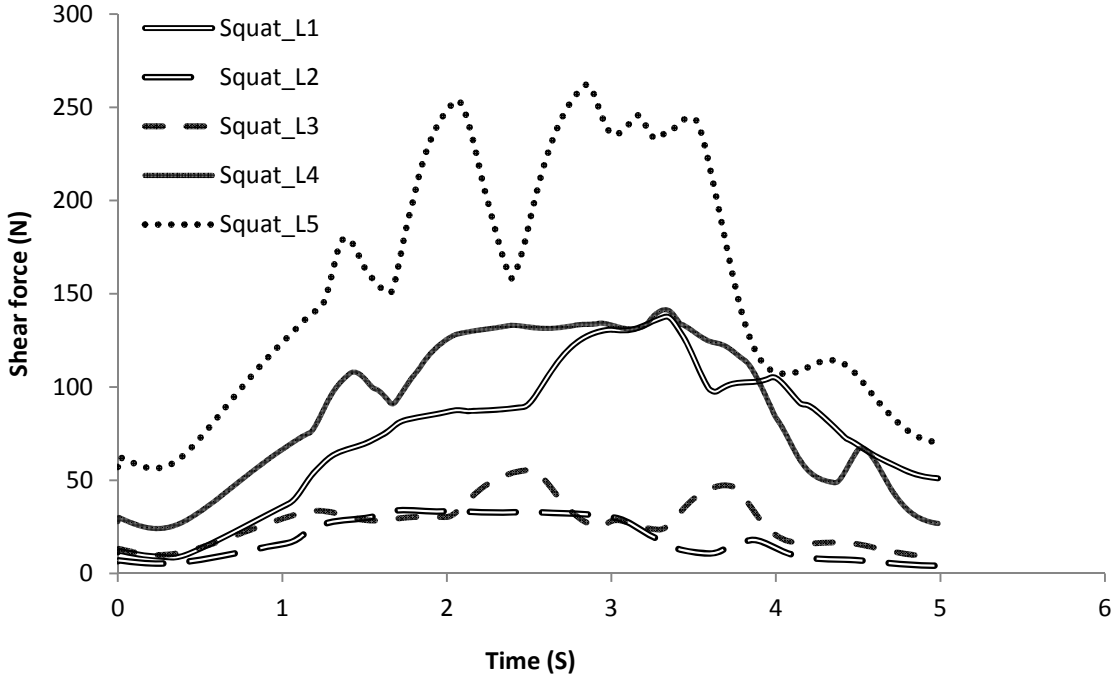

Figure C4: Shear forces on discs L1 to S1 for squatting without load.

Appendix D: Anthropometric Data

Table D1: Anthropometric data at each segmnet for total body weight of 74 kg [6, 81].

Segment	Definition	Segment Weight / Total Body Weight
Hand	Wrist axis / knuckle II middle finger	0.444
Forearm	Elbow axis / ulnar styloid	1.184
Upper arm	Glenohumeral axis / elbow axis	2.072
Forearm and hand	Elbow axis / ulnar styloid	1.628
Total arm	Glenohumeral joint / ulnar styloid	3.7
Foot	Lateral malleolus / head metatarsal II	1.073
Leg	Femoral condyles / medial malleolus	3.441
Thigh	Greater trochanter / femoral condyles	7.4
Foot and leg	Femoral condyles / medial malleolus	4.514
Total leg	Greater trochanter / medial malleolus	11.914

Table D1: Anthropometric data at each segmnet for total body weight of 70 kg [29, 81].

Segment	Definition	Segment Weight / Total Body Weight
Hand	Wrist axis / knuckle II middle finger	0.42
Forearm	Elbow axis / ulnar styloid	1.12
Upper arm	Glenohumeral axis / elbow axis	1.96
Forearm and hand	Elbow axis / ulnar styloid	1.54
Total arm	Glenohumeral joint / ulnar styloid	3.5
Foot	Lateral malleolus / head metatarsal II	1.015
Leg	Femoral condyles / medial malleolus	3.255
Thigh	Greater trochanter / femoral condyles	7.0
Foot and leg	Femoral condyles / medial malleolus	4.27
Total leg	Greater trochanter / medial malleolus	11.27

References

[1] Abrahams P, (2002) Atlas of the Human Body: *A Complete Guide to how the Body Works*. Silverdale Bools an imprint of Bookmart Ltd.

[2] NHS to give back pain acupuncture, *BBC New*. Retrieved on May 6th 2010. <http://news.bbc.co.uk/2/hi/health/8068427.stm>

[3] Geffen P. van, Reenalda J, Veltink P. H, and Koopman B. F. J. M, (2010) Decoupled pelvis adjustment to induce lumbar motion: A technique that controls low back load in sitting, *Int. J. Ind. Ergonomics* 40: 47-54.

[4] Low Back Pain Fact Sheet: National Institute of Neurological Disorders and Stroke (NINDS), National institute of Health. Retrieved on May 4th 2010.
<http://www.ninds.nih.gov/disorders/backpain/detail_backpain.htm>

[5] Ahmadi A, Maroufi N, Behtash H, Zekavat H, and Parnianpour M, (2009) Kinematics analysis of dynamic lumbar motion in patients with lumbar segmental instability using digital videofluoroscopy, *European Spine Journal,* 18: 1677-1685.

[6] Bazrgari B, Shirazi-Adl A, and Arjmand N, (2007) Analysis of squat and stoop dynamic liftings: Muscle forces and internal spinal loads, *European Spine Journal* 16: 687-699.

[7] Indahl A, (2004) Low back pain: Diagnosis, treatment and prognos*is,* Scand. J. Rheumatol 33:199-209.

[8] Hainline, B. (1995). Low back injury, *Clinics in Sports Medicine,* (14): 241- 265.

[9] Søndergaard K. H. E, Olesen C. G, Søndergaard E. K, Zee M. de and Madeleine P, (2010) The variability and complexity of sitting postural control are associated with discomfort, *J. Biomech.,* 43: 1997-2001.

[10] Wang J. L, Parnianpour M, Shirazi-Adl A, and Engin A. E, (1999) Rate effect on sharing of passive lumbar motion segment under load-controlled sagittal flexion: Viscoelastic finite elemnt analysis, *Theor. Appl. Fract. Mech.,* 32: 119-128.

[11] Bertagnoli R, Karg A, and Voigt S, (2005) Lumbar partial disc replacement, *Orthop. Clin.* North Am. 36: 341-347.

[12] Keller T. S, Colloca C. J, and Béliveau J, (2002) Force-deformation response of the lumbar spine: A sagittal plane model of posteroanterior manipulation and mobilization, *Clin. Biomech*., 17: 185-196.

[13] Geffen P. van, Reenalda J, Veltink P. H, and Koopman B. F. J. M, (2010) Decoupled pelvis adjustment to induce lumbar motion: A technique that controls low back load in sitting, *Int. J. Ind. Ergonomics,* 40: 47-54.

[14] Tanaka M. L, Ross S. D, and Nussbaum M. A, (2010) Mathematical modeling and simulation of seated stability*, J. Biomech.,* 43: 906-912.

[15] Bazrgari B, Shirazi-Adl A, and Parnianpour M, (2009) Transient analysis of trunk response in sudden release loading using kinematics-driven finite element model, *Clin. Biomech.,* 24: 341-347, 2009.

[16] Lengsfeld M, Frank A, Deursen D. L. Van and Griss P, (2001) Lumbar spine curvature during office chair sitting, *Medical Engineering and Physics,* 22: 665-669.

[17] Tay S. K, Gibson I, and Jagdish B. N, (2009) Detailed spine modeling with LifeMOD™, in *ICREATE '09 - International Convention on Rehabilitation Engineering and Assistive Technolog.*

[18] Pankoke S, Buck B, Woelfel H.P, (1998) Dynamic FE model of sitting man adjustable to body height, body mass and posture used for calculating internal forces in the lumbar vertebral disks, *J. Sound Vibrat.,* 215: 827-839.

[19] Fritz M, (2000) Simulating the response of a standing operator to vibration stress by means of a biomechanical model, *J. Biomech.,* 33: 795-802.

[20] Hess J. A, Kincl L. D, and Davis K, (2010) The impact of drywall handling tools on the low back, *Appl. Ergon.,* 41: 305-312.

[21] Roffey D. M, Wai E. K, Bishop P, Kwon B. K, and Dagenais S, (2010) Causal assessment of awkward occupational postures and low back pain: results of a systematic review, *Spine Journal,* 10: 89-99.

[22] Marras W. S, Lavender S. A, Ferguson S. A, Splittstoesser R. E, and Yang G, (2010) Quantitative biomechanical workplace exposure measures: Distribution centers, *Journal of Electromyography and Kinesiology,* 20: 813-822.

[23] Wai E. K, Roffey D. M, Bishop P, Kwon B. K, and Dagenais S, (2010) Causal assessment of occupational carrying and low back pain: results of a systematic review, *Spine Journal,* 10: 628-638.

[24] Damecour C, Abdoli-Eramaki M, Ghasempoor A, and Neumann W. P, (2010) Comparison of two heights for forward-placed trunk support with standing work, *Appl. Ergon.,* 41: 536-541.

[25] Callaghan J. P, Salewytsch A. J, and Andrews D. M, (2001) An evaluation of predictive methods for estimating cumulative spinal loading, *Ergonomics,* 44: 825-837.

[26] Adams M. A., (2004) Biomechanics of back pain, *Acupuncture in Medicine,* 22: 178-188.

[27] Harvey J. and Tanner S, (1991) Low back pain in young athletes. A practical approach, *Sports Medicine,* 12: 394-406.

[28] Dieën J. H. Van, (1996) Asymmetry of erector spinae muscle activity in twisted postures and consistency of muscle activation patterns across subjects, *Spine,* 21: 2651-2661.

[29] Wilke H. J-, Neef P, Hinz B, Seidel H, and Claes L, (2001) Intradiscal pressure together with anthropometric data - A data set for the validation of models, *Clin. Biomech.,* 16: S111-S126.

[30] Seraj-Zadeh R, (2009) A Three-dimensional multibody computational model of lumbar spine, Ryerson University, pp 1-60.

[31] Corlett E. N, (2006) Background to sitting at work: Research-based requirements for the design of work seats, *Ergonomics,* 49: 1538-1546.

[32] Pope M. H, Goh K. L, and Magnusson M. L, (2002) Spine ergonomics, *Annual Review of Biomedical Engineering,* 4: 49-68.

[33] Rasmussen J, Tørholm S, and Zee M. de, (2009) Computational analysis of the influence of seat pan inclination and friction on muscle activity and spinal joint forces, *Int. J. Ind. Ergonomics,* 39: 52-57.

[34] Arjmand N, Gagnon D, Plamondon A, Shirazi-Adl A, and Larivière C, (2009) Comparison of trunk muscle forces and spinal loads estimated by two biomechanical models, *Clin. Biomech.,* 24: 533-541.

[35] Sun L. W, Lee R. Y. W, Lu W, and Luk K. D. K, (2004) Modelling and simulation of the intervertebral movements of the lumbar spine using an inverse kinematic algorithm, *Medical and Biological Engineering and Computing,* 42: 740-746.

[36] Zee M. de, Hansen L, Wong C, Rasmussen J, and Simonsen E. B, (2007) A generic detailed rigid-body lumbar spine model," *J. Biomech.,* 40: 1219-1227.

[37] Ezquerro F, Simón A, Prado M, an. Pérez A, (2004) Combination of finite element modeling and optimization for the study of lumbar spine biomechanics considering the 3D thorax-pelvis orientation, *Medical Engineering and Physics,* 26: 11-22.

[38] Rohlmann A, Zander T, Schmidt H, Wilke H. J-, and Bergmann G, (2006) Analysis of the influence of disc degeneration on the mechanical behaviour of a lumbar motion segment using the finite element method, *J. Biomech.,* 39: 2484-2490.

[39] Little J. P, Pearcy M. J, and Adam C. J, (2007) Coupled rotations in the lumbar spine - are these a consequence of passive spinal anatomy in *WIT Transactions on Biomedicine and Health,* 83-92.

[40] Latham F, (1957) A study in body ballistics: seat ejection. *Proceedings of the Royal Society of London.Series B, Containing Papers of a Biological Character.Royal Society (Great Britain),* 147: 121-139.

[41] Toth R, (1996) Multiplying degree of freedom, non-linear spinal model, in *19Th Annual Conference on Engineering in Medicine and Biology,* pp. 8.

[42] Orne D, and Liu Y. K, (1971) A mathematical model of spinal response to impact, *J. Biomech.,* 4: 49-71.

[43] Goto K, Tajima N, Chosa E, Tororibe K, Kuroki H, Arizumi Y, and Arai T, (2002) Mechanical analysis of the lumbar vertebrae in a three-dimensional finite element method model in which intradiscal pressure in the nucleus pulposus was used to establish the model, Journal of Orthopaedic, 7: 243-246.

[44] El-Rich M, and Shirazi-Adl A, (2005) Effect of load position on muscle forces, internal loads and stability of the human spine in upright postures. *Comput. Methods Biomech. Biomed. Engin.,* 8:359-368.

[45] Shirazi-Adl A, and Parnianpour M, (1996) Stabilizing role of moments and pelvic rotation on the human spine in compression, *J. Biomech. Eng.,* 118: 26-31.

[46] Arjmand N, Shirazi-Adl A, and Parnianpour M, (2008) Trunk biomechanics during maximum isometric axial torque exertions in upright standing, *Clin. Biomech.,* 23: 969-978.

[47] Arjmand N, Gagnon D, Plamondon A, Shirazi-Adl A, and Larivière C, (2010) A comparative study of two trunk biomechanical models under symmetric and asymmetric loadings, *J. Biomech.,* 43: 485-491.

[48] Adams M. A, Bogduk N, Burton K, and Dolan P, (2002) *The Biomechanics of Back Pain.* Churchill Livingstone.

[49] Zhang Q. H, and Teo E. C, (2008) Finite element application in implant research for treatment of lumbar degenerative disc disease, *Med. Eng. Phys.,* 30: 1246-1256.

[50] Goel V. K, Kong W, Han J. S, Weinstein J. N, and Gilbertson L. G, (1993) A combined finite element and optimization investigation of lumbar spine mechanics with and without muscles, *Spine,* 18: 1531-1541.

[51] Shin D. S, Lee K, and Kim D, (2007) Biomechanical study of lumbar spine with dynamic stabilization device using finite element method, *CAD Computer Aided Design,* 39: 559-567.

[52] Yamamoto I, Panjabi M. M, Crisco T, and Oxland T, (1989) Three-dimensional movements of the whole lumbar spine and lumbosacral joint, *Spine,* 14: 1256-1260.

[53] Shirazi-Adl A, and Parnianpour M, (2000) Load-bearing and stress analysis of the human spine under a novel wrapping compression loading, *Clin. Biomech.,* 15: 718-725.

[54] A. Shirazi-Adl, Analysis of large compression loads on lumbar spine in flexion and in torsion using a novel wrapping element, *J. Biomech.,* vol. 39, pp. 267-275, 2006.

[55] Kuo C, Hu H, Lin R, Huang K, Lin P, Zhong Z, and Hseih M, (2010) Biomechanical analysis of the lumbar spine on facet joint force and intradiscal pressure - A finite element study, *BMC Musculoskeletal Disorders, Vol.* 11.

[56] Kong W. Z, Goel V. K, and Gilbertson L. G, (1998) Prediction of biomechanical parameters in the lumbar spine during static sagittal plane lifting, *J. Biomech. Eng.,* 120: 273-280.

[57] Fritz M, (1991) An improved biomechanical model for simulating the strain of the hand-arm system under vibration stress, *J. Biomech.,* 24: 1165-1171.

[58] Fritz M, (1997) Estimation of spine forces under whole-body vibration by means of a biomechanical model and transfer functions, *Aviation Space and Environmental Medicine,* 68: 512-519.

[59] Fritz M, (1998) Three-dimensional biomechanical model for simulating the response of the human body to vibration stress, *Medical and Biological Engineering and Computing,* 36: 686-692.

[60] Keller T. S, and Colloca C. J, (2002) A rigid body model of the dynamic posteroanterior motion response of the human lumbar spine, *J. Manipulative Physiol. Ther.,* 25: 485-496.

[61] Kassem A. H, and Sameh A, (2008) A general framework for lumbar spine modelling and simulation, *International Journal of Human Factors Modelling and Simulation,* 1: 211-224.

[62] Tsung B, Evans J, Tong P, and Lee R. Y. W, (2005) Measurement of lumbar spine loads and motions during rotational mobilization, *J. Manipulative Physiol. Ther.,* 28: 238-244.

[63] Ralph E, B Gay, Iharreborde L, Berglund K, and Kai-Nan A, (2005) The neutral zone in human lumbar spine sagittal plane motion: A compression of in vitro quasistatic and dynamic force displacement curves, in ISB XXth Congress-ASB 29th Annual Meeting, 302.

[64] Daggfeldt K, and Thorstensson A, (2003) The mechanics of back-extensor torque production about the lumbar spine, *Journal of Biomechanics.,* 36: 815-825.

[65] Hodges W. P, Cresswell A. G, Daggfeldt K, and Thorstensson A, (2001) In vivo measurement of the effect of intraabdominal pressure on the human spine, *Journal of Biomechanics*., 34: 347-353.

[66] Eberlein R, Holzapfel G. A, and Fröhlich M, (2004) Multi-segment FEA of the human lumbar spine including the heterogeneity of the annulus fibrosus, *Comput. Mech.,* 34: 147-163.

[67] Psoas major, Muscular System - Hip Flexor Muscles Retrieved on June 10th 2010. < http://www.criticalbench.com/hip-flexor-muscles.htm>

[68] Psoas Major, The Free Dictionary, Retrieved on May 18th 2011. <http://medical-dictionary.thefreedictionary.com/psoas+major>.

[69] Quadratus Lumborum, Retrieved on May 17th 2011. < http://www.exrx.net/Muscles/QuadratusLumborum.html>.

[70] Quadratus Lumborum, Craddock & Associates, Retrieved on June 28th 2010. < http://professionalmassagetherapist.org/anatomy/anatomy_Results.php>.

[71] Quadratus Lumborum, Obliques and Quadratus Lumborum, Retrieved on June 20th 2010. < http://muscul.az.free.fr/uk/anaplus/anifo_oblic.htm>.

[72] Bruno D, Multifidus, Spine strong. Retrieved on May 18th 2011. <http://spinestrong.files.wordpress.com/2011/05/core-muscle-anatomy2.jpg>.

[73] Multifidus, D G Lee Physical Therapist corp. and associates. Retrieved on April 10th 2011. <http://dianelee.ca/education/article_deep_core.php#multifidus>.

[74] Iliopsoas, Nicolle's Massage Therapy Spot, Retrieved on June 10th 2010. < http://solacenmt.blogspot.com/2010/11/pelvic-tilt-and-its-effect-on-lower.html>.

[75] Song D, Cheng E, Brown I, Davoodi R, and Loeb G. E, (2008) *Virtual Muscle 4.0.1: Muscle* for MATLAB.

[76] Brinckmann P, Frobin W, and Leivseth G, (2002) *Musculoskeletal Biomechanics.* Thieme.

[77] Stuart McGill, (2002) *Low Back Disorders: Evidence-Based Prevention and Rehabilitation.* United States of America: Human Kinetics.

[78] Keith B, Intervertebral Discs, Retrieved on May 6th 2010. < http://www.spineuniverse.com/anatomy/intervertebral-discs>

[79] Transverse section of an intervertebral disc showing the subarachnoid space, Anaesthesia, *The Medicine Publishing Company Ltd.* Retrieved on August 10th, 2010. < http://www.frca.co.uk/article.aspx?articleid=100361>.

[80] El-Rich M, Arnoux P, Wagnac E, Brunet C, and Aubin C, (2009) Finite elemnet investigantion of the loading rate effect on the spine load-sharing changes under impact conditions, *Journal of Biomechanics.,* 42: 1252-1262.

[81] Pintar F. A, Yogonandan N, Myers T, Elhagediab A, and Sances Jr. A, (1992) Biomechanical properties of human lumbar spine ligaments, *Journal of Biomechanics*. 25: 1351-1356.

[82] Craig J. J, (1955) Introduction to Robotics: Mechanics and control. *Addison-Wesley Publishing Company Inc.*

[83] Hibbler R. C, (2010) Engineering Mechanics: Dynamics. United State of America: Pearson Prentice Hall 12th edition: 600-603.

[84] Winter D. A, (2005) *Biomechanics and Motor Control of Human Movement.* John Wiley & Sons.